



TECHNICKÁ UNIVERZITA V LIBERCI  
Fakulta mechatroniky, informatiky  
a mezioborových studií ■

# SYNTÉZA A FUNKCIONALIZACE UHLÍKATÝCH NANOMATERIÁLŮ PRO TKÁŇOVÉ INŽENÝRSTVÍ

## SYNTHESIS AND FUNCTIONALISATION OF CARBON NANOMATERIALS FOR TISSUE ENGINEERING

### Disertační práce

*Studijní program:* P 3901 Aplikované vědy v inženýrství  
*Studijní obor:* 3901V055 Aplikované vědy v inženýrství

*Autor práce:* Mgr. Jana Karpíšková  
*Školitel:* Prof. Ing. Ivan Stibor, CSc.

## **DECLARATION**

I hereby certify that I have been informed that Act 121/2000, the Copyright Act of the Czech Republic, namely Section 60, Schoolwork, applies to my master thesis in full scope. I acknowledge that the Technical University of Liberec (TUL) does not infringe my copyrights by using my master thesis for TUL's internal purposes.

I am aware of my obligation to inform TUL on having used or licensed to use my master thesis in which event TUL may require compensation of costs incurred in creating the work at up to their actual amount.

I have written my master thesis myself using literature listed therein and consulting it with my supervisor.

I hereby also declare that the hard copy of my master thesis is identical with its electronic form as saved at the IS STAG portal.

Date:

Signature:

## **ACKNOWLEDGEMENTS**

I would like to express my gratitude to Prof. Ing. Ivan Stibor, CSc., for his valuable advice, patience and extraordinarily professional yet humane approach. I wish all students had such a great supervisor.

I would also like to thank to my co-workers, Mgr. Veronika Zajícová, PhD., RNDr. Michal Řezanka, PhD., Ing. Jan Lukášek and our students, who created an unbelievably friendly and supportive working environment and filled my PhD years with lots of laughter.

Many thanks belong to my co-workers from the group of Prof. Ing. Václav Švorčík, DrSc., whose research I was allowed to participate in, and the group of Ing. Věra Jenčová, PhD., mainly Mgr. Kateřina Strnadová, who provided supervision for fibrous materials production and testing.

Finally, I would like to thank to my family, who always listened to me, although they had no idea what I was talking about.

### **Fundings:**

Surface area and pore size distribution measurements were funded via Research Infrastructure NanoEnviCz, supported by the Ministry of Education, Youth and Sports of the Czech Republic under Project No. LM2015073.

Attendance at international conferences was supported by the Ministry of Education of the Czech Republic within the SGS project 21066/115 and Mobility Funds at the Technical University of Liberec.

## ANNOTATION

Research of materials suitable for tissue engineering is a rapidly developing area. Among many other, various carbon materials have been successfully used for cell cultivation. There are a lot of factors that have been proved to affect cell adhesion and proliferation, such as the presence of various chemical groups, wettability of the surface, surface energy, morphology, mechanical properties etc.

In this work, a novel type of functionalisation was performed, in which carbon nanoparticles (CNPs) were successfully functionalised with amide-amine groups. The size and form of the CNPs was investigated by transmission electron microscopy (TEM). The specific surface areas and pore volumes of the particles were measured via nitrogen adsorption and calculated from Brunauer-Emmet-Teller (BET) equation. The chemical composition was studied via X-ray photoelectron spectroscopy (XPS) and organic elemental analysis (OEA). Differential scanning calorimetry (DSC) was used to investigate thermal stability of CNPs.

The functionalised CNPs were grafted onto the surface of polyethylene terephthalate (PET) and high density polyethylene (HDPE) pre-activated in argon plasma. The chemical composition of the modified polymer surfaces was determined by Raman and X-ray photoelectron spectroscopies and by electrokinetic analysis (zeta potential). Surface roughness and morphology of polymers grafted with CNPs was studied by atomic force microscopy (AFM), surface contact angle was measured by goniometry. Adhesion and proliferation of rat vascular smooth muscle cells (VSMC) on HDPE and PET surfaces grafted with functionalised CNPs were studied *in vitro*.

Using the aforementioned CNPs, four types of composite scaffolds were prepared via sputtering the CNPs into electrospun polycaprolactone (PCL) nanofibers: three of them with three types of functionalised CNPs and one with plain activated CNPs. Plain PCL nanofibers and the composite nanofibrous scaffold with plain activated CNPs were used as comparative samples. The structure of the materials was studied using scanning electron microscopy (SEM). The specific surface area of the scaffolds was measured via nitrogen and krypton adsorption and calculated from BET equation. Cytocompatibility of the materials was tested using 3T3 mouse fibroblasts. Cell viability and proliferation was measured by MTT assay on days 1, 3, 8 and 14

after cell seeding. The samples were then stained using fluorescent dyes and examined via fluorescence microscopy (FM). During the FM analyses, all scaffolds containing CNPs underwent structural degradation when irradiated with either green or blue light. The scaffolds with functionalised CNPs showed better cytocompatibility than the scaffold with plain CNPs.

The PCL scaffold with plain CNPs was also tested for antibacterial activity (in comparison with plain PCL nanofibers) using the following bacterial strains: *Escherichia coli*, *Staphylococcus aureus*, *Pseudomonas aeruginosa* and *Enterococcus faecalis*. However, no antibacterial effect was found.

A substantial part of the thesis is also focused on the synthesis of mesoporous carbon particles via soft- and hard-templating. The materials were analysed using SEM and gas adsorption analyses. Selected synthesised materials were functionalised using the above mentioned amide-amine functionalisation and characterised using OEA and gas adsorption. These materials are to be used for grafting on plasma treated polymer surfaces.

As this study is highly interdisciplinary, the author wanted to manage as many procedures as possible to make a complex piece of work. She therefore focused on being trained not only in synthesis, but also production of fibrous materials, plasma treatment, gas physisorption, basics of tissue engineering and fluorescence microscopy. Not only did she use the skills gained to prepare the materials, but also actively participated in the majority of the procedures and analyses performed throughout the study.

**Keywords:** carbon nanomaterials, functionalisation, tissue engineering, cytocompatibility, amine

## ANOTACE

Výzkum materiálů vhodných pro tkáňové inženýrství patří mezi rychle se rozvíjející oblasti; pro kultivaci buněk jsou, mimo jiné, úspěšně používány různé uhlíkaté materiály. Bylo prokázáno, že adheze a proliferace buněk závisí na mnoha faktorech, jako například přítomnost určitých funkčních chemických skupin, smáčivost povrchu, jeho povrchová energie, morfologie, mechanické vlastnosti apod.

Tato práce představuje nový typ funkcionalizace, při němž byl povrch uhlíkatých nanomateriálů modifikován amid-aminovými skupinami. Velikost a struktura částic byly zkoumány transmisí elektronovou mikroskopií. Specifický měrný povrch a objem pórů byl stanoven pomocí dusíkové adsorpce a vypočten z Brunauer-Emmet-Tellerovy rovnice. Chemické složení připravených materiálů bylo zkoumáno prostřednictvím rentgenové fotoelektronové spektroskopie a organické elementární analýzy, teplotní stabilita pomocí diferenční snímání kalorimetrie.

Funkcionalizované částice byly navázány na povrch polymerních povrchů z polyethylentereftalátu a vysokohustotního polyethylenu, aktivovaných argonovým plasmováním. Chemické složení modifikovaných povrchů bylo analyzováno pomocí Ramanovy a rentgenové fotoelektronové spektroskopie a měřením elektrokinetického potenciálu. Drsnost povrchu byla měřena pomocí mikroskopu atomárních sil, jeho smáčivost pak měřením kontaktního úhlu. Adheze a proliferace potkaních hladkosvalových buněk na modifikovaných povrchích byla zkoumána *in vitro*.

Výše zmíněné funkcionalizované uhlíkaté nanočástice byly dále využity k přípravě kompozitních nanovlákných nosičů z polykaprolaktonu. Tyto materiály pak byly porovnávány s čistými polykaprolaktonovými nanovláknými a nanovlákným kompozitem, obsahujícím pouze neupravené uhlíkaté částice. Struktura připravených nosičů byla zkoumána skenovacím elektronovým mikroskopem, specifický měrný povrch stanoven pomocí dusíkové a kryptonové adsorpce. Cytokompatibilita byla studována v rámci MTT testování na linii 3T3 myších fibroblastů. Vzorky byly dále obarveny pro fluorescenční mikroskopii, během níž při ozařování modrým a zeleným světlem došlo u vzorků obsahujících uhlíkaté částice k tepelnému natavení nanovlákné polymerní matrice. Nosiče s funkcionalizovanými uhlíkatými částicemi vykazovaly mnohem vyšší cytokompatibilitu než vzorek s neupravenými částicemi.

Dále byly testovány antibiotické vlastnosti nosiče obsahujícího neupravené částice (v porovnání s čistými polykaprolaktonovými nanovlákný) za použití bakteriálních kmenů *Escherichia coli*, *Staphylococcus aureus*, *Pseudomonas aeruginosa* and *Enterococcus faecalis*. Žádná antibakteriální aktivita nebyla prokázána.

Podstatná část práce je též zaměřena na syntézu mezoporézních uhlíkatých materiálů pomocí soft a hard templátování. Připravené materiály byly analyzovány pomocí skenovací elektronové mikroskopie a dusíkové adsorpce. Vybrané materiály byly dále funkcionalizovány výše zmíněným způsobem a charakterizovány za použití organické elementární analýzy a dusíkové adsorpce. Tyto materiály jsou určeny pro budoucí experimenty s navazováním částic na polymerní povrchy pro tkáňové inženýrství.

Vzhledem k interdisciplinární povaze této studie se její autorka snažila osvojit si co nejvíce užité metody, aby byla schopna vytvořit komplexní práci. Zaměřila se tedy nejen na syntézu a funkcionalizaci uhlíkatých částic, ale také na přípravu nanovláknenných materiálů, plasmování, analýzu specifického měrného povrchu a porosity plynovou adsorpcí, základy tkáňového inženýrství a fluorescenční mikroskopie. Aktivně se podílela na převážné většině provedených experimentů a analýz.

**Klíčová slova:** uhlíkaté nanomateriály, funkcionalizace, tkáňové inženýrství, cytokompatibilita, amin

## Contents

1. INTRODUCTION .....	10
2. OBJECTIVES .....	11
3. THEORETICAL PART .....	12
3.1. Tissue engineering .....	12
3.1.1. Cell-material interaction .....	12
3.2. Carbon materials in tissue engineering and biomedicine .....	15
3.2.1. Activated carbon .....	16
3.2.2. Fullerenes .....	16
3.2.3. Graphene .....	18
3.2.4. Carbon nanotubes .....	21
3.2.5. Carbon nanodiamonds .....	23
3.2.6. Carbon nanohorns .....	24
3.2.7. Carbon dots .....	24
3.2.8. Toxicity of carbon nanomaterials .....	25
4. RESULTS AND DISCUSSION .....	27
4.1. Functionalisation of Commercially Available Carbon Particles .....	27
4.1.1. Transmission electron microscopy .....	31
4.1.2. X-ray photoelectron spectroscopy .....	31
4.1.3. Organic elementary analysis .....	34
4.1.4. Surface area, pore size distribution and pore volume analysis .....	36
4.1.5. Electrokinetic analysis – zeta potential .....	38
4.1.6. Differential scanning calorimetry .....	39
4.2. Grafting of the functionalised CNPs on polymer surfaces and their cytocompatibility testing .....	40
4.3. Nano-microfibrous Scaffolds Containing Carbon Particles .....	41
4.3.1. Surface area .....	41
4.3.2. Cytocompatibility with 3T3 mouse fibroblasts – MTT assay .....	44
4.3.3. Scanning electron microscopy .....	49
4.3.4. Thermogravimetric analysis .....	51
4.3.5. Differential scanning calorimetry .....	53
4.3.6. Antibacterial properties testing .....	53
4.4. Templated Mesoporous Carbon Materials .....	55
4.4.1. Hard-templated Materials .....	55
4.4.2. Soft-templated Materials .....	60
4.4.3. Functionalised Materials .....	64
5. EXPERIMENTAL PART .....	69

5.1. Functionalisation of Commercially Available Carbon Particles .....	69
5.1.1. Amine formation .....	69
5.1.2. Amide-amine formation .....	69
5.1.3. Oxidation of commercially available carbon nanoparticles .....	70
5.2. Preparation of Nanofibrous Scaffolds Containing Carbon Particles .....	70
5.3. Cytocompatibility of Nanofibrous Scaffolds Containing Carbon Particles – MTT Assay .....	70
5.4. Antibacterial Testing of PCL Nanofibers and PCL+C Scaffolds.....	71
5.5. Synthesis of Templated Mesoporous Carbon Materials.....	72
5.5.1. Hard-templated Materials .....	72
5.5.2. Soft-templated Materials .....	74
5.6. Functionalisation of the Synthesised Mesoporous Carbons .....	74
5.7. Equipment specifications.....	75
6. CONCLUSIONS .....	77
7. ABBREVIATIONS .....	80
8. REFERENCES .....	83
9. LIST OF PUBLICATIONS.....	95
9.1. Articles in impacted journals.....	95
9.2. Articles in non-impacted journals .....	95
9.3. Conferences .....	95

# 1. INTRODUCTION

Carbon materials can be found literally everywhere, widely used from home to industrial settings (Hirsch, 2010; Inagaki et al., 2014). The versatility of carbon stems from its ability to form three hybridisation types, which leads to a huge variety of allotropes of either natural or artificial origin (Falcao and Wudl, 2007; Enyashin and Ivanovskii, 2014). Countless carbon-based composites have been prepared and investigated, the interest in this area being not declining for sure, still providing scientists with new challenges.

From the broad spectrum of carbon-based materials, this work focuses *only* on activated carbon nanoparticles (CNPs) and mesoporous carbon materials. If suitably functionalised, their unique properties may be improved and tailored for specific applications. In this work, functionalisation of commercially available CNPs and synthesis of templated mesoporous carbon nanostructures and their functionalisation are primarily aimed at the field of tissue engineering, but the products might also find their use in catalysis and other areas.

Because of a highly interdisciplinary nature of this study, the author believes that, to thoroughly understand the issue, it is essential to manage and participate in as many procedures as possible. Starting with synthesis of the materials, continuing with the production of fibrous materials and plasma treatment, she also aims at analysing and testing via gas physisorption, basics of tissue engineering and fluorescence microscopy.

## 2. OBJECTIVES

The aim of this work is to prepare and/or modify carbon nanostructures with functional groups that would potentially be useful in tissue engineering and possibly other fields, such as catalysis. For such carbon materials' modifications, a novel type of functionalisation with amide-amine groups was selected. This kind of functionalisation should improve the materials' cytocompatibility, making their surface more suitable for cell adhesion. The influence of various oligoamines, varying in the number and type of amino groups and the length of alkyl chains, will be studied.

After the first experiments with the surface modification of commercially available carbon nanoparticles, prepared templated mesoporous carbon materials could also be used as substrates for functionalisation.

Such structures shall be grafted on plasma treated polymers and tested *in vitro* for cell adhesion and proliferation. Grafting with functionalised carbon nanostructures should enhance the wettability of such polymer surfaces, modify surface roughness and provide the presence of chemical functional groups that support cell adhesion and proliferation.

The functionalised CNPs could also be incorporated into nanofibrous scaffolds, which would be tested *in vitro* for cell adhesion and proliferation.

Properties of the prepared materials will be analysed using various analytical methods.

Besides the aims regarding the synthesis and functionalisation, one of the author's main aims is to manage and practice the majority of skills needed to conduct this study. Among others, these shall include production of fibrous materials, plasma treatment, gas physisorption, tissue engineering basics and fluorescence microscopy.

## **3. THEORETICAL PART**

### **3.1. Tissue engineering**

In 1993, Langer and Vacanti defined tissue engineering as an interdisciplinary field that applies the principles of engineering and life sciences toward the development of biological substitutes that restore, maintain, or improve tissue function or a whole organ (Langer and Vacanti, 1993). As there are many health problems connected with organ/tissue loss or damage, this area is of a great importance and therefore being extensively researched.

A cell carrier, usually called a biomaterial, is in a direct interaction with the biological environment. Biomaterials can be both, of biological origin (proteins of extracellular matrix (ECM) such as fibronectin, collagen, laminin, fibrin, etc.) or artificial (carbon materials, synthetic polymers, metals, ceramics). They have to be biocompatible, i. e. tolerated by cells, without any cytotoxic, mutagenic and immunogenic effects.

Biomaterials can be either bioinert or bioactive. While the bioinert ones do not directly support cell adhesion, the bioactive materials try to mimic some specific features of the biological environment (e. g. properties of ECM molecules, growth factors, enzymes, etc.). In other words, they should lead to specific, controllable cell behaviour.

#### **3.1.1. Cell-material interaction**

To be able to grow and proliferate, tissue cells need to attach themselves to a material. Surface characteristics of such a material play a key role in cell adhesion and further influence the cells' behaviour. The cell adhesion can be achieved via two mechanisms.

##### **3.1.1.1. Non-receptor mediated cell adhesion**

Non-receptor mediated cell adhesion is a non-specific cell-material interaction via weak chemical bonds (hydrogen bonding, electrostatic, Van der Waals interactions) between molecules present on a material and a cell membrane. This kind of interactions is not mediated via the extracellular matrix, and therefore does not support a long term adhesion and proliferation (Bacakova et al., 2000).

### 3.1.1.2. Receptor-mediated cell adhesion

Tissues consist of cells and extracellular matrix, which is secreted by cells and provides not only structural but also biochemical support for them. ECM is specific for each tissue; depending on cell types, its composition and structure varies to a large extent. It is usually a flexible system that is constantly being remodelled.

ECM is composed of various proteins (fibrous proteins such as collagen, elastin, laminin and fibronectin) and polysaccharides glycosaminoglycans, which are covalently bound to ECM proteins to form proteoglycans (except for hyaluronan). To ensure mechanical strength, also inorganic components are present in bone and teeth tissues.

ECM strongly influences the cell behaviour, such as cell adhesion, cell shape, cell phenotype, migration, proliferation, differentiation, apoptosis etc. The cell-ECM communication is enabled via receptors for specific ECM proteins on cell membranes. *In vitro*, the ECM proteins are spontaneously adsorbed on a material from cell culturing media, *in vivo* from body fluids. Cells' adhesion receptors are able to recognize some specific amino acid sequences in the ECM proteins. After binding to them, the receptors are driven into nano- or micro-domains called focal adhesions (Rosso et al., 2004; Bacakova et al., 2011).

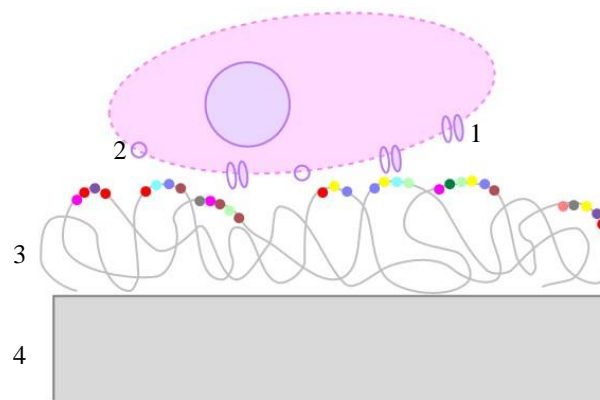


*Fig. 1: Scheme of receptor-mediated cell adhesion; 1 – integrin receptors, 2 – non-integrin receptors, 3 – ECM proteins (with specific sequences of amino-acids) adsorbed on 4– a substrate.*

A successful adsorption of ECM proteins (and therefore also cell adhesion) depends on specific properties of a material – polarity, wettability, presence of certain chemical functional groups,

electrical charge and conductivity, surface roughness and topography (Bacakova et al., 2007, 2011).

**Polarity, wettability:** A moderately hydrophilic surface is usually considered the most beneficial for cell adhesion. Both highly hydrophobic and highly hydrophilic materials do not allow such adhesion; while highly hydrophilic surfaces do not allow proper adsorption of ECM proteins and therefore a stable cell attachment, on highly hydrophobic surfaces, the ECM proteins are absorbed in a rigid form, in which the specific amino acid sequences are not accessible for cells' adhesion receptors (Bacakova et al., 2011).

**Electrical charge and conductivity:** Positive charge of a surface is favourable for a good cell adhesion as a large portion of cell or serum protein surface is recognised as negatively charged (Lee et al., 1994). ECM proteins are usually adsorbed in a geometrical conformation that is easily accessible by cell adhesion receptors.

**Chemical functional groups:** Oxygen containing groups (hydroxyl, carboxyl, ester, carbonyl, aldehyde, etc.) and amino groups on a material's surface usually increase its wettability and therefore have a positive impact on cell adhesion (Lee et al., 1991, 1994; Bacakova and Svorcik, 2008). As for amino groups, they also bring a positive electrical charge to the surface.

**Surface roughness and topography:** A particular structure of a material also plays an important role in cell adhesion. While macroroughness (i.e. irregularities distinguishable by the human eye-cca from 100  $\mu\text{m}$ ) is too large to be "noticed" by cells, microroughness (i.e. dimensions in micrometres) exhibits a dual effect on cell adhesion (Bacakova et al., 2011). Cases where microroughness supported (Zhao et al., 2005) or negatively influenced (Kim et al., 2005) cell attachment are known. Lately, nanoroughness and nanotopography (i.e. irregularities smaller than 100 nm) have been studied extensively, because nanostructured materials shall naturally mimic structures similar to cell membranes and ECM proteins. ECM adhesion molecules are adsorbed in a favourable orientation, which enables the cells' receptor access to the specific amino acid sequences (Webster et al., 1999; Price et al., 2004).

### 3.2. Carbon materials in tissue engineering and biomedicine

Various forms of elemental carbon represent a wide range of biomaterials. From fullerenes through nanotubes and graphene to many nanostructured carbon materials (e.g. nanooxions, nanohorns, nanodiamonds, templated particles, etc.), their mechanical, electrical and optical properties present new possibilities for the field of tissue engineering. Such a diversity in structure and properties makes them a unique class of materials (Ratner et al., 2009).

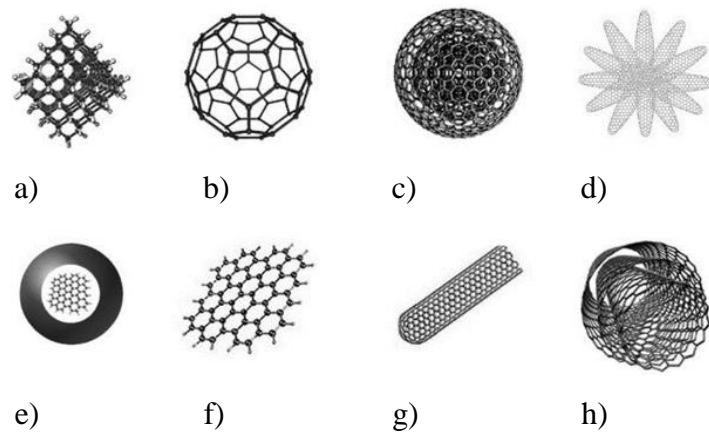


*Fig. 2: Schematic pictures of selected carbon nanomaterials: a) nanodiamond, b) fullerene C60, c) nano-onion, d) nanohorn, e) carbon dot, f) graphene, g) single-walled carbon nanotube, h) multi-walled carbon nanotube; (Baptista et al., 2015).*

Carbon-based nanomaterials have been successfully demonstrated as biocompatible substrates for the growth and differentiation of various mammalian cells (including neurons, osteoblasts, and stem cells); their physicochemical properties (e.g., reduction state, surface functionalisation, and surface roughness) modulated the differential behaviour of the cells. In terms of chemical composition and physical structure, carbon nanomaterials are also able to provide a microenvironment similar to biological extracellular matrix, which makes them potential candidates for the development of artificial scaffolds (Ku et al., 2013).

A “breakthrough” in using carbon materials in tissue engineering came in 1968, when a mechanical heart valve made of pyrolytic carbon was first implanted. Since then, 95 % of the mechanical heart valves implanted worldwide have had at least one component made of pyrolytic carbon (Ratner, 2004).

### **3.2.1. Activated carbon**

Activated carbon (AC) does not belong to a group of materials extensively researched for tissue engineering purposes; its main use stems from its adsorptive properties due to its extraordinarily large surface area. It is usually used e. g. in filtration, electrodes, waste decontamination, catalysis, and removal of various substances or bacteria. Its physical characteristics (particle size, shape, porosity etc.) can be tuned during the manufacturing process, and, actually, any organic matter can be turned into a kind of AC.

Nevertheless, AC in various forms, such as films, cloths, fibres or nanoparticles, has been reported e.g. to promote human embryonic stem cell differentiation towards neuronal lineage (Chen et al., 2012), support adhesion and proliferation of neuronal cells (Jain et al., 2013), osteoblasts (Rodil et al., 2005) and VSMC (Parizek et al., 2009), accelerate wound healing (Blazewicz, 2001) (facilitating fibroblast growth and enhancing fibronectin and type I collagen expression (Huang et al., 2012)), and support mesenchymal stem cell growth and differentiation (Peñalver et al., 2009).

### **3.2.2. Fullerenes**

Since their discovery in 1985, fullerenes in various forms have attracted the attention of scientists in many fields. In tissue engineering, they are considered particularly special because their size enables them to penetrate tissues and organelles (Andreev et al., 2008), which cannot be easily achieved using other submicron materials (Yamashita et al., 2012). They have therefore been proved to be useful carriers; for example, their usage as intracellular carriers was tested by (Foley et al., 2002), who demonstrated their crossing the external cellular membrane and preferential localisation to mitochondria. Drug-delivery capabilities for low-molecular weight agents or oligonucleotides and a slow drug release were reported by (Sitharaman et al., 2008) and (Zakharian et al., 2005), respectively. In addition, successful *in vivo* gene delivery by tetraamino fullerenes was reported by (Maeda-Mamiya et al., 2010).

Due to their anti-oxidative properties (Gharbi et al., 2005), they have also been used as anti-inflammatory (Dellinger et al., 2009; Shershakova et al., 2016) and neuroprotective agents (Huang et al., 2001).

Briefly, research on biomedical applications of functionalised fullerenes and their derivatives has been reviewed in (Partha and Conyers, 2009; Grebowski et al., 2013; Djordjevic et al., 2015; Bogdanovic and Djordjevic, 2016). A comprehensive table of functionalised fullerenes and their potential applications in biomedicine can be seen in Tab. 1.

<b>Type of functionalized fullerene</b>	<b>Potential application</b>	<b>References</b>
Amphiphilic fullerene (AF-1, buckysomes, PEB)	Drug delivery	(Brettreich et al., 2000) (Burghardt et al., 2005) (Partha et al., 2008)
Dendrofullerene (DF-1)	Radioprotection	(Brettreich and Hirsch, 1998) (Daroczi et al., 2006)
Fullerene–paclitaxel	Cancer therapy	(Zakharian et al., 2005)
Fullerene polyamine (tetraamino fullerene)	Gene delivery, transfection	(Nakamura et al., 2000; Isobe et al., 2001, 2006)
Amino-fullerene adducts	Nonviral gene delivery	(Sitharaman et al., 2008)
Fullerene-based amino acids and peptides	Peptide delivery	(Bianco et al., 2001; Hu et al., 2007a; Yang et al., 2007a, 2007b)
Cystine C <sub>60</sub> , Beta-alanine C <sub>60</sub>	H <sub>2</sub> O <sub>2</sub> -induced apoptosis Protection	(Hu et al., 2007b)
Fullerene lipidosome	Anti-viral activity	(Ji et al., 2008)
Fullerene doped liposomes (LMIC)	Photodynamic cancer therapy	(Ikeda et al., 2008) (Doi et al., 2008)
Fullerene-liposomes	Antioxidant	(Lens et al., 2008)
Fullerene vesicle	Oxidative stress reduction	(Maeda et al., 2008)
Gadofullerenes	MRI contrast agents	(Bolskar et al., 2003; Toth et al., 2005; Fatouros et al., 2006; Sitharaman et al., 2007; Bolskar, 2008)
Hydrophilic or cationic fullerenes	Photodynamic cancer therapy	(Mroz et al., 2007a) (Mroz et al., 2007b)
Human serum albumin-fullerene		(Qu et al., 2008)
Fullerene hexaadducts		(Rancan et al., 2002)
Fullerenol	Free radical scavenger	(Dugan et al., 1996(Tsai et al., 1997; Lai et al., 2000; Injac et al., 2008))
Carboxy fullerene		(Dugan et al., 1997)
Polymer encapsulated fullerene		(Murthy et al., 2002)
Hydrated fullerene	Treating alcohol-induced encephalopathy	(Tykhomyrov et al., 2008)

<b>Type of functionalized fullerene</b>	<b>Potential application</b>	<b>References</b>
Fullerene based nanocationite	Myocardial hypoxia	(Amirshahi et al., 2008)
C3-F-tris-MDC	Oxidative stress reduction	(Bisaglia et al., 2000)
Carboxy fullerene	Antioxidant	(Lin et al., 1999)
Ascorbic acid-fullerene		(Monti et al., 2000; Santos et al., 2008)
Bisphosphonate fullerene	Bone therapeutic agent	(Gonzalez et al., 2002)

*Tab. 1: A comprehensive table of functionalised fullerenes and their potential applications in biomedicine according to (Partha and Conyers, 2009), slightly altered. Amphiphilic fullerene-1, AF-1; paclitaxel-embedded buckysomes, PEB; dendrofullerene-1, DF-1; Lipid membrane incorporated fullerenes, LMIC; C3-fullero-tris-methanodicarboxylic acid, C3-F-tris-MDC.*

A special type of multi-layered fullerenes was discovered in 1992 (Ugarte, 1992). These so-called carbon nano-onions (CNOs) are formed by concentric shells of carbon atoms. Similarly to carbon nanotubes, CNOs exhibit insufficient solubility in both aqueous and organic solvents due to strong intermolecular interactions (Van der Waals forces). Their tendency to aggregate can be overcome by means of functionalisation (Bartelmess and Giordani, 2014; Frascioni et al., 2015). Their main potential for biomedical applications lies in bioimaging and biosensing. For example, (Ghosh et al., 2011) used CNOs for *in vivo* life cycle imaging of *Drosophila melanogaster*, followed by (Giordani et al., 2014), who functionalised CNOs with fluorescein and tested them in a comparative toxicological study both *in vitro* and *in vivo* in comparison to analogously functionalised carbon nanotubes.

### **3.2.3. Graphene**

As its existence used to be considered impossible, graphene has been paid a lot of attention to since its first single layer isolation in 2004 (Monaco and Giugliano, 2014). Its structure, i. e. mono-atomic two-dimensional sheet of sp<sup>2</sup>-hybridised carbon atoms arranged as a honeycomb lattice, gives it not only unique electronic properties (Novoselov et al., 2007; Bolotin et al., 2008), but also high transparency (Nair et al., 2008), mechanical strength (Lee et al., 2008) and large surface area (Stoller et al., 2008), making it a promising material for both technological and biomedical applications. As biocompatibility of graphene and its derivatives (graphene oxide and reduced graphene oxide) is disputed (Monaco and Giugliano, 2014), its highest potential for tissue engineering seems to lie mainly in the area of biosensors (Kuila et al., 2011;

Zhu et al., 2015); biomolecular imaging (Sun et al., 2008; Hong et al., 2012) and in electrodes for neural stimulation (Heo et al., 2011).

However, its usage for drug delivery systems and tissue scaffolds has also been actively investigated (Ku et al., 2013; Ding et al., 2015), especially for electroactive tissue repair and regeneration (Li et al., 2016). This is particularly useful in the area of bone tissue engineering, as electric stimulation is known to be vital for the attachment, proliferation and later differentiation of osteoblasts. The recent advances in this area have been thoroughly reviewed by (Shadjou and Hasanzadeh, 2016). Another, not less important, area is neural tissue engineering; comprehensive tables 2 and 3 with the most recent strategies using graphene-based materials for bone and nerve regeneration can be found in (Ding et al., 2015). Generally, in brain repair and neural regeneration, it is crucial to induce more human neural stem cells differentiation towards neurons rather than glial cells, which is achieved by means of graphene-based materials.

The importance of functionalisation of graphene-based nanomaterials to minimise their possible cytotoxic effects has been highlighted and thoroughly summarised in (Menaar et al., 2015).

<b>Materials</b>	<b>Highlights of the study</b>	<b>References</b>
Graphene on a glass substrate	Graphene could induce the differentiation of hNSCs more toward neurons than glial cells.	(Park et al., 2011)
3D-GFs	3D-GFs could promote the mNSCs differentiation towards astrocytes and especially neurons.	(Li et al., 2013)
Hydrazine-rGO films, Ginseng-rGO films and GO films	More differentiation of hNSCs into neurons on the hydrazine-rGO and especially the ginseng-rGO films than the GO film.	(Akhavan et al., 2014)
Fluorinated graphene	FG could enhance cell adhesion, proliferation, and neuroinduction of MSCs.	(Akhavan and Ghaderi, 2014)
G and GO	The rGO sheets stimulated by pulsed laser irradiation provided an accelerated differentiation of the hNSCs into neurons.	(Wang et al., 2012)

<b>Materials</b>	<b>Highlights of the study</b>	<b>References</b>
CNTs, GO and graphene	GO could significantly promote dopamine neuron differentiation.	(Yang et al., 2014a)(Yang et al., 2014)

*Tab. 2: The most recent strategies that combine various stem cells with graphene-based materials for neural regeneration (Ding et al., 2015). Human neural stem cells, hNSCs; mouse neural stem cells, mNSCs; graphene oxide, GO; reduced graphene oxide, rGO; graphene foams, GFs; fluorinated graphene, FG; mesenchymal stem cells, MSCs.*

<b>Materials</b>	<b>Highlights of the study</b>	<b>References</b>
Single layer graphene produced by CVD	Graphene is promising for bone reconstructive surgery with an increased likelihood of inducing MSC differentiation into the osteoblast lineage.	(Kalbacova et al., 2010)
Graphene coated with PMMA	Graphene could accelerate the differentiation of hMSCs at a rate comparable to differentiation under the influence of BMP-2.	(Nayak et al., 2011)
Graphene and GO films	Graphene and GO are demonstrated to be effective preconcentration platforms for accelerated stem cell growth and differentiation.	(Lee et al., 2011)
GO-coated Ti substrate	The BMP-2-adsorbed Ti/GO substrates could significantly enhance in vitro osteogenic differentiation of hMSCs and induce more robust bone formation.	(La et al., 2013)
Graphene nanogrids	rGONR grids showed the fastest osteogenic differentiation of the hMSCs reported up to now in short time of 7 days in the presence of chemical inducers.	(Akhavan et al., 2013)
Self-supporting graphene hydrogel films	The SGH film alone is able to stimulate osteogenic differentiation of stem cells without the need for any additional inducer.	(Lu et al., 2013)
Graphene-coated plates	GO supports proliferation and osteogenic differentiation of gMSCs without the addition of any glucocorticoid or specific growth factors.	(Elkhenany et al., 2015)
3D graphene foams	3D graphene foams can support the attachment and viability of hMSCs, and induce spontaneous osteogenic differentiation.	(Crowder et al., 2013)

<b>Materials</b>	<b>Highlights of the study</b>	<b>References</b>
Graphene-incorporated substrata	CS Nanotopographic cues of the substrata promoted adhesion and differentiation of hMSCs.	(Kim et al., 2013)
GO/PLL composite films	GO/PLL composite film could not only support the growth of MSCs with a high proliferation rate, but also could accelerate the osteogenic differentiation of MSCs.	(Qi et al., 2014)
PLLA nanofibrous scaffolds containing CNT and graphene	Graphene showed stronger effect on promoting osteogenic differentiation of BMSCs and inducing osteogenesis in vivo than CNT.	(Duan et al., 2015)
GO-CaP nanocomposites	GO-CaP nanocomposites significantly facilitated the osteogenesis of hMSCs and further enhanced calcium deposition.	(Tatavarty et al., 2014)

*Tab. 3: The most recent strategies that combine various stem cells with graphene-based materials for bone regeneration (Ding et al., 2015). Chemical vapour deposition, CVD; poly methyl methacrylate, PMMA; bone morphogenetic protein-2, BMP-2; reduced graphene oxide nanoribbon, rGONR; goat adult mesenchymal stem cells, gMSC; self-supporting graphene hydrogel, SGH; poly L-lysine, PLL; poly L-lactide, PLLA; calcium phosphate, CaP; bone marrow stromal stem cells, BMSCs.*

### **3.2.4. Carbon nanotubes**

First described by Iijima in 1991, these tubes are made of one or more graphene sheets; single-walled CNTs (SWCNTs) represent one graphene layer, seamlessly rolled up to form a cylindrical tube, while multi-walled CNTs (MWCNTs) comprise an array of concentric cylinders, coaxially arranged around a central hollow core with Van der Waals forces between adjacent layers. They have increasingly drawn the attention of research because of their interesting properties such as excellent mechanical and physical properties, low density, tuneable semiconductivity, high modulus and high electrical/thermal properties. These outstanding properties make them useful materials for applications in many various fields, including biomedicine (Singh et al., 2012; Alshehri et al., 2016; Mallakpour and Soltanian, 2016). Nevertheless, their high cytotoxicity limits their use in biological systems. The biocompatibility and cytotoxicity of CNTs are related to size (resp. aspect ratio), dose, exposition, testing systems, residual impurities and surface functionalisation. Not only does functionalisation of CNTs improve their solubility and biocompatibility, but it also alters their

cellular interaction pathways, resulting in a significant reduction of their cytotoxic effects. A comprehensive table of effects of CNTs functionalisation according to (Singh et al., 2012) can be seen in Tab. 4.

<b>Material</b>	<b>Toxicological studies</b>	<b>Application</b>	<b>References</b>
Acid-oxidised SWCNTs	Apoptosis studies showed no apparent cell toxicity	Intracellular protein transporters	(Kam and Dai, 2005)
Acid-treated, water-soluble SWCNTs	No changes in cell viability or structure in lysosomes and cytoplasm		(Porter et al., 2009)
Purified COOH-SWCNTs	No cytotoxicity	Pharmacological applications	(Wang et al., 2011)
Oxidised ultrashort SWCNTs	Showed no cytotoxic effects	Intracellular delivery of oligonucleotide molecules	(Crinelli et al., 2010)
Amine-terminated CNTs	Cross cellular membrane without cytotoxicity	Delivery of amino acids, peptides, nucleic acids or drugs	(Pantarotto et al., 2004b, 2004a; Singh et al., 2005; Liu et al., 2009)
SWCNT-PL-PEG	Gene silencing with no apparent cytotoxic effects	SH-small interfering RNA delivery	(Liu et al., 2007)
SWCNT-PEG-drug	Decreased reactive oxygen species-mediated toxicological response and exhibited less cytotoxicity	Drug delivery	(Zhang et al., 2011)
SWCNT-PEG-cisplatin/ doxorubicin	Remarkable reduction of cytotoxicity	Drug-delivery and imaging tool	(Bhirde et al., 2010; Bottini et al., 2011)
SWCNT-PEG-mAb ( $\alpha_v\beta_3$ )	Without harming adjacent normal cells	Cancer-cell targeting	(Portney and Ozkan, 2006)
SWCNT-PEG	Revealed no evidence of toxicity over 4 months		(Schipper et al., 2008)
MWNT-CS-(PC)	Chitosan and PC reduced the cytotoxic effects on normal cells with specific photo-induced toxicity towards malignant cells	Photothermal therapy	(Liao et al., 2011)
Polyoxyethylene sorbitan monooleate (PS80) CNTs	Suppressed cytotoxicity		(Wick et al., 2007)
HMDA-SWCNTs; PDDA chloride-SWCNTs	Negligible cytotoxic effects	Intracellular delivery of negatively	(Krajcik et al., 2008)

Material	Toxicological studies	Application	References
		charged biomolecules	
SWCNTs with human serum proteins	Blood proteins altered SWCNT cellular interaction pathways and reduced cytotoxicity	Biological applications	(Ge et al., 2011)
BSA-dispersed SWCNTs	No acute deleterious cellular effects		(Holt et al., 2011)
Albumin–SWCNTs	Induced cyclooxygenase-2 and modulating toxicity effects of SWCNTs		(Dutta et al., 2007)
Streptavidin–CNT–protein conjugates	No cytotoxic effects on adjacent cells	Specific drug delivery	(Balavoine et al., 1999)
DNA-encased MWCNTs	Does not exert cytotoxic effect on lymphocytes	Selective thermal ablation of malignant tissue in vivo	(Ghosh et al., 2009)
Lectin-functionalized CNTs	Increase in cell viability without signs of apoptosis	Nanovaccine fabrication	(Lorena Montes-Fonseca et al., 2012)
Fluorescent–CNT–FITC/ biotin conjugates	Reduced cytotoxicity	Delivery systems	(Bianco et al., 2005)
Cationic fCNTs	Lowers cytotoxicity <i>in vitro</i>	Delivery of drugs and biomolecules	(Kam et al., 2004)

Tab. 4: Functionalised carbon nanotubes and reduced cytotoxic effects (Singh et al., 2012). Carbon nanotubes, CNTs; functionalised carbon nanotubes, fCNTs; single-walled carbon nanotubes, SWCNTs; phospholipid, PL; poly ethylene glycol, PEG; monoclonal antibody, mAb; multiwalled carbon nanotubes, MWCNTs; chitosan, CS; phycocyanin, PC; cetyltrimethylammonium bromide, CTAB; hexamethylenediamine, HMDA; polydiallyldimethylammonium, PDDA; bovine serum albumin, BSA.

### 3.2.5. Carbon nanodiamonds

Carbon nanodiamonds (CNDs) are mainly composed of carbon  $sp^3$  structures in their core and  $sp^2$  and disorder/defect carbons on the surface, with their size ranging from 1 to cca 150 nm. For biomedical applications, films produced by means of chemical vapour deposition and ultrananocrystalline CNDs with particle sizes between cca 2 and 10 nm are of particular interest, with the focus largely aimed at detonation CNDs (with a particle size around 5 nm). The harsh conditions during detonation lead to the presence of impurities, such as carbides, soot and oxides of iron, chromium copper, potassium, etc., and possible creation of reactive sites forming

various functional groups, which then interact via e.g. Van der Waals and dipole interactions, resulting in aggregates (Mochalin et al., 2011; Badea and Kaur, 2013; Perevedentseva et al., 2013). A detailed scheme of CNDs surface modification approaches can be found in (Badea and Kaur, 2013).

With their low cytotoxicity, dense structure, high surface roughness and surface dangling bonds, ultrananocrystalline CND films have been described as an outstanding coating for biomedical implants, as reported e. g. by (Bajaj et al., 2007; Auciello et al., 2014). Another area of potential application is biosensing (Yang et al., 2002; Hupert et al., 2003). CNDs have been extensively studied for their usage in drug delivery (Chen et al., 2009; Liu et al., 2010; Martín et al., 2010) and biomaging both *in vitro* and *in vivo* (Perevedentseva et al., 2007; Mohan et al., 2010). Their suitability as a carrier arises from their high loading capacity and ability to protect/retain the therapeutic effects of their cargo; CNDs as controlled- and sustained-release delivery agents are mainly aimed at cancer therapy applications (Badea and Kaur, 2013).

### **3.2.6. Carbon nanohorns**

Sometimes also called nanocones, carbon nanohorns (CNHs) are conical nanostructures formed by  $sp^2$  carbon sheets. They can be considered as an alternative to CNTs, although their morphology allows for their own unique properties. Their significant advantages are the possibility of industrial scale production, no need of potentially toxic metal catalysts during their synthesis and the lack of toxicology related high aspect ratio issue (which can be found with CNTs). On the other hand, they tend to aggregate into so called “dahlia clusters” during synthesis, which makes their functionalisation slightly more difficult. Despite this fact, it seems that CNHs may find their use in bioapplications (Karousis et al., 2016), and there have been successful studies exploring CNHs as e.g. drug delivery carriers (Murakami et al., 2008; Xu et al., 2008), biosensors (Yang et al., 2014b), biofuel cells (Wen et al., 2010) and photothermal cancer treatment agents (Whitney et al., 2011, 2013).

### **3.2.7. Carbon dots**

Although they were first discovered as by-products during purification of SWCNTs (Xu et al., 2004), luminescent carbon dots (CDs) quickly gained attention. Thanks to their low cytotoxicity, high stability, low cost and tuneable optical behaviour, they have been studied for their biomedical application potential (Wang and Qiu, 2016), mainly in biosensing, bioimaging

(Kong et al., 2012; Wang et al., 2015) and catalysis (Zhang et al., 2015). Their outstanding optical properties can be even improved by means of surface passivation or modification. For example, doping CDs with nitrogen considerably enhanced their fluorescence, such doped CDs readily entered the cytoplasm of cancer cells *in vivo* and showed no significant toxicity, demonstrating the potential for multicolour live cell labelling, tracking and imaging (Du et al., 2015).

### **3.2.8. Toxicity of carbon nanomaterials**

The use of carbon nanomaterials in biomedical applications and their (cyto)toxicity have been areas of great interest during the last decades (Zhang and Olin, 2012). Carbon materials are generally considered biocompatible and well accepted by the biological environment (Blazewicz, 2001); however, cytotoxicity of the graphene-family (including nanotubes) (Guo and Mei, 2014; Orecchioni et al., 2014; Alshehri et al., 2016) fibrous (Guseva Canu et al., 2016) and fullerene (Trpkovic et al., 2012) materials is still quite a controversial issue, which has not been thoroughly resolved yet (Ding et al., 2015). They have the ability to e.g. damage the DNA and cell membrane, cause oxidative stress, modify mitochondrial activity, alter intracellular metabolic routes and protein synthesis (Singh et al., 2012).

Toxicity of carbon-based nanomaterials is size-dependent (Magrez et al., 2006; Yamashita et al., 2012), but there are also other factors, such as manufacturing methods, surface-to-volume ratio, shape, concentration, composition and quality of purification (Alshehri et al., 2016), that play an important role.

On the other hand, according to some research works, activated and amorphous carbon materials seem to be biocompatible, without any cytotoxic effects (Rodil et al., 2005; Barnes et al., 2009; Chen et al., 2012; Jain et al., 2013). However, overall nanotoxicological research has shown that the potential risks of using nanomaterials must always be taken into consideration, and that more research on this matter is certainly needed (Oberdörster et al., 2005; Fadeel et al., 2015; Piperigkou et al., 2016; Shvedova et al., 2016) because the interactions between nanomaterials and the biological environment are very complex and difficult to predict (Alshehri et al., 2016).

Valuable reference sources with up to date information regarding carbon nanomaterials' biomedical applications and toxicity have lately been summarised in handbooks by (Chen and Wang, 2016; Zhang et al., 2016).

Besides their toxicity issues, another major obstacle to the biological applications of carbonaceous materials is their non-degradability (Ku et al., 2013). Nevertheless, although there are still many challenges to face regarding these topics, carbon-based nanomaterials are and will be highly promising for the use in the field of tissue engineering.

## 4. RESULTS AND DISCUSSION

### 4.1. Functionalisation of Commercially Available Carbon Particles

For this part, commercially available active carbon nanoparticles Darco KB-G from Aldrich (batch 4769TH) were used as a substrate. Although the supplier claims that the particle size shall be around 45  $\mu\text{m}$  or larger, the TEM measurements showed that the particles were about 20 to 40 nm in diameter (see Fig. 8 in chapter 4.1.1.). The adsorption-desorption isotherms obtained from nitrogen adsorption measurements represent Type H2 hysteresis loop, which is typical for micro-mesoporous carbon materials (Thommes et al., 2015). The pore size distribution (PSD) was calculated using Density Functional Theory (DFT), for which the slit/cylindrical pore model was chosen as the most suitable, and the PSD plot can be seen later in chapter 4.1.4., Fig. 10.

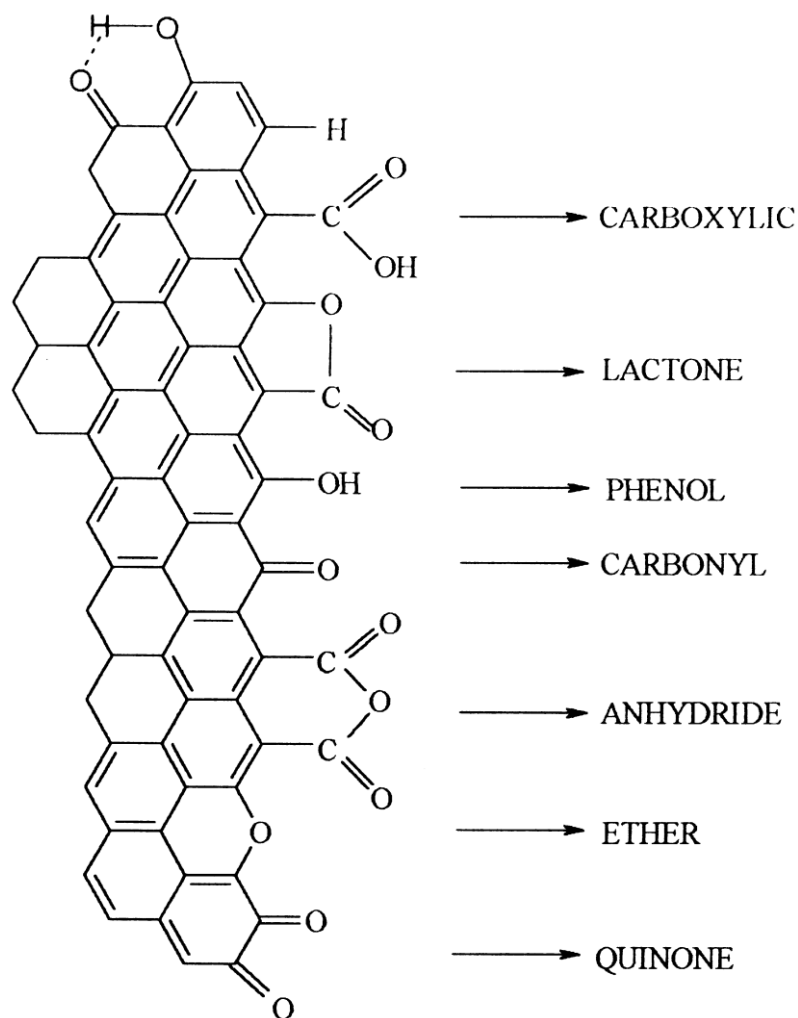


Fig. 3: Surface oxygen groups present on activated carbon (Figueiredo et al., 1999).

Generally, the surface of activated carbon is covered with various oxygen groups, such as carboxyl groups, lactones, phenols, carbonyls, anhydrides, ethers or quinones (Figueiredo et al., 1999), the schematic drawing of which can be seen in Fig. 3.

The general scheme of the procedure used for amide-amine functionalisation can be seen in Fig. 4 and the detailed descriptions of each step are mentioned later in this chapter. Briefly, the CNPs were first oxidised with  $(\text{NH}_4)_2\text{S}_2\text{O}_8$ . The carboxylic groups thus formed were then chlorinated using thionyl chloride. The acyl chloride thus formed further reacted with oligoamines to form amide-amine groups. The list of the oligoamines used for functionalisation and the names of the corresponding materials prepared can be seen in Tab. 5., the structures of particular amide-amine functional groups grafted on CNPs in Fig. 5.

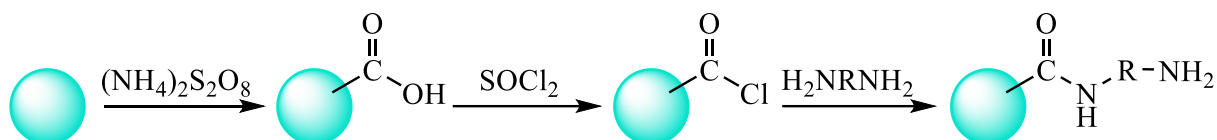
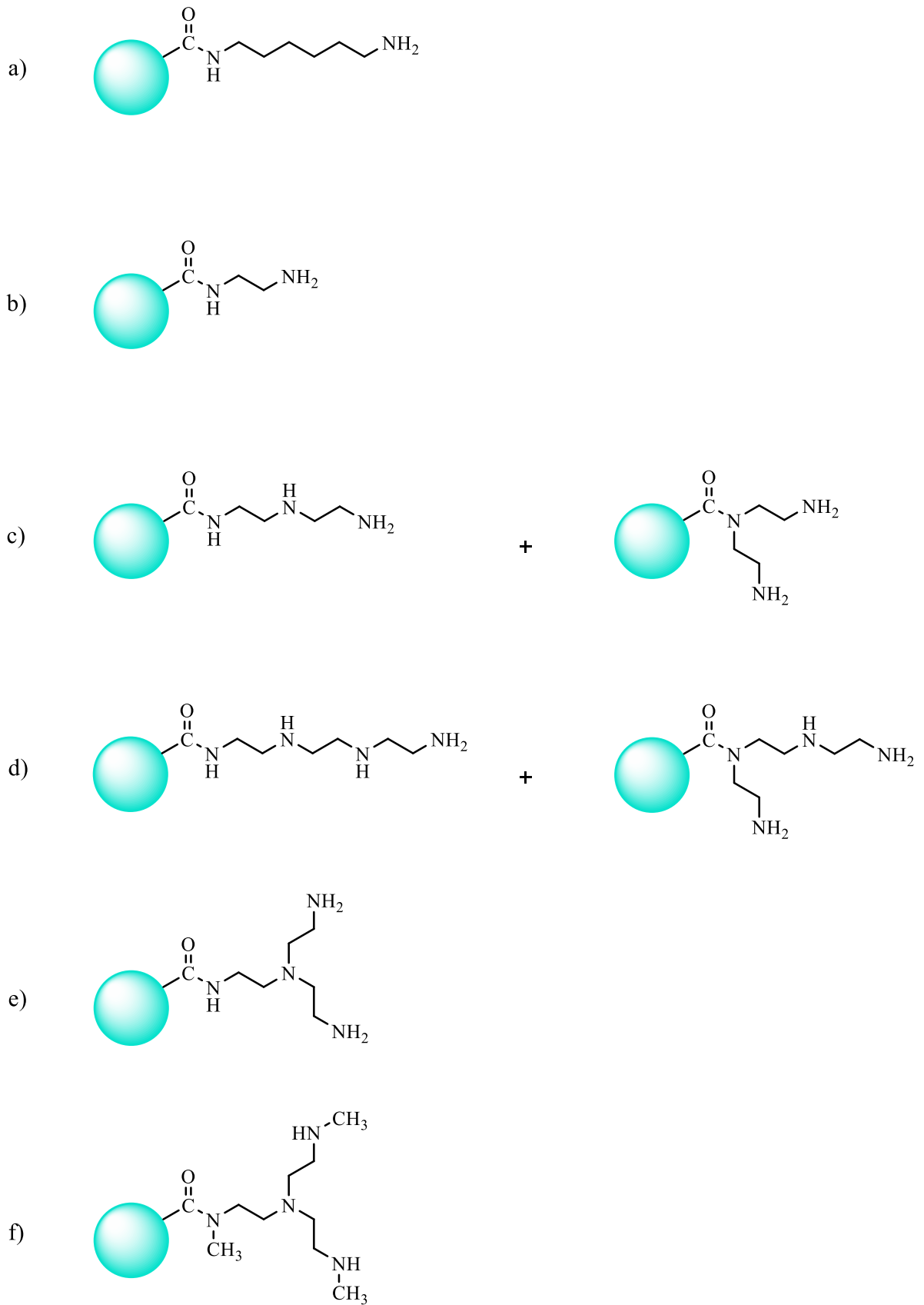


Fig. 4: The scheme of amide-amine functionalisation.

	The oligoamine used	The material's name
a)	hexamethylenediamine	C-HMD
b)	ethylenediamine	C-ED
c)	diethylenetriamine	C-DET
d)	triethylenetetramine	C-TET
e)	tris(2-aminoethyl)amine	C-TAE
f)	tris[2-(methylamino)ethyl]amine	C-TMAE

Tab. 5: The list of the oligoamines used for functionalisation and the corresponding materials prepared.



*Fig. 5: Structures of particular amide-amine functional groups grafted on CNPs.*

There are many methods to oxidise carbon materials, using e.g. O<sub>2</sub> or O<sub>3</sub> atmosphere, hydrogen peroxide, nitric acid or ammonium persulfate (Gómez-Serrano et al., 1994; Jaramillo et al., 2010; Guedidi et al., 2013). However, for the purpose of this work, a method leading mainly to formation of carboxylic groups was essential. Wet methods using HNO<sub>3</sub> and (NH<sub>4</sub>)<sub>2</sub>S<sub>2</sub>O<sub>8</sub> have been proved to work this way (Haydar et al., 2003; Lemus-Yegres et al., 2007). As the method using (NH<sub>4</sub>)<sub>2</sub>S<sub>2</sub>O<sub>8</sub> described in (Lemus-Yegres et al., 2007) was considered well reproducible and most straightforward, it was selected as the starting step of the functionalisation procedure.

Another step, i. e. conversion of the carboxylic groups into chlorides, was performed via nucleophilic substitution, resp. addition/elimination, using thionyl chloride (Fig. 6). As the carboxylic acid attacks thionyl chloride, a chloride ion leaves, resulting in the formation of oxonium ion, which is activated towards nucleophilic attack. The oxonium ion is then attacked by chloride ion, and a tetrahedral intermediate chlorosulfite is formed. Chlorosulfite then collapses, losing sulphur dioxide and chloride ion, ending up as a protonated acyl chloride. The hydrogen proton can be removed by chloride ion, forming HCl and leaving acyl chloride.

The advantage of using thionyl chloride is that the byproducts of this reaction are gaseous and can therefore be separated easily. The excess of thionyl chloride is removed by distillation.

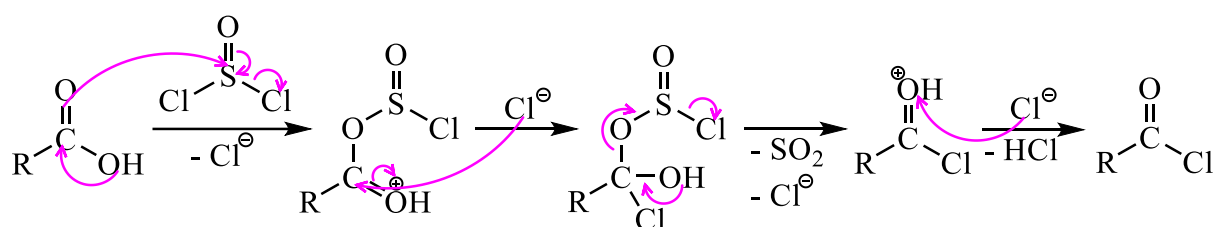


Fig. 6: The reaction scheme of the chlorination step.

Generally, the reaction of an acyl chloride with an amine proceeds in a similar addition/elimination manner (Fig. 7). At first, there is the nucleophilic attack of the lone electron pair on a nitrogen atom of the amine on the partially positive carbon atom of the acyl chloride. With the double bond reformed, the chloride ion is eliminated, which can then remove a hydrogen ion on nitrogen, forming HCl, immediately reacting with the excess of an amine to form alkylammonium chloride. However, a hydrogen can also be removed from the nitrogen directly by an amine.

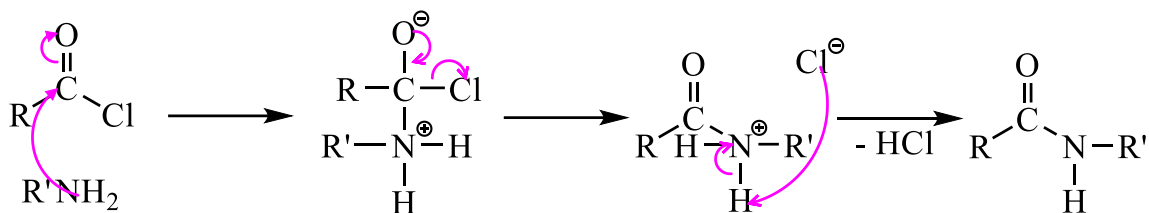


Fig. 7: The reaction scheme of the reaction of acyl chlorides with amines.

Due to the mechanism of such a reaction with oligoamines, it is advisable to use the oligoamines in a high excess, which facilitates the acylation on the primary amino group while suppressing the multiple acylation at the same time.

#### 4.1.1. Transmission electron microscopy

There were no significant visible differences in the structure of the particles; the functionalised CNPs, however, seem to be less sharp. The size of the CNPs can be estimated from the images, varying from 20 to 40 nm (Švorčík et al., 2014). Functionalisation improved wettability of the CNPs and therefore facilitated preparation of CNPs suspension in water.

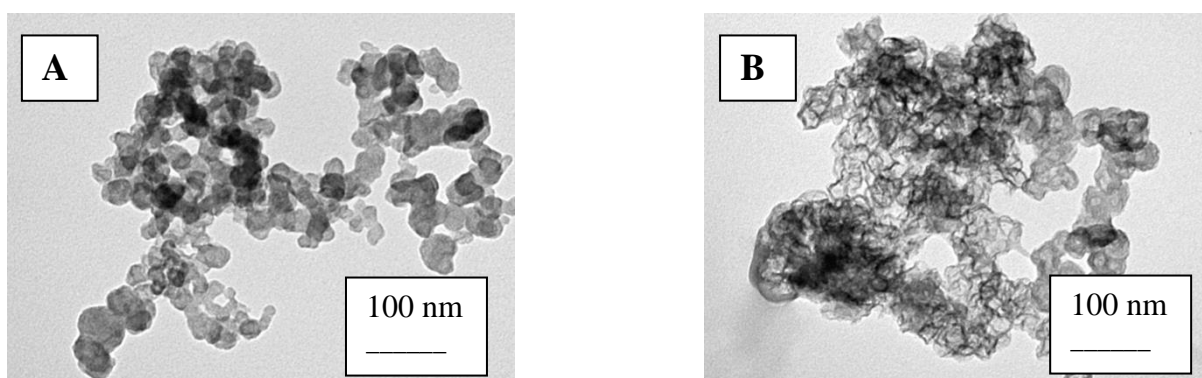


Fig. 8: TEM images of pristine (A) and functionalised (B) CNPs.

#### 4.1.2. X-ray photoelectron spectroscopy

The chemical composition of 6–8 atomic layers on CNP surface was determined, the results of which can be seen in Tab. 6. Nitrogen, chlorine and sulphur were introduced into the structures by functionalisation; an increase in nitrogen concentration on the CNP surface indicates a successful introduction of amino groups onto the CNPs surface. Trace amounts of chlorine on the CNP surface are a result of an incomplete  $\text{-COCl}$  conversion during the functionalisation process.

	<b>Pristine C</b>	<b>C-ED</b>	<b>C-DET</b>	<b>C-TET</b>	<b>C-TAE</b>	<b>C-TMAE</b>
Element	<b>XPS [at. %]</b>					
<b>C (1s)</b>	89.30	77.06	73.49	78.67	66.37	80.17
<b>N (1s)</b>	-	7.12	10.73	7.44	12.93	4.38
<b>O (1s)</b>	10.70	11.30	14.81	10.90	17.53	12.31
<b>Cl (2p)</b>	-	2.00	0.57	1.77	2.02	1.31
<b>S (2p)</b>	-	2.52	0.40	1.22	1.15	1.83

*Tab. 6: Results of XPS measurements of atomic concentrations of C(1s), N(1s), O(1s), Cl(2p) and S(2p) for pristine and functionalised CNPs (ethylenediamine, C-ED; diethylenetriamine, C-DET; triethylenetetramine, C-TET; tris(2-aminoethyl)amine, C-TAE; tris[2-(methylamino)ethyl]amine, C-TMAE).*

In the case of C-ED, the results might indicate that this least branched and shortest oligoamine may mostly be positioned in pores of the CNPs.

In the case of acylation of primary amino groups of DET and TET, the linear structures on C-DET and C-TET may also be partially positioned in the pores of CNPs. However, in the case of acylation of secondary amino groups, which is much less likely, the more branched structures shall rather be located on the very surface.

As for the high amount of nitrogen in the case of C-TAE, it can be assumed that these results may have stemmed from the combination of three primary amino groups, which positively influenced the process of acylation, and the overall higher weight ratio of N/C in this branched oligoamine.

On the other hand, as it had been expected, the reaction did not proceed well with the secondary amino groups of the most branched TMAE. The weight ratio of N/C in TMAE was also lower in comparison to the other oligoamines used. The combination of these features resulted in the lowest amount of nitrogen on the surface of C-TMAE.

The lower amounts of nitrogen on C-TET and C-TMAE surfaces correspond with the results of organic elemental analysis (see Tab.8).

To observe the differences between the composition on the very surface and of the lower layers, the following experiment was performed using CNPs functionalised with triethylene tetramine (Švorčík et al., 2014): the analysis was first carried out without Ar<sup>+</sup> ion etching and then after 5 min of Ar<sup>+</sup> ion etching (ions energy 5 keV), as 5 min etching should remove a few nanometres thick surface layer. After ion etching, the concentration of both nitrogen and oxygen decreased by 4.9 % and 10.6 % respectively, which confirms that the functionalisation took place mainly on the very surface of the CNPs (Tab. 7).

	<b>Element atomic concentrations [at. %]</b>					
	<b>Etching time [min]</b>					
	<b>C (1s)</b>		<b>O (1s)</b>		<b>N (1s)</b>	
	<b>0</b>	<b>5</b>	<b>0</b>	<b>5</b>	<b>0</b>	<b>5</b>
<b>Pristine CNPs</b>	97.8	98.5	3.2	1.5	-	-
<b>C-TET</b>	75.5	91.0	15.0	4.4	9.5	4.6

*Tab. 7: Results of XPS measurements of atomic concentrations of C(1s), O(1s) and N(1s) for pristine and CNPs functionalised with triethylenetetramine (C-TET) without and after 5 min Ar<sup>+</sup> ion etching.*

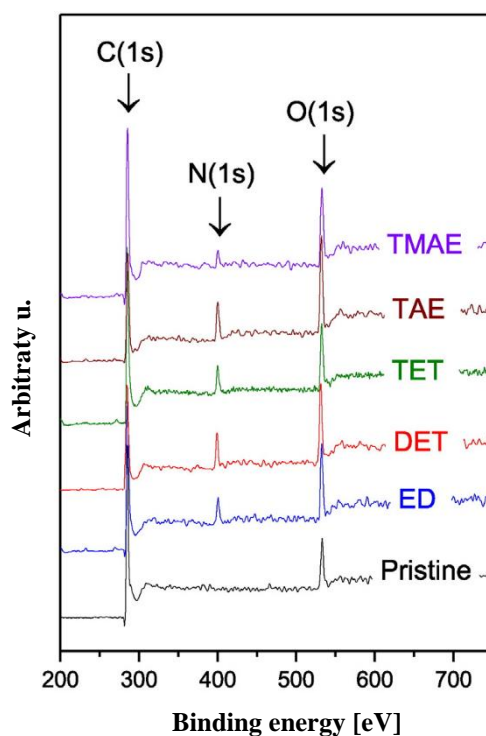


Fig. 9: XPS spectra of the pristine (pristine C) and functionalised CNPs (ethylenediamine, ED; diethylenetriamine, DET; triethylenetetramine, TET; tris(2-aminoethyl)amine, TAE; tris[2-(methylamino)ethyl]amine, TMAE).

#### 4.1.3. Organic elementary analysis

The results of OEA can be seen in Tab. 8. As it has already been mentioned, nitrogen and sulphur were introduced into the structures by functionalisation. The lower amount of nitrogen in the functionalised CNPs structures of C-TET and C-TMAE suggest that the amines in question may be bonded in lower amounts due to their three-dimensional arrangements (Žáková et al., 2016) and secondary amino groups.

	<b>Pristine C</b>	<b>C-ED</b>	<b>C-DET</b>	<b>C-TET</b>	<b>C-TAE</b>	<b>C-TMAE</b>
Element	<b>OEA [wt. %]</b>					
<b>C</b>	77.76	58.90	56.65	67.74	58.50	64.44
<b>N</b>	-	11.31	11.33	5.67	11.82	6.01
<b>S</b>	-	0.72	0.74	1.79	0.73	1.32
<b>H</b>	2.55	4.37	4.61	3.69	5.02	4.42

*Tab. 8: Results of OEA of the pristine (pristine C) and functionalised CNPs (ethylenediamine, C-ED; diethylenetriamine, C-DET; triethylenetetramine, C-TET; tris(2-aminoethyl)amine, C-TAE; tris[2-(methylamino)ethyl]amine, C-TMAE).*

After a few successfully functionalised batches, some new batches seemed to have slightly different properties, which caused problems with grafting the functionalised CNPs on plasma treated polymer surfaces (see chapter 4.2.). The results of OEA showed that such batches contained cca twice as much nitrogen in comparison to the original nitrogen content (which was about 82 wt. %). After a thorough evaluation of the whole process, the oxidation step was considered the most probable cause.

	<b>C</b>	<b>S</b>	<b>H</b>	<b>N</b>
Sample	<b>OEA [wt. %]</b>			
<b>original</b>	81.72	-	3.006	-
<b>2 hours uncooled</b>	73.84	0.577	2.616	-
<b>4 hours uncooled</b>	71.53	0.777	2.631	-
<b>8 hours uncooled</b>	71.03	0.769	2.725	-
<b>12 hours uncooled</b>	70.85	0.680	2.794	-
<b>24 hours uncooled</b>	68.07	0.454	2.735	-
<b>48 hours uncooled</b>	67.22	0.394	2.834	-
<b>30 minutes cooled</b>	77.83	-	2.867	-
<b>60 minutes cooled</b>	76.89	-	2.935	-
<b>90 minutes cooled</b>	77.67	-	2.951	-

*Tab. 9: Results of OEA of newly oxidised CNP samples.*

When checking the composition of newly oxidised samples (named 24 hours uncooled) via OEA, it was found that the new samples were ‘overoxidised’ in comparison to the original batches. The procedure was therefore optimised using various times of oxidation and cooling. Examples of the OEA results can be seen in Tab. 9, the adjusted procedure is described later in chapter 5.1.3.

It also seemed that  $(\text{NH}_4)_2\text{S}_2\text{O}_8$  used for oxidation of the first batches might not have been as strong an oxidation agent (possibly e.g. due to storage conditions). Nevertheless, the procedure was successfully optimised, using always a freshly opened batch of  $(\text{NH}_4)_2\text{S}_2\text{O}_8$  and cooling. The more oxidised a sample, the lower the carbon content in the sample was, as oxidation introduced more oxygen into the structures (mainly carboxylic groups, as it has been discussed earlier in chapter 4.1.). Surface area and pore size distribution changes are discussed in the following chapter.

#### **4.1.4. Surface area, pore size distribution and pore volume analysis**

Because oxidation may result in changes in the porous structure of the material, which can then affect its behaviour (Jaramillo et al., 2010), PSDs of pristine, oxidised and functionalised CNPs were measured and can be seen in Fig. 10. As mentioned before in chapter 4.1., the adsorption-desorption isotherms obtained from nitrogen adsorption measurements represent Type H2 hysteresis loop, which is typical for micro-mesoporous carbon materials (Thommes et al., 2015). The pore size distribution (PSD) was calculated using Density Functional Theory (DFT), for which the slit/cylindrical pore model was chosen as the most suitable.

As can be seen in Fig. 10, oxidation did not significantly change the pore size distribution. However, due to oxidation, the surface area decreased by  $199 \text{ m}^2 \text{ g}^{-1}$ . A noticeable change in both PSD and surface area can be observed for C-TET, the surface area of which decreased by more than  $1130 \text{ m}^2 \text{ g}^{-1}$  in comparison to pristine C. The PSD of C-TET followed the trend similar to pristine and oxidised CNPs, nevertheless, a prominent decrease in microporosity and pores with diametres above 8 nm can be seen. Slit/cylindrical DFT pore model fitted well to all three samples in Fig. 10.

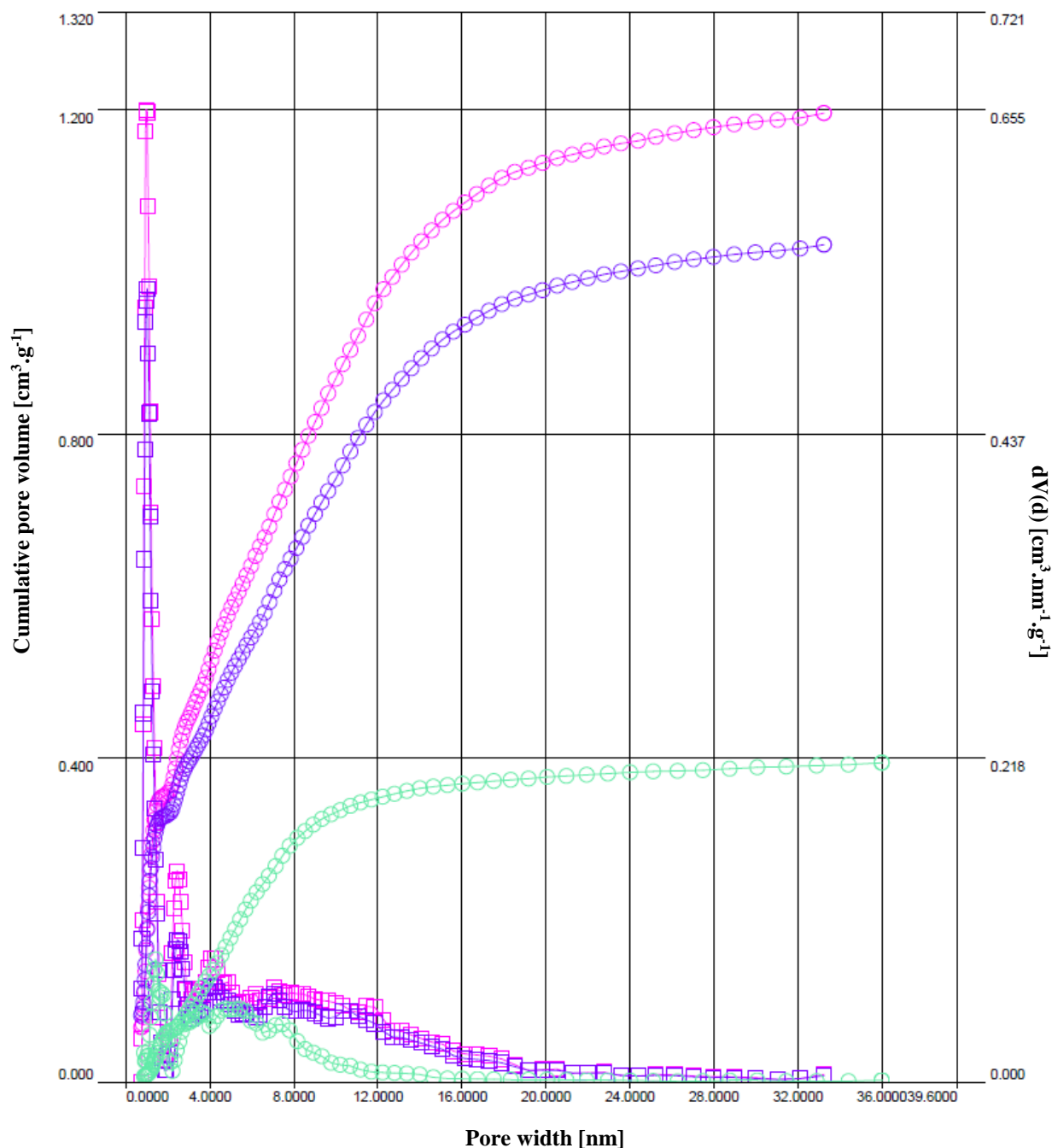


Fig. 10: The pore size distribution curves of pristine CNPs (magenta), oxidised CNPs (violet) and C-TET (green).

Results of surface area and pore volume analyses of the pristine and functionalised CNPs can be seen in Tab. 10. Functionalised samples were degassed at 150 °C for several hours, then adsorption and desorption isotherms were measured with nitrogen. Five points Brunauer–Emmett–Teller (BET) analysis was applied for the total surface area determination and 40 points Barrett–Joyner–Halenda (BJH) model for pore volume (Žáková et al., 2016). The functionalisation caused a distinct decrease in the total surface area from 1518 m<sup>2</sup> g<sup>-1</sup> (for

unmodified CNPs), which indicates the coverage of the surfaces by the grafted amines. In addition, the pore volume decrease confirmed the amines grafted onto CNPs surface and into their pores.

<b>Pristine C</b>	<b>ED</b>	<b>DET</b>	<b>TET</b>	<b>TAE</b>	<b>TMAE</b>
<b>Surface area [m<sup>2</sup> g<sup>-1</sup>]</b>					
1518	74.2	156.5	386.1	150.4	81.4
<b>Pore volume [cm<sup>3</sup> g<sup>-1</sup>]</b>					
0.602	0.154	0.264	0.420	0.349	0.169

*Tab. 10: Results of surface area and pore volume analyses of the pristine (pristine C) and functionalised CNPs (ethylenediamine, ED; diethylenetriamine, DET; triethylenetetramine, TET; tris(2-aminoethyl)amine, TAE; tris[2-(methylamino)ethyl]amine, TMAE).*

#### 4.1.5. Electrokinetic analysis – zeta potential

Colloidal samples of CNPs (0.01 g) dispersed in KCl water solution (4 ml of 0.01 mol l<sup>-1</sup>) were tested by dynamic light scattering. The electrokinetic analysis, the results of which can be found in Tab. 11, also confirmed the successful grafting of amino-compounds onto the CNP surface. While the zeta potential of pristine CNPs of -10.5 mV is negative, zeta potential of all amino-grafted CNPs shifted to positive values. There is a good correlation between the amounts of amino-groups in grafted molecules and the shift of the surface charge to positive values (Žáková et al., 2016). It is known that the presence of amino groups on CNP surface results in zeta potential increase and shifting to the positive values (Reznickova et al., 2012).

<b>Pristine C</b>	<b>ED</b>	<b>DET</b>	<b>TET</b>	<b>TAE</b>	<b>TMAE</b>
<b>Zeta potential [mV]</b>					
-10.5	15.9	19.4	21.3	27.5	21.0

*Tab. 11: Results of electrokinetic analysis of the pristine (pristine C) and functionalised CNPs (ethylenediamine, ED; diethylenetriamine, DET; triethylenetetramine, TET; tris(2-aminoethyl)amine, TAE; tris[2-(methylamino)ethyl]amine, TMAE).*

#### 4.1.6. Differential scanning calorimetry

Differential scanning calorimetry was used to examine the thermal stability of the pristine and functionalised CNPs. The measurements were performed in a range of 25–1000 °C in oxygen at a flow rate of about 50 ml/min. The heating/cooling rate was 10 °C/min. DSC peak for the pristine CNPs at 445 °C is shifted to slightly higher temperatures for modified samples. This can be explained by a decrease in CNPs surface area during the treatment. Degradation/oxidation of amine groups starts above approx. 150 °C and the relevant parts of DSC curves differ depending on the amines used. In the case of pristine TET (not bonded with CNPs), complete degradation bellow 210 °C was observed (Silva et al., 2012). Our observation of a broad bump (see Fig. 11) with a tiny maximum at 250 °C for TET modified CNPs thus demonstrates chemical bonding of TET on CNPs (Žáková et al., 2016).

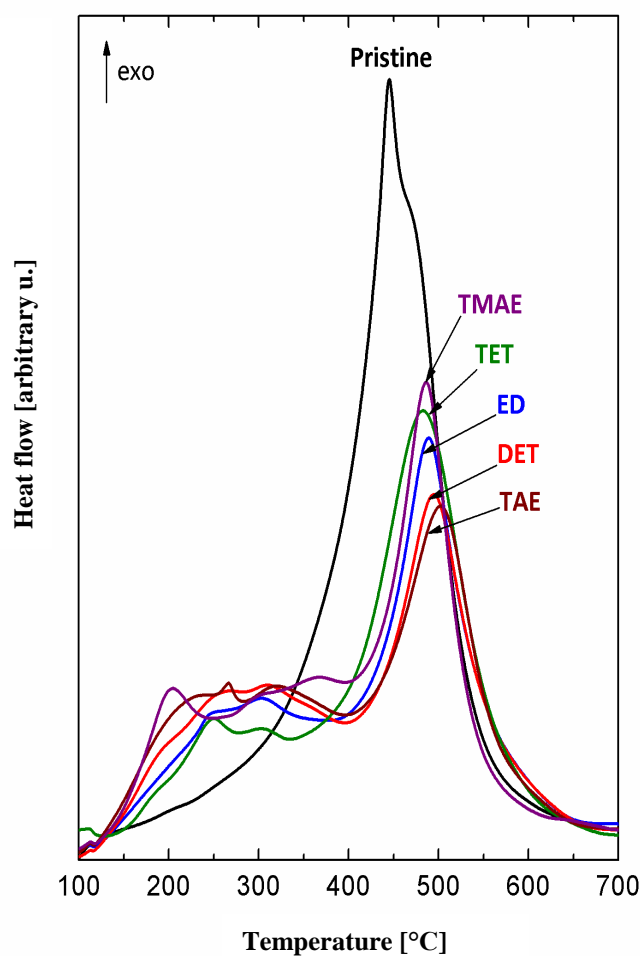


Fig. 11: DSC scans of the pristine (pristine C) and functionalised CNPs (ethylenediamine, ED; diethylenetriamine, DET; triethylenetetramine, TET; tris(2-aminoethyl)amine, TAE; tris[2-(methylamino)ethyl]amine, TMAE).

## 4.2. Grafting of the functionalised CNPs on polymer surfaces and their cytocompatibility testing

As this part was not the author's own work, the results will be described only briefly. The detailed information about the research can be found in the following articles: (Trostová et al., 2013, 833; Švorčík et al., 2014; Žáková et al., 2016). The scheme of the experiments is depicted in Fig. 12.

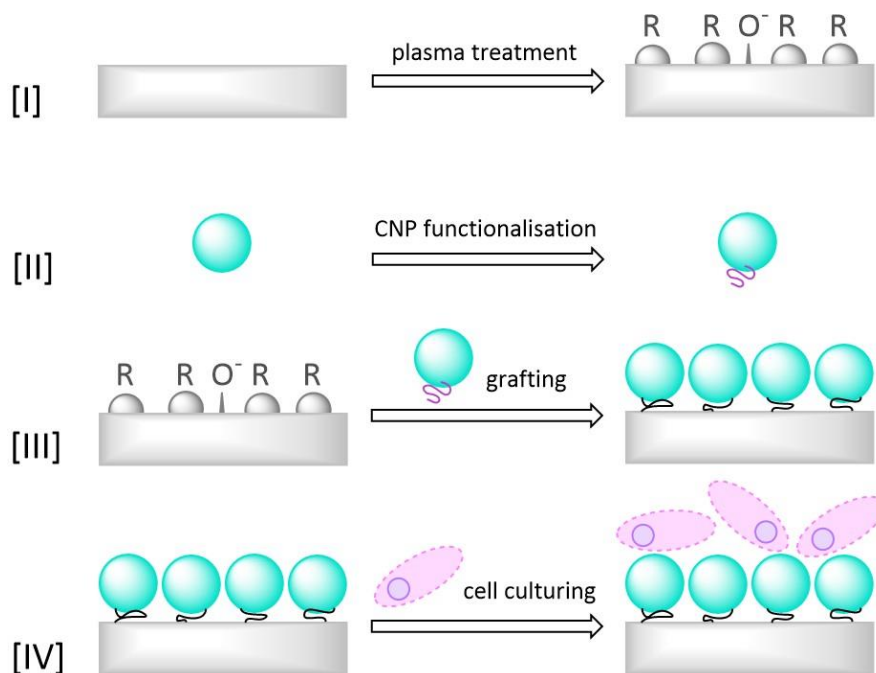


Fig. 12: The scheme of the experiments: [I] Ar plasma treatment of a polymer, [II] functionalisation of CNPs, [III] grafting of functionalised CNPs on the plasma treated polymer, [IV] cytocompatibility testing

The functionalised CNPs were chemically grafted on polyethylene terephthalate and high density polyethylene the surfaces of which had been treated with argon plasma. The chemical composition of the modified polymer surfaces was determined by Raman and X-ray photoelectron spectroscopies. Graphitic peaks attributed to CNPs could be observed in Raman spectra. The presence of nitrogen on the very surface of the materials was confirmed by means of angle resolved XPS.

Surface roughness and morphology of polymers grafted with CNPs was studied by atomic force microscopy, surface contact angle was measured by goniometry. AFM images showed that the

CNPs were spread relatively homogeneously on the polymer surface, however, they did not form a continuous coverage. As the functionalisation improved wettability of the CNPs surfaces, the wettability of the polymers grafted with functionalised CNPs also increased, which can be indicated from the increase in water contact angle.

Adhesion and proliferation of vascular smooth muscle cells on HDPE and PET surfaces grafted with functionalised CNPs were studied *in vitro*. Functionalised CNPs grafting on the plasma activated polymers had a positive effect on VSMCs adhesion and proliferation. In comparison with pristine, plasma treated or methanol etched surfaces there was a significant increment in the numbers of cultivated cells on the substrates grafted with CNPs. The viability of cells cultivated on all grafted types of functionalised CPs was extremely high. In all cases (except for the 1<sup>st</sup> day, on which the cells were still adapting to modified surface), the cell viability was above 95 %. However, there were no significant differences in the numbers of cultivated cells among the individual types of the grafted CNPs (Žáková et al., 2016). We can therefore assume that the structure of the amino chains did not play an important role in cell adhesion. Some deviations were caused by various parts of the samples being covered more densely.

To sum up this set of experiments, it can be stated that grafting PET and HDPE with amide-amine functionalised CNPs had positive effects on cytocompatibility of these polymers with VSMCs.

### **4.3. Nano-microfibrous Scaffolds Containing Carbon Particles**

Four types of nanofibrous scaffolds containing the aforementioned particles were prepared via sputtering CNPs into electrospun polycaprolactone (PCL) micro-nanofibres: three of them with three types of functionalised CNPs (C-ED, C-TAE and C-TMAE) and one with plain activated CNPs. First, a micro-nanofibrous layer was electrospun, on which the particles were sputtered and subsequently covered with another micro-nanofibrous layer.

#### **4.3.1. Surface area**

The surface areas of the scaffolds containing CNPs were determined from adsorption and desorption isotherms. Samples were degassed at 40 °C for 24 hours (not to alter the PCL fibres), then adsorption and desorption isotherms were measured with nitrogen or krypton adsorption

(Linde, 99.999% purity). Seven points BET analysis was applied for the total surface area determination.

Incorporation of CNPs caused a distinct increase in the total surface area from  $4.3 \text{ m}^2 \text{ g}^{-1}$  for pristine PCL nanofibres to  $15.9 \pm 3.5 \text{ m}^2 \text{ g}^{-1}$  for scaffolds containing the functionalised CNPs and  $235.8 \text{ m}^2 \text{ g}^{-1}$  for the scaffold containing the pristine CNPs (see Tab. 12). The surface area increments roughly correlate with the surface areas of the CNPs, except for sample PCL+CTAE. It can be assumed that there might have been a lower amount of the TAE functionalised CNPs, the scaffold might have been thicker (i.e. consisting mainly of PCL fibres) or that the particles were somehow covered with PCL, which could have blocked their accessible surface area. Although there was the same amount of CNPs sputtered into the PCL fibres during electrospinning, electrospinning itself is a highly sensitive process and every little, seemingly insignificant, change may result in noticeable differences in materials' properties.

<b>Particles</b>	<b>Surface area [<math>\text{m}^2 \text{ g}^{-1}</math>]</b>	<b>Scaffolds</b>	<b>Surface area [<math>\text{m}^2 \text{ g}^{-1}</math>]</b>
pristine C	1058.9	PCL+C	235.8
ED	74.2	PCL+CED	15.5
TAE	150.4	PCL+CTAE	12.9
TMAE	81.4	PCL+CTMAE	19.4
		PCL	4.3

*Tab. 12: The results of the surface area analyses of CNPs and PCL scaffolds (ethylenediamine, ED; tris(2-aminoethyl)amine, TAE; tris[2-(methylamino)ethyl]amine, TMAE).*

PCL scaffold exhibited Type II isotherm according to IUPAC classification (Fig.13, squared curve in cyan) (Thommes et al., 2015). Adding CNPs in the structure significantly altered the materials' properties and the hysteresis loops measured resembled H4 type, which is a composite of type I and II isotherms. Such hysteresis loops are typically found with micro-mesoporous carbon materials. PCL+C scaffold can clearly be distinguished from the others (Fig. 13, x curve in apricot), as the volume of adsorbed nitrogen is much higher due to the much larger specific surface area of the pristine CNPs, the surface of which had not been blocked by the amide-amine functions.

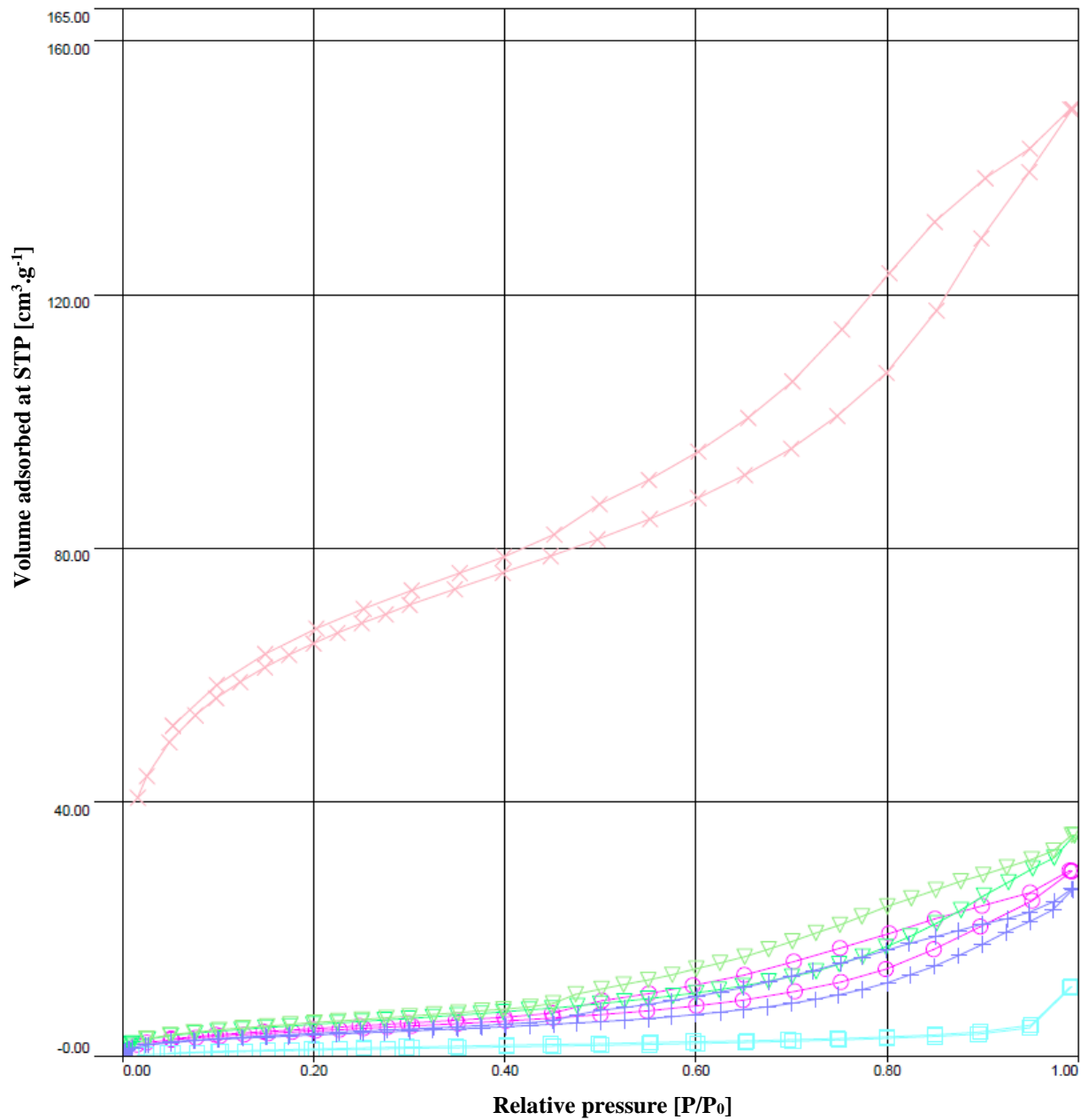


Fig. 13: Adsorption and desorption isotherms for all fibrous scaffolds: PCL (square, cyan), PCL+C (X, salmon), PCL+CTAE (cross, purple), PCL+CTMAE (triangle, green) and PCL+CED (circle, magenta).

### 4.3.2. Cytocompatibility with 3T3 mouse fibroblasts – MTT assay

The cell viability was estimated via measurements of absorbance of a formazane solution, as formazane is formed when yellow tetrazole 3-(4,5-dimethylthiazol-2-yl)-2,5-diphenyltetrazolium bromide is reduced to purple formazan in living cells by a mitochondrial reductase. As can be seen in Fig. 14, cell adhesion on the first day was similar for all scaffolds except for PCL+C. On day 3, however, pristine PCL scaffold started to overtake the others and on day 8, the absorbance measured for pristine PCL clearly indicated higher cell viability than for the other scaffolds. Nevertheless, the performance of the scaffolds with the functionalised CNPs was also quite good. The results for PCL+C are really poor in comparison to all the other scaffolds, which showed that functionalisation of CNPs had a positive effect on cell adhesion and proliferation. The differences among the individual types of oligoamines are noticeable but not too big. On day 14, pristine PCL was still by far the most suitable material for 3T3 mice fibroblasts while PCL+C seemed to have created the most hostile environment for them. PCL+CED and PCL+CTAE ended almost the same, with moderately good cell viability. Again, the functionalised CNPs exhibited better results than the pristine CNPs.

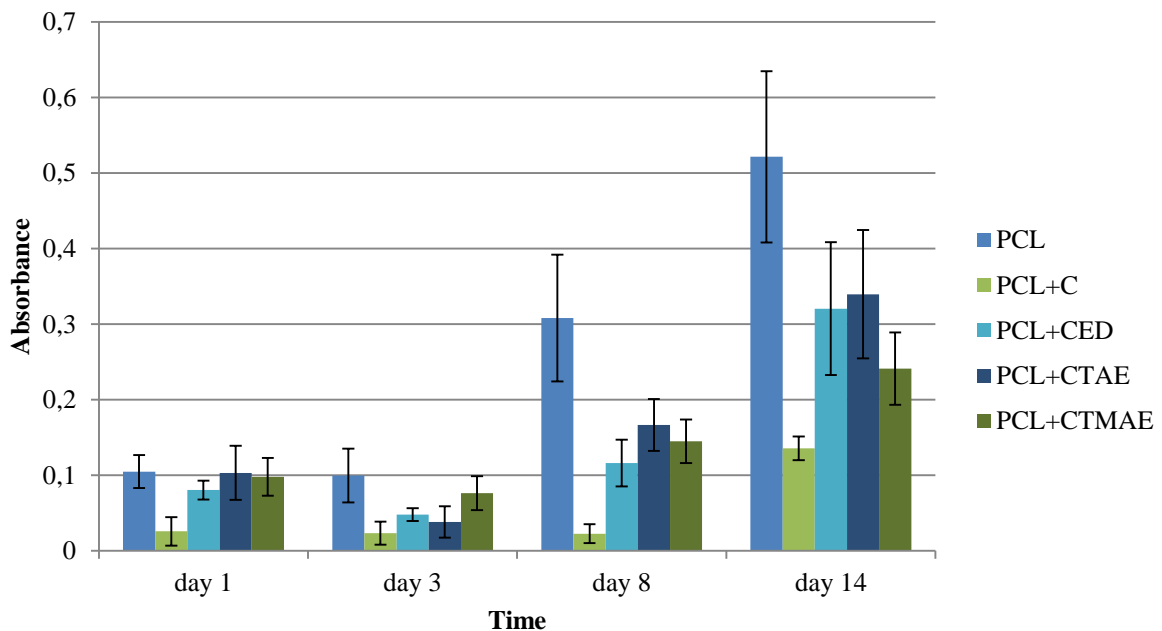


Fig. 14: Results of MTT assay sorted by days.

Fig. 15 shows the same data from another perspective, i. e. sorted by the scaffolds. It is therefore possible to see the different trends in cell viability for all the individual materials.

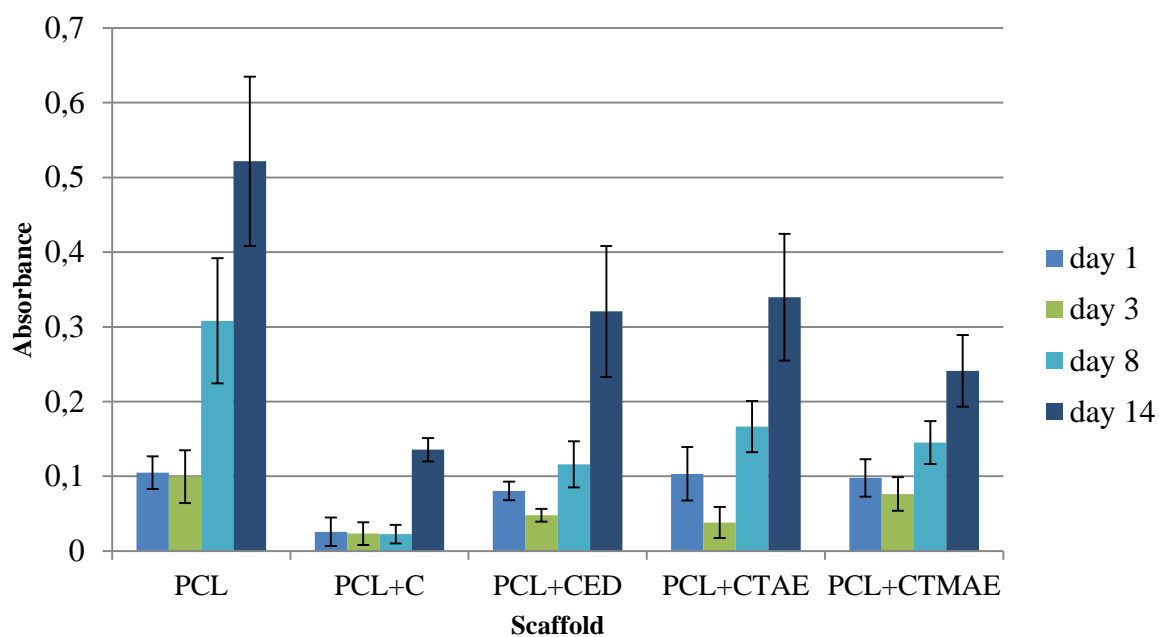
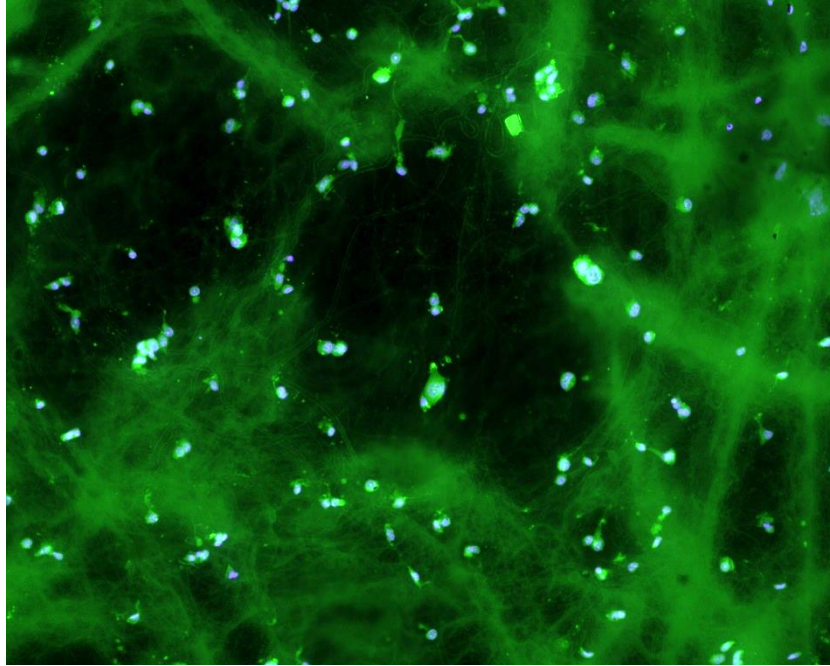


Fig. 15: Results of MTT assay sorted by types of scaffolds.

#### 4.3.2.1. Fluorescent microscopy

The samples were examined via fluorescent microscopy. As more fluorescent dyes were used (propidium iodide and DAPI in combination with phalloidin-FITC), the photographs were taken using UV, blue and green light filters (i. e. emissions at 420 nm, 515 nm and 610 nm, respectively). Generally, when staining one sample with more dyes that are excited at different wavelengths, more photographs are taken, each one using a different filter. They are then collated into one final photograph, in which the cells and their parts shall overlap. A photograph of a cell culture stained with DAPI with phalloidin-FITC can be seen in Fig. 16, which shows the pristine PCL nanofibrous scaffold.

The same procedure was applied to take FM photographs of the other scaffolds, i. e. those containing CNPs. However, the cells and their parts did not overlap in any of the cases. An example of such a phenomenon can be seen in Fig. 17.



*Fig. 16: Fluorescent microscopy photograph of PCL scaffold with 3T3 mouse fibroblasts on day 1, stained with DAPI (nuclei, blue) and phalloidin-FITC (actin fibres, green). Note: the larger green structures are fibres of the PCL scaffold.*

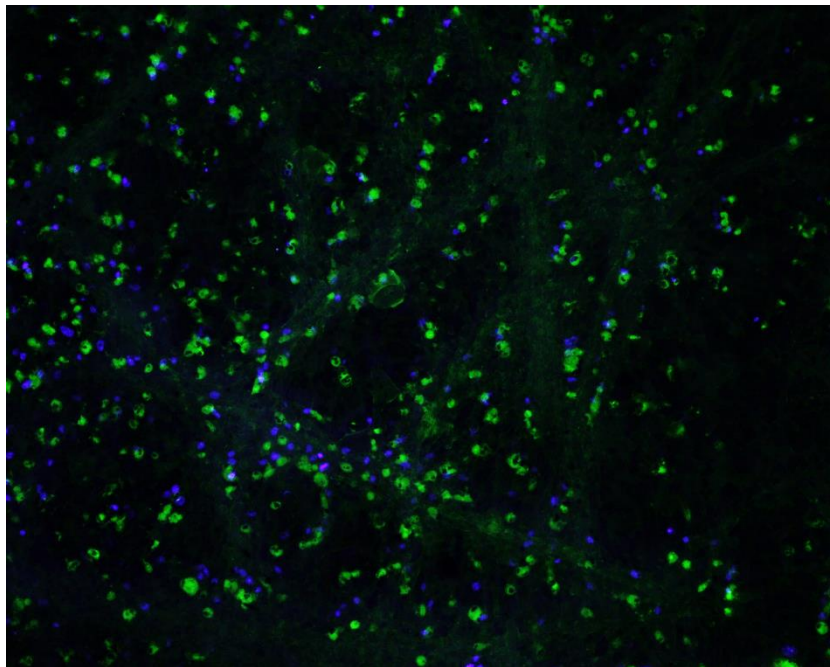


*Fig. 17: Fluorescent microscopy photograph of PCL+CTMAE scaffold with 3T3 mouse fibroblasts on day 1, stained with DAPI (nuclei, blue) and phalloidin-FITC (actin fibres, green); the cell nuclei do not overlap with the actin fibres.*

As the cells on the images were not *just* shifted in one direction but simply occupied different locations in random directions, it was clear that this phenomenon had not been caused by a careless manipulation, e. g. moving the samples. As the cells had already been dead, they could not have moved by themselves. The only logical explanation was that something must have happened with the material itself during taking the photographs, causing its morphological changes and thus changing the position of the cells.

It was then found that all scaffolds containing CNPs were sensitive to irradiation when using the blue and green filters. The morphological changes started immediately after the beginning of irradiation, leading to literally tearing the materials and holes formation within a few seconds. It happened to all the scaffolds containing CNPs, regardless the functionalisation. Irradiation with UV light did not have such an effect, which is not surprising considering the fact that carbon materials, especially carbon black, are widely used as UV stabilisers in polymer production.

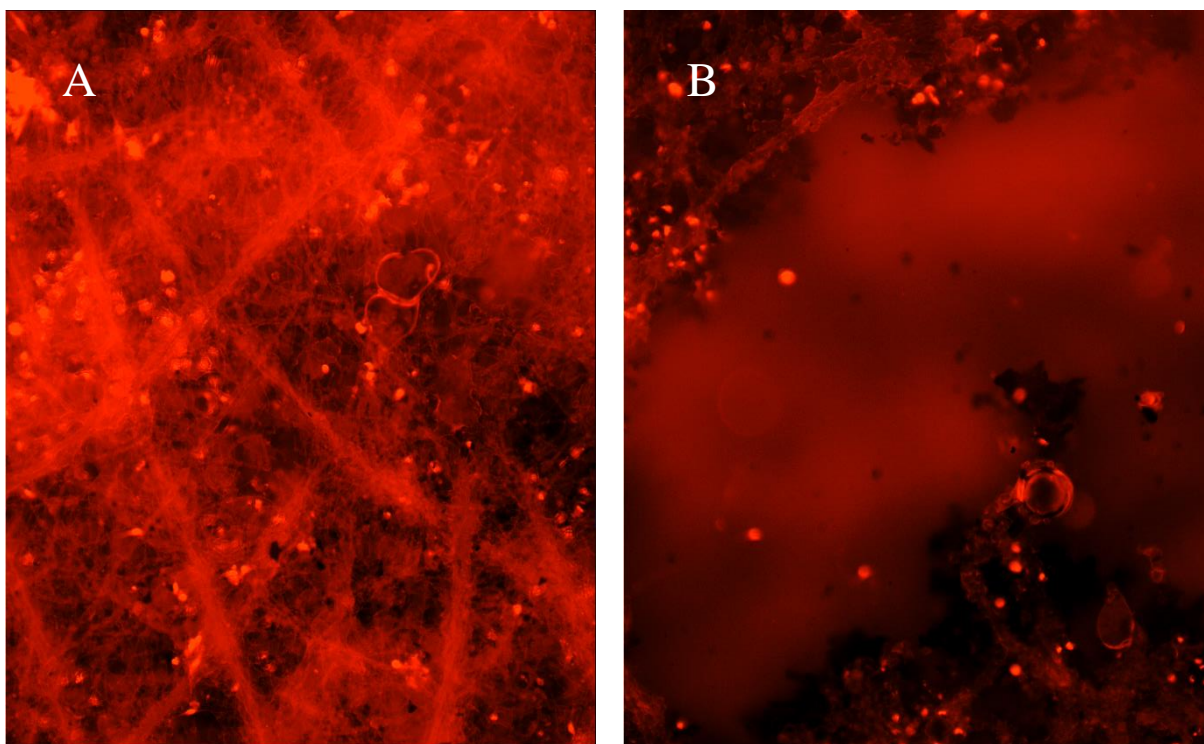


*Fig. 18: Fluorescent microscopy photographs of 3T3 mouse fibroblasts on PCL+CTMAE scaffold on day 8 during irradiation with the green filter after: A) 0 seconds, B) 15 seconds*

Pictures A and B in Fig. 18 were taken from a short film that had captured a structural degradation of PCL+CTMAE sample in real time. In the film, which can be found on a CD attached to this work, a few changes can be seen during the first seconds, while larger breaks occur in around the tenth second. They then spread wider, joining into one, which continues growing with time.

It was further examined whether the presence of the fluorescent dyes and the overall methodology of FM sample preparation affected the materials' selective light sensitivity. No such effects have been observed.

The CNPs containing scaffolds were also checked using Raman DXR microscope (laser at a wavelength of 532 nm, objective: 10x/0.25 BD). Using the 25  $\mu\text{m}$  pin hole aperture, even with the weakest power, i. e. 2 mW, it took only a few seconds to create holes in the substrates.

### 4.3.3. Scanning electron microscopy

Although all the scaffolds were prepared at the same conditions, the photographs revealed significant morphological differences among them. While the pristine PCL scaffold can be described as predominantly nanofibrous (Fig. 19), the other ones containing the CNPs were rather microfibrinous with some nanofibres present in the structures (Fig. 20). CNPs also aggregated into larger agglomerates during sputtering into the electrospun fibrous layers. The presence of the conductive CNPs might have altered the usual behaviour of the newly developing fibres during the electrospinning process, which is extremely sensitive to even the slightest, seemingly insignificant, alterations in conditions.

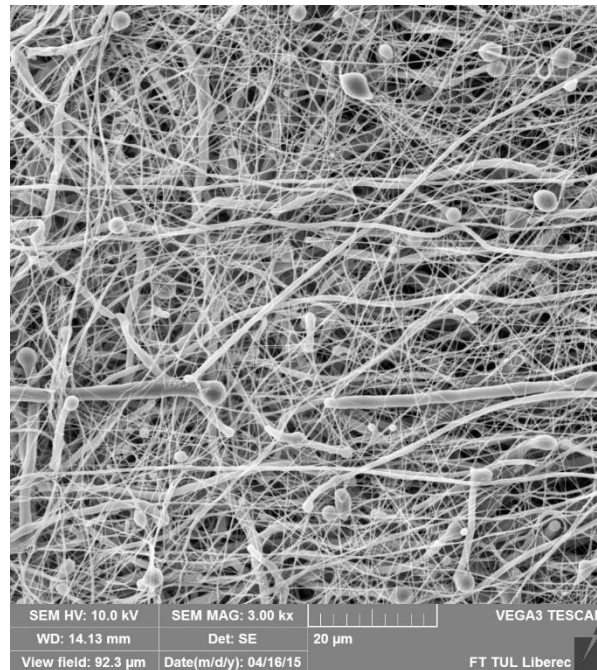


*Fig. 19: Scanning electron photograph of PCL nanofibrous scaffold.*

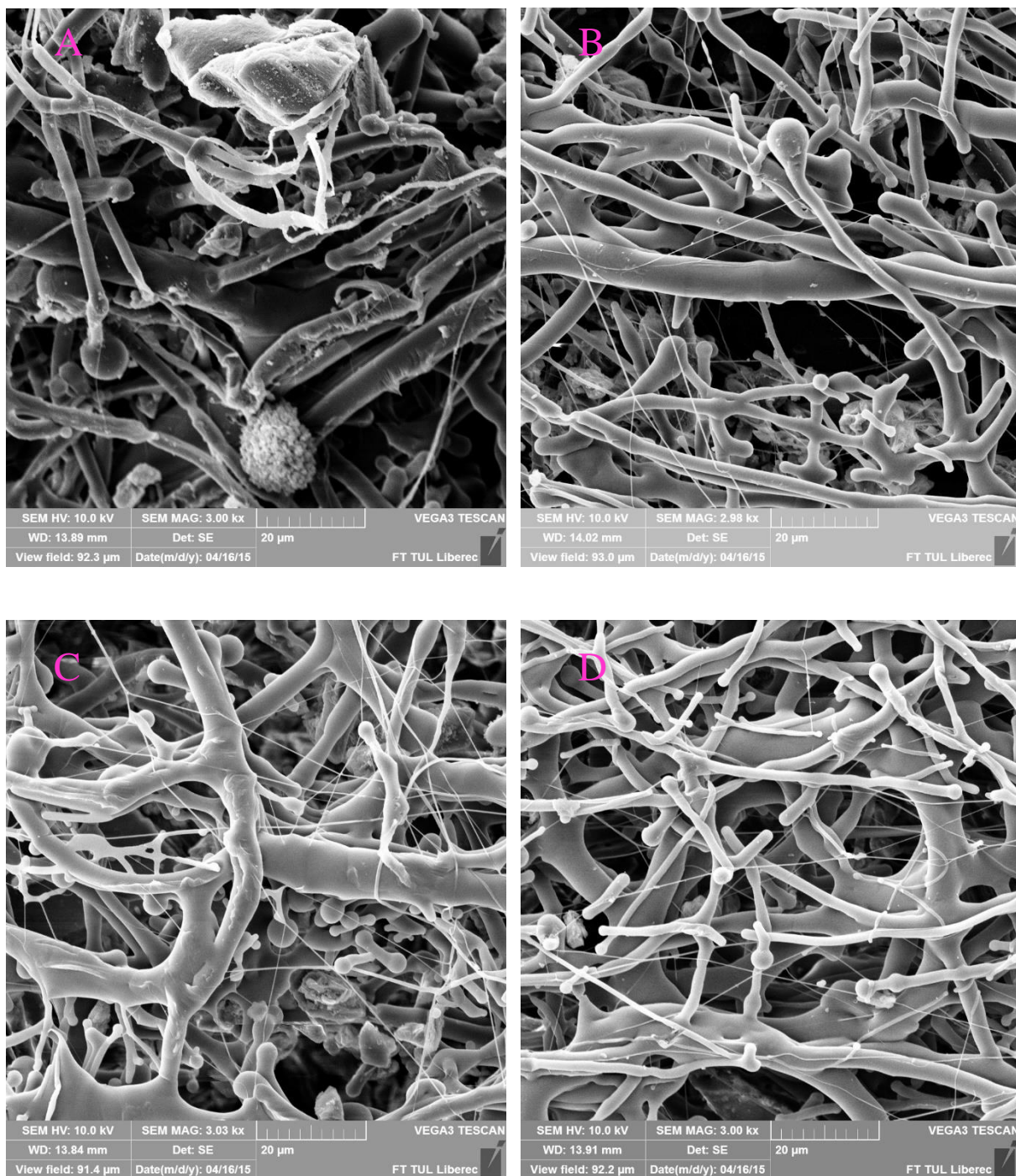


*Fig. 20: Scanning electron photographs of PCL micro-nanofibrous scaffolds containing CNPs: A) PCL+C, B) PCL+CED, C) PCL+CTAE, D) PCL+CTMAE.*

The structures of CNPs containing scaffolds after green light irradiation were also studied using SEM. The fibres seemed to have melted, which resulted in creating holes in the materials, as can be seen in Fig. 21.

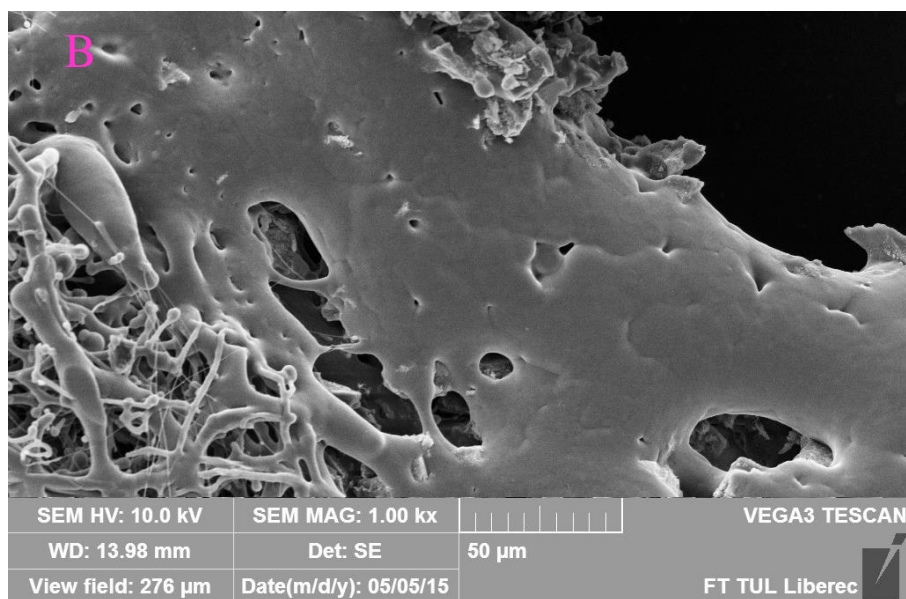
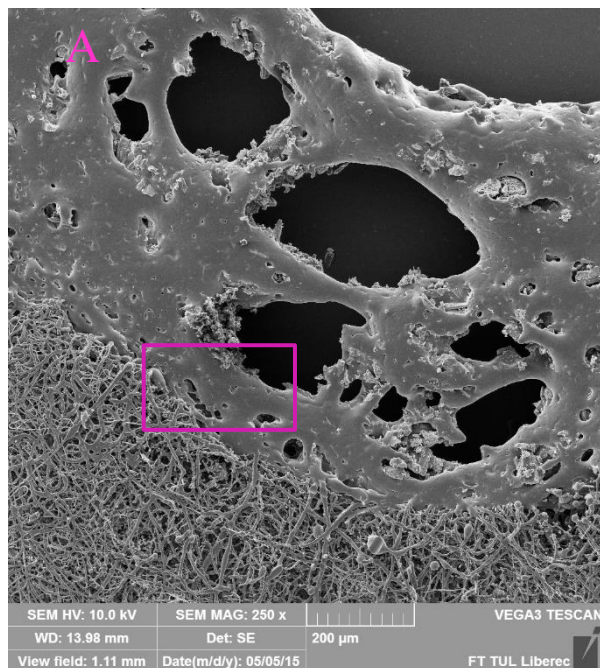


*Fig. 21: Scanning electron photographs of a melted part of PCL+CTAE scaffold (A) with the detail of the middle hole (B).*

#### **4.3.4. Thermogravimetric analysis**

Samples PCL and PCL-C were analysed via thermogravimetric analysis. Cca 10 mg of each material was heated to 650 °C at a rate of 10 °C/min under nitrogen flow at a rate of 60 ml/min. It was then kept at that temperature for 10 min. After that, the sample was exposed to synthetic air with the same flow rate at the same temperature for 15 minutes.

As can be seen in Fig. 22, the carbonisation residue is very low, approximately 0.2 weight %. It is therefore possible to assume that all combustible content from PCL-C at 650 °C may correspond with the amount of carbon present in the fibres. The amount of non-combustible residues for PCL and PCL-C are 1.64 % and 2.25 % respectively. The second significant peak in Fig. 23 can be assigned mainly to oxidation of CNPs, which might have formed cca 25 weight % of PCL-C sample.

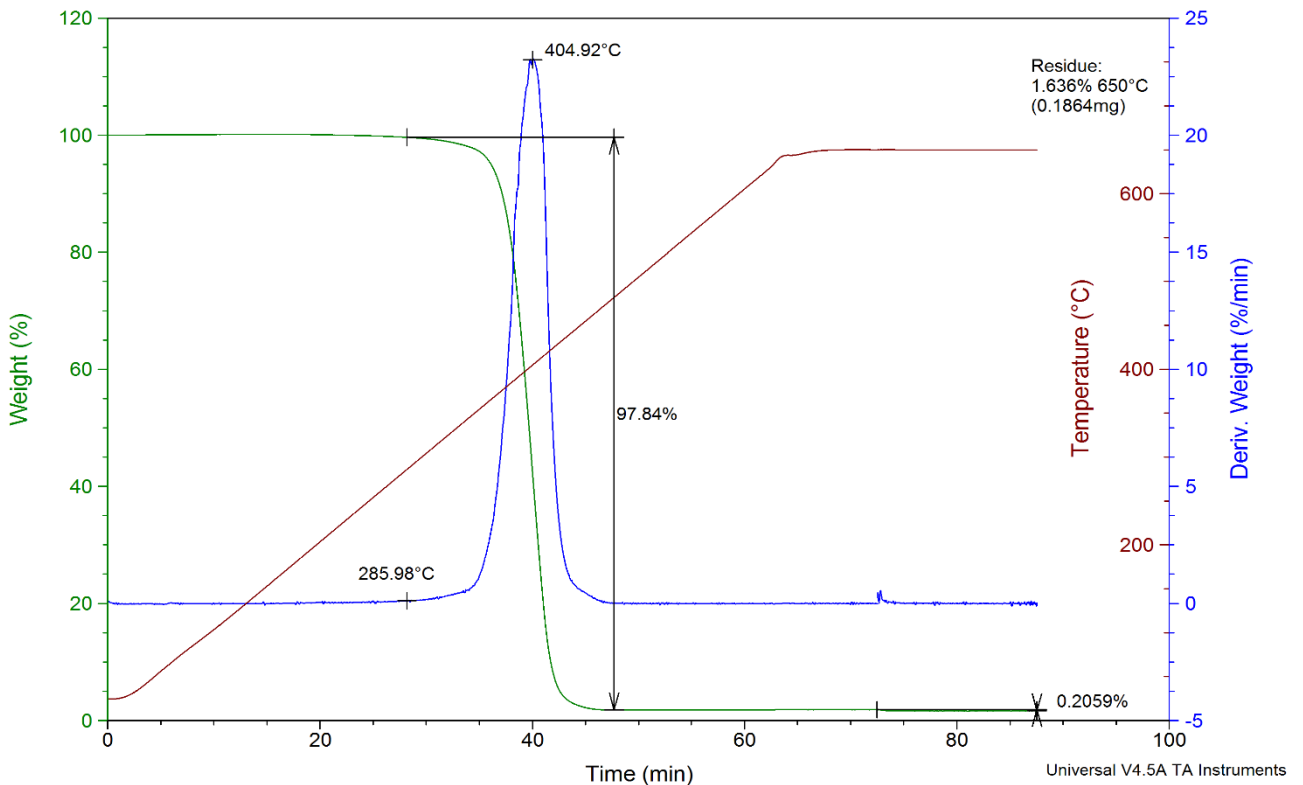


Fig. 22: The TGA plot for PCL nanofibrous scaffold.

Both materials started to decompose at similar temperatures, i.e. above 280 °C. However, the temperature at which the decomposition proceeded at the highest speed was cca 30 °C lower for PCL-C material. The presence of CNPs might facilitate decomposition of PCL in PCL-C in comparison to pristine PCL. However, the slower speed/higher temperature of PCL decomposition in PCL sample may be also influenced by the higher amount of PCL, which may have taken longer to heat and subsequently decompose.

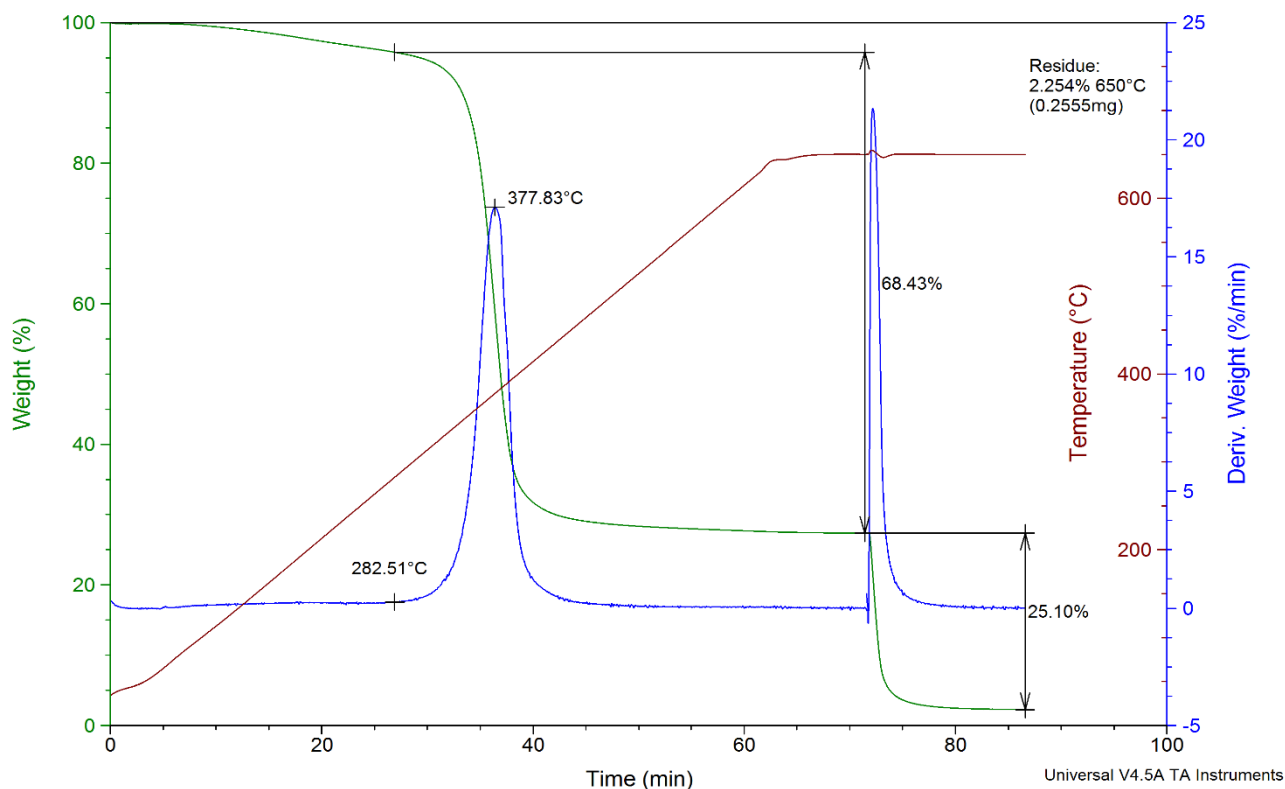


Fig. 23: The TGA plot for PCL+C micro-nanofibrous scaffold.

#### 4.3.5. Differential scanning calorimetry

DSC was used to examine the thermal behaviour of the pristine PCL s and PCL+C scaffolds. The measurements were performed in a range of -20–100 °C in nitrogen at a flow rate of 50 ml/min, the heating/cooling rate was 10 °C/min. The measurements were based on the Boersma and heat flow principles.

The first heating reflected structural properties of a sample, as well as some feature of its preparation, such as solvent residues or different conditions. The measurement showed a non-standard curve for the PCL+C sample; nevertheless, it can be said that a lower energy/temperature was needed to change the structure of PCL+C material in comparison to pristine PCL fibres.

#### 4.3.6. Antibacterial properties testing

Because the cell adhesion and viability of 3T3 mice fibroblasts was very poor on PCL+C sample, an idea whether this composite might exhibit antibacterial properties came into question. Therefore, a series of antibacterial testing experiments was carried out. The procedure

was similar to the one described in (Padil et al., 2015). The antibacterial activity of the plain PCL nanofibres and PCL-C scaffold was investigated by a qualitative method determining the zone of inhibition. Using the bacterial strains of Gram-negative *Escherichia coli* and *Pseudomonas aeruginosa* and Gram-positive *Staphylococcus aureus* and *Enterococcus faecalis*, no inhibition zones around the samples were detected. It can be therefore assumed that the nanofibrous scaffolds loaded with CNPs possess no antibacterial effect.

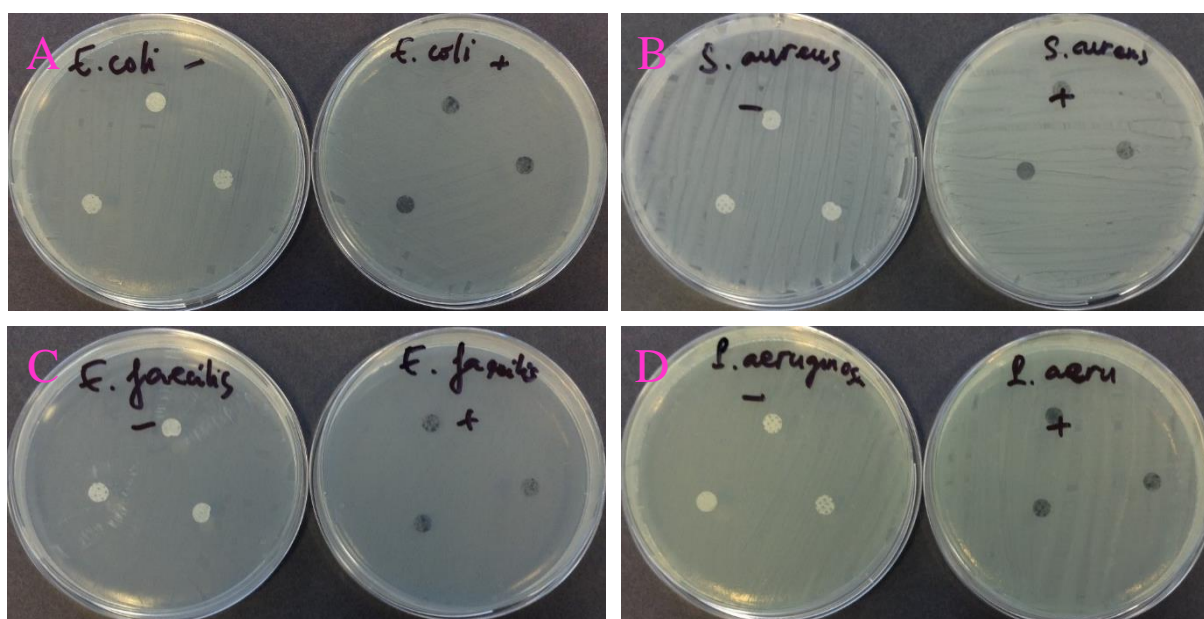


Fig. 24: Photographs of agar plates inoculated with A) *E. coli*, B) *S. Aureus*, C) *E. faecalis*, D) *S. Aeruginosa* with pristine PCL nanofibers (white, -) and PCL+C micro-nanofibrous scaffolds (black, +).

## **4.4. Templated Mesoporous Carbon Materials**

Several mesoporous carbon materials were prepared via hard- and soft-templating methods. The morphology of all the synthesised materials was studied using SEM.

The surface areas and pore size distributions were calculated using ASiQwin software based on adsorption-desorption isotherms. The pristine and functionalised samples were degassed at 300 °C or 150 °C, respectively, for at least 12 hours, after which nitrogen (Linde, 99.999% purity) 40-point adsorption and desorption isotherms were measured at the temperature of liquid nitrogen. 7-point BET analysis was applied for the total surface area determination. Various models of Density Functional Theory were used for the pore size distribution calculations. The previously widely used BJH model is no longer recommended for such applications in micro-mesoporous materials examination (Thommes et al., 2015), as it can significantly underestimate the pore size for narrow mesopores (for pore diameter smaller than 10 nm the pore size may be underestimated even by 30 %) (Lowell et al., 2012).

### **4.4.1. Hard-templated Materials**

#### **4.4.1.1. Ordered Mesoporous Carbon Materials Based on SBA-15 Silica Template**

Two types of mesoporous carbon materials were obtained using SBA-15 as their template: JAK017A, where no boric acid was used, and JAK017B with boric acid used as a pore expanding agent.

SEM photographs did not show any noticeable differences, as can be seen in Fig. 25. However, it can be seen that the materials are porous.

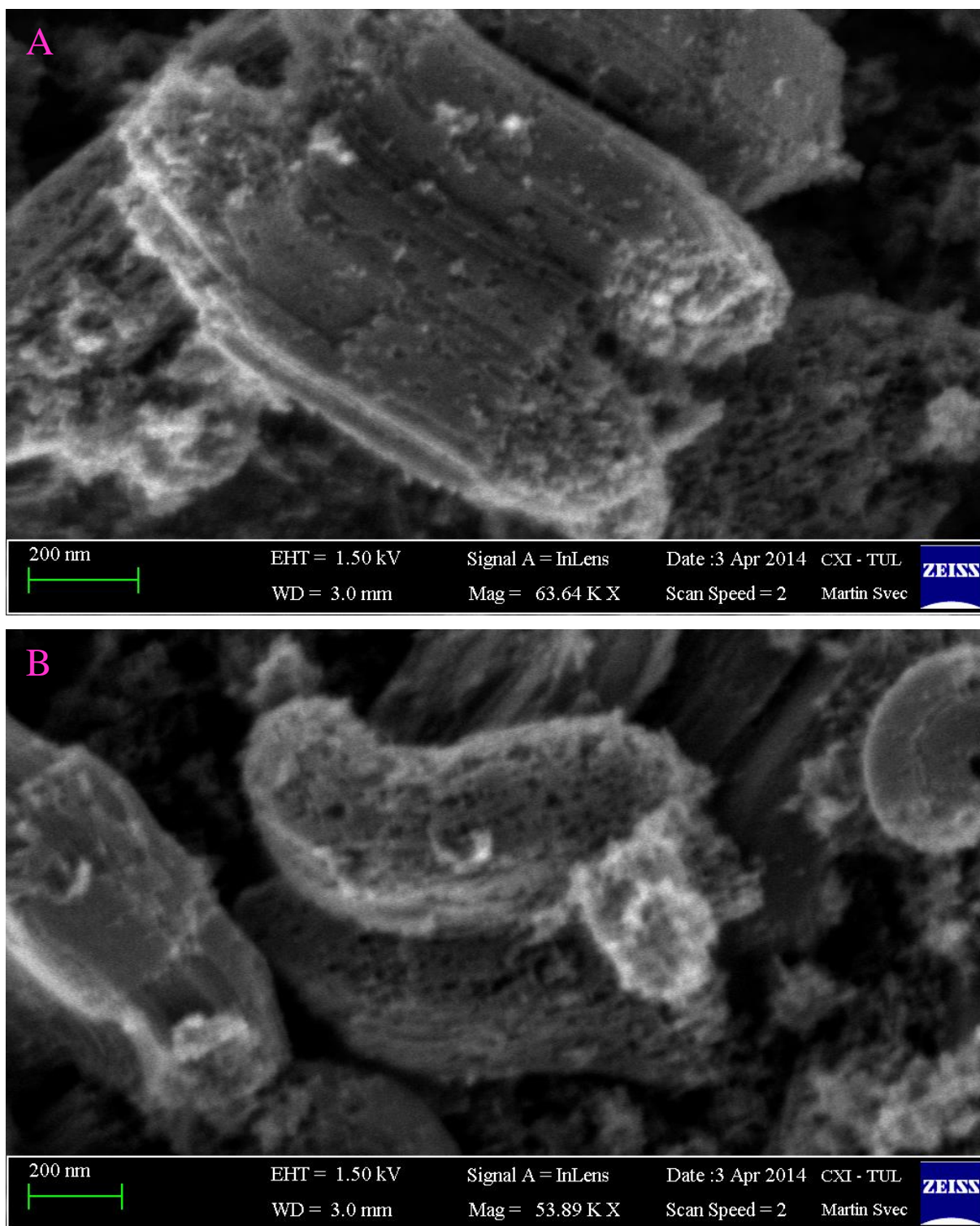


*Fig. 25: Scanning electron photographs of JAK017A (A) and JAK017B (B).*

Surface area and pore size distribution (PSD) analyses provided more information about the materials' morphology. While the surface area of SBA-15 was  $522.4 \text{ m}^2 \text{ g}^{-1}$ , the surface area of JAK017A and JAK017B were much higher,  $2234 \text{ m}^2 \text{ g}^{-1}$  and  $1927 \text{ m}^2 \text{ g}^{-1}$ , respectively. According to the PSD curve for SBA-15 (in pink), which can be seen in Fig.26, the structure of

the material is ordered, with the slightly wider peak at around 11 nm. The structure of JAK017A, represented by the blue curve, can also be considered ordered. There are two significant narrow peaks, the first one in the micropore region and the second one at around 6 nm. Nevertheless, some wider pores are also present in the structure.

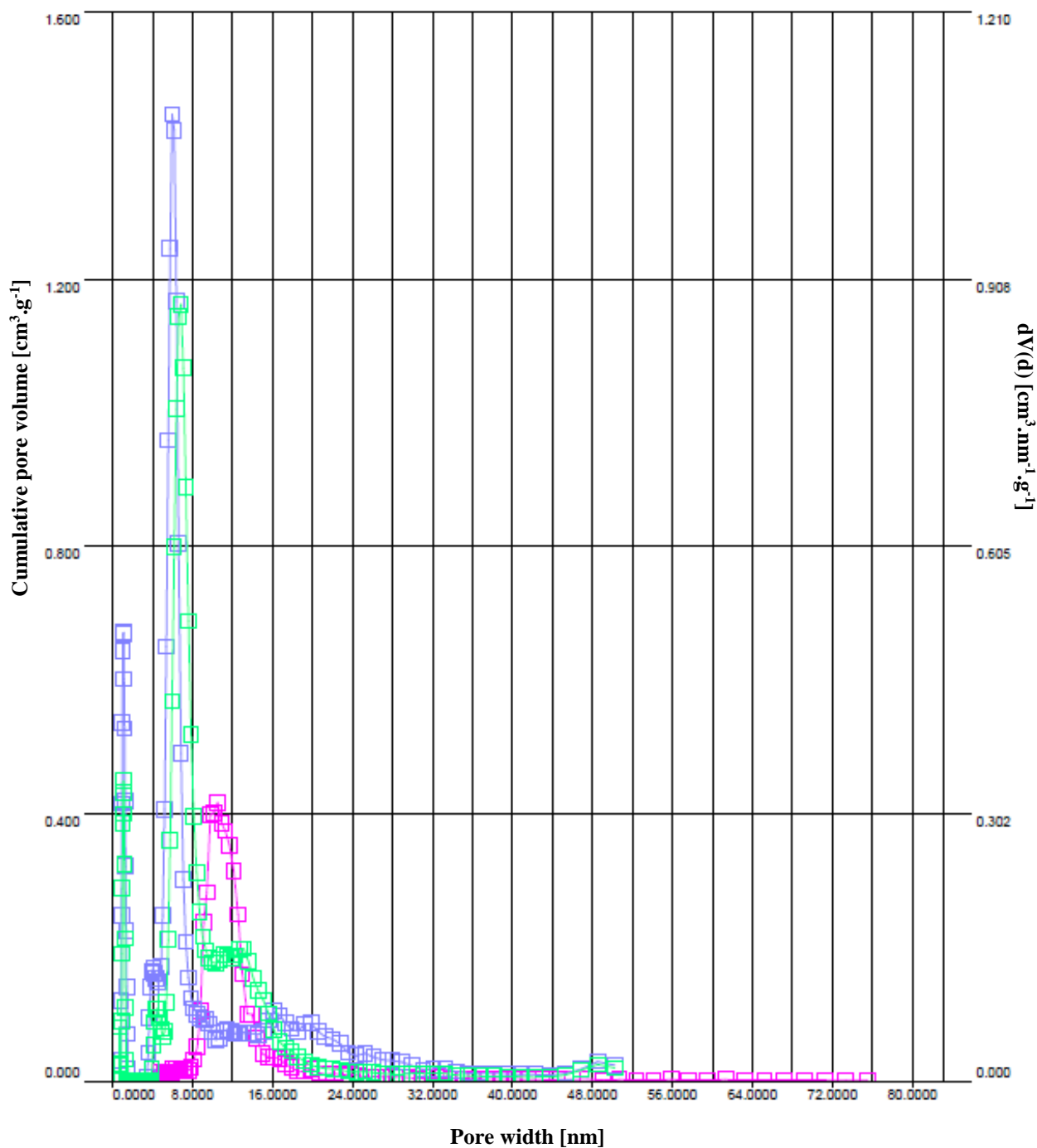


Fig. 26: The pore size distribution curves of SBA-15 (magenta), JAK017A (blue) and JAK017B (green).

The structure of JAK017B (green curve) is also ordered, with one sharp peak in the micropore region, the other at around 6.7 nm, and with some larger pores present. It can be therefore assumed that boric acid worked as the pore expanding agent, indeed. However, the structures are not as highly ordered as they were supposed to be according to (Li et al., 2011), and the average pore size of JAK017A is larger than that of a corresponding material mentioned in the study.

JAK017B was chosen for further functionalisation.

#### 4.4.1.2. Ordered Mesoporous Carbon Materials Based on Monodisperse Silica Nanospheres (JAK019)

According to SEM photographs in Fig. 27, the template looks monodisperse and the average diameter of the silica nanospheres was 60 nm. The pores in the carbon material, which are based on the nanospheres and can be seen in Fig. 28, are also spherical (which corresponds with the DFT model chosen for the assessment of PSD). However, the PSD is not narrow and the material cannot be considered ordered (Fig. 29).

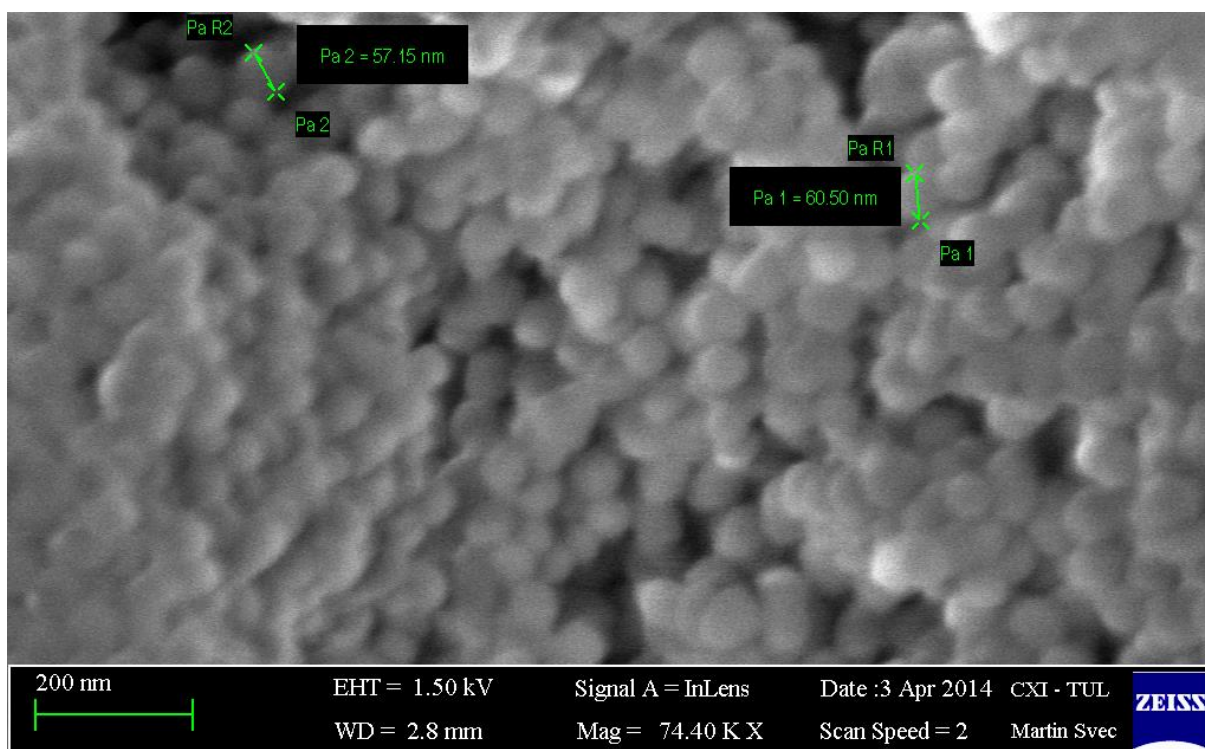
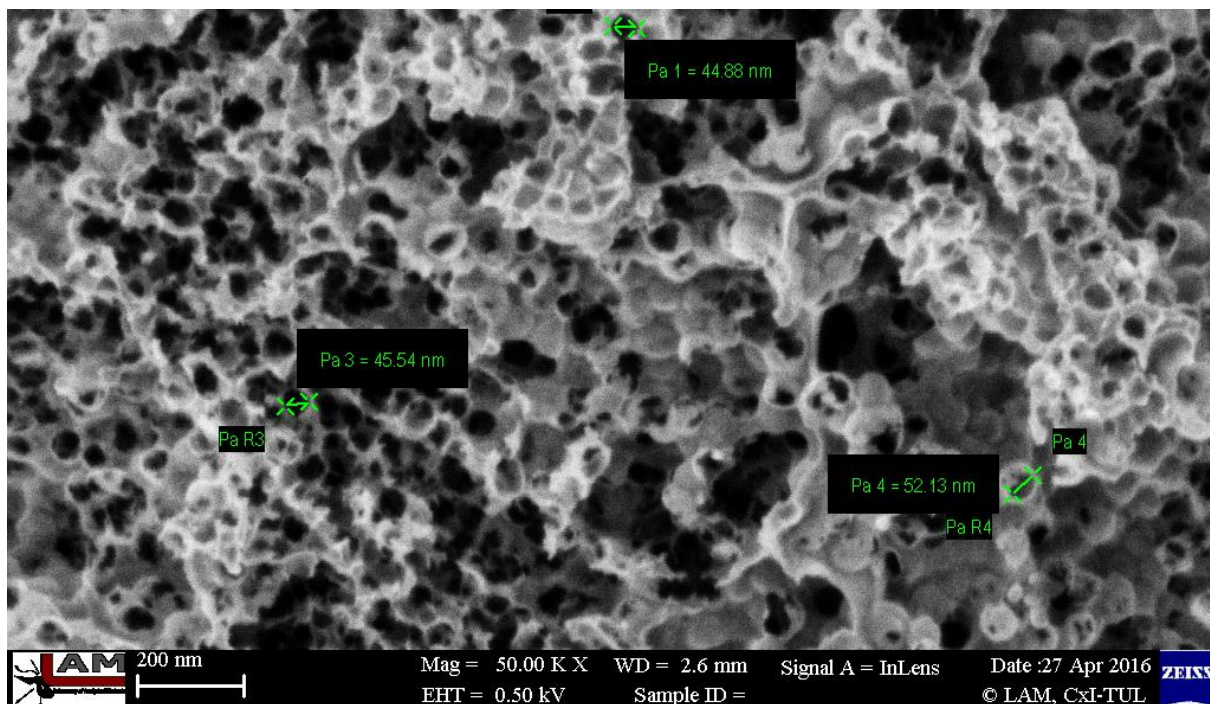


Fig. 27.: Scanning electron photograph of the silica template for JAK019.



*Fig. 28: Scanning electron photograph of JAK019.*

The surface area of the material is  $155 \text{ m}^2 \text{ g}^{-1}$ , which is not very high, taking into consideration that surface areas of carbon materials commonly exceed  $500 \text{ m}^2 \text{ g}^{-1}$ , and even values above  $1500 \text{ m}^2 \text{ g}^{-1}$  are not exceptionally high. It is also possible that some silica spheres might have stayed inside their carbon wrapping, which would have increased the weight of the sample and thus made the surface area seem smaller. According to the PSD curve in Fig. 29, micropores and mesopores are present. The overall shape of the hysteresis loop can be described as H3 type, which also suggests the presence of macropores that were not completely filled with pore condensate (Thommes et al., 2015). The presence of macropores would be in accordance with the SEM photograph in Fig. 28.

JAK019 was chosen for further functionalisation.

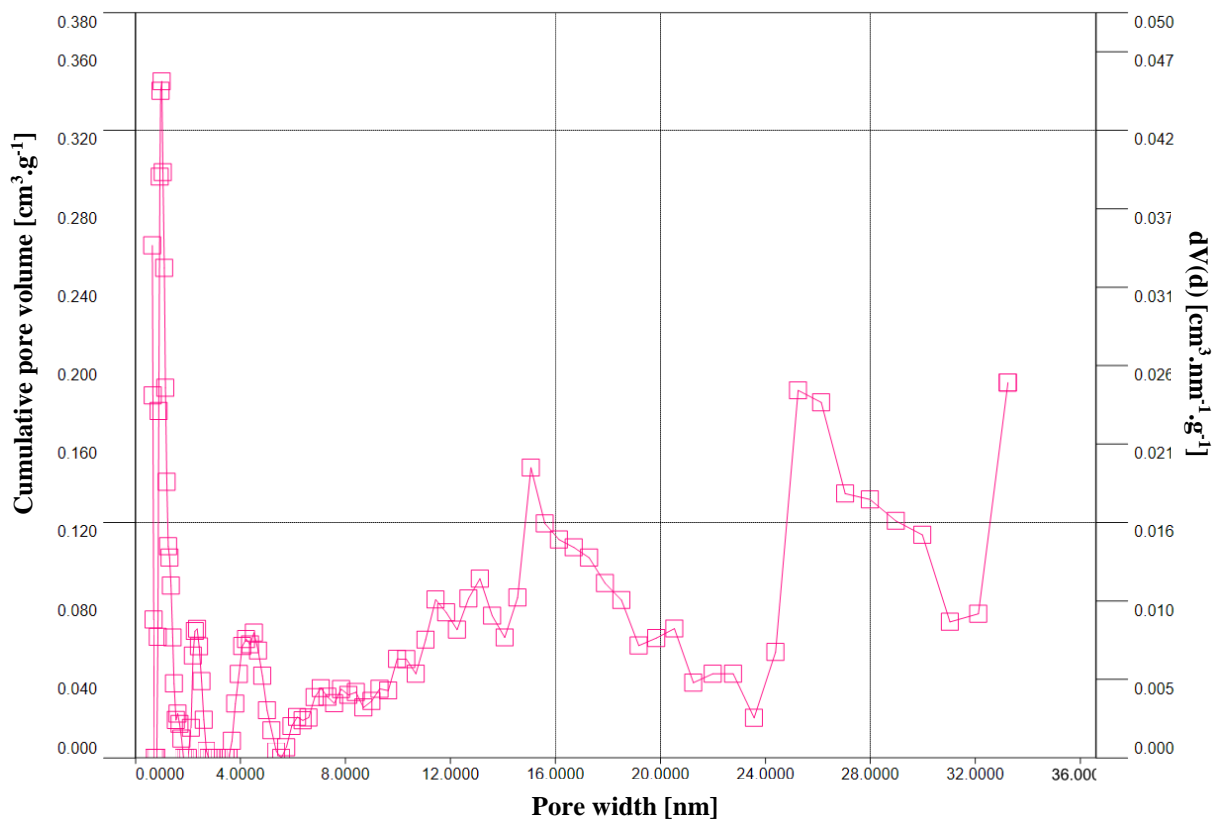


Fig. 29: The pore size distribution of JAK019 based on DFT.

## 4.4.2. Soft-templated Materials

### 4.4.2.1. Porous Carbon Nanospheres (JAK045)

Two batches of this material were prepared via a low-concentration hydrothermal synthesis (chapter 5.5.2.1.). Although the procedure was the same, the resulting materials, named JAK045A and JAK045B, were different. None of them exhibited either a narrow particle or pore size distribution, as can be seen from the SEM photographs shown in Fig. 30. and PSD curves in Fig. 31. The majority of JAK045A nanospheres were around 40 nm in diameter, but larger particles of cca 120 nm in diameter were also present in the mixture. However, in comparison with JAK045B, the particle size distribution was much narrower; the smallest particles observed in JAK045B were around 70 nm in diameter, while even particles larger than 1  $\mu\text{m}$  in diameter could be found in SEM photographs.

The surface area differed by cca 120 m<sup>2</sup>g<sup>-1</sup> (the surface areas of the batches JAK045A and JAK045B were 617 m<sup>2</sup>g<sup>-1</sup> and 737.3 m<sup>2</sup>g<sup>-1</sup>, respectively).

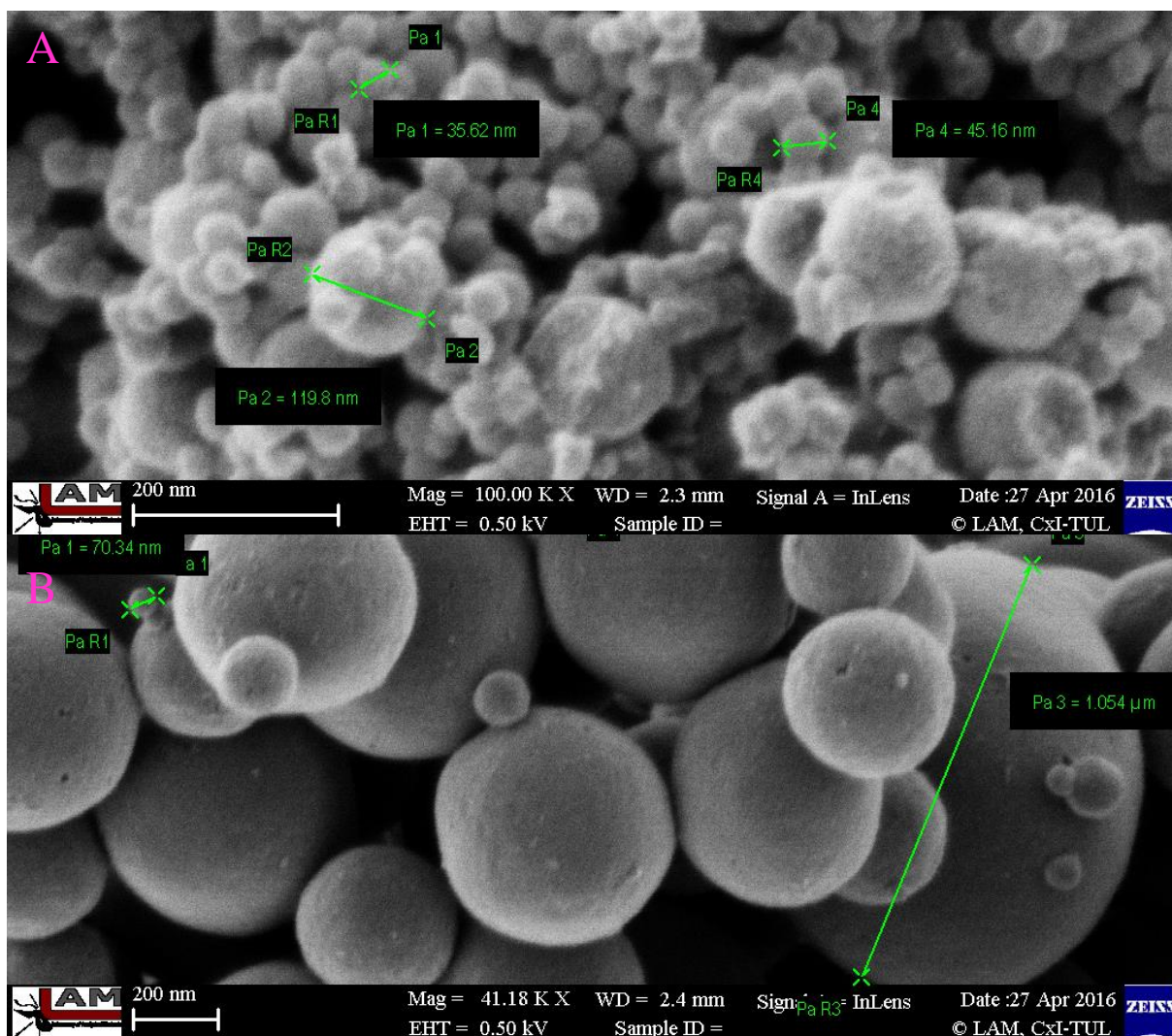


*Fig. 30: SEM photographs of JAK045A (A) and JAK045B (B).*

These differences could have been caused by the oscillating temperatures during the hydrothermal treatment in the autoclave, which was a drawback impossible to fix in our conditions. Further experiments with this kind of nanospheres were therefore discontinued.

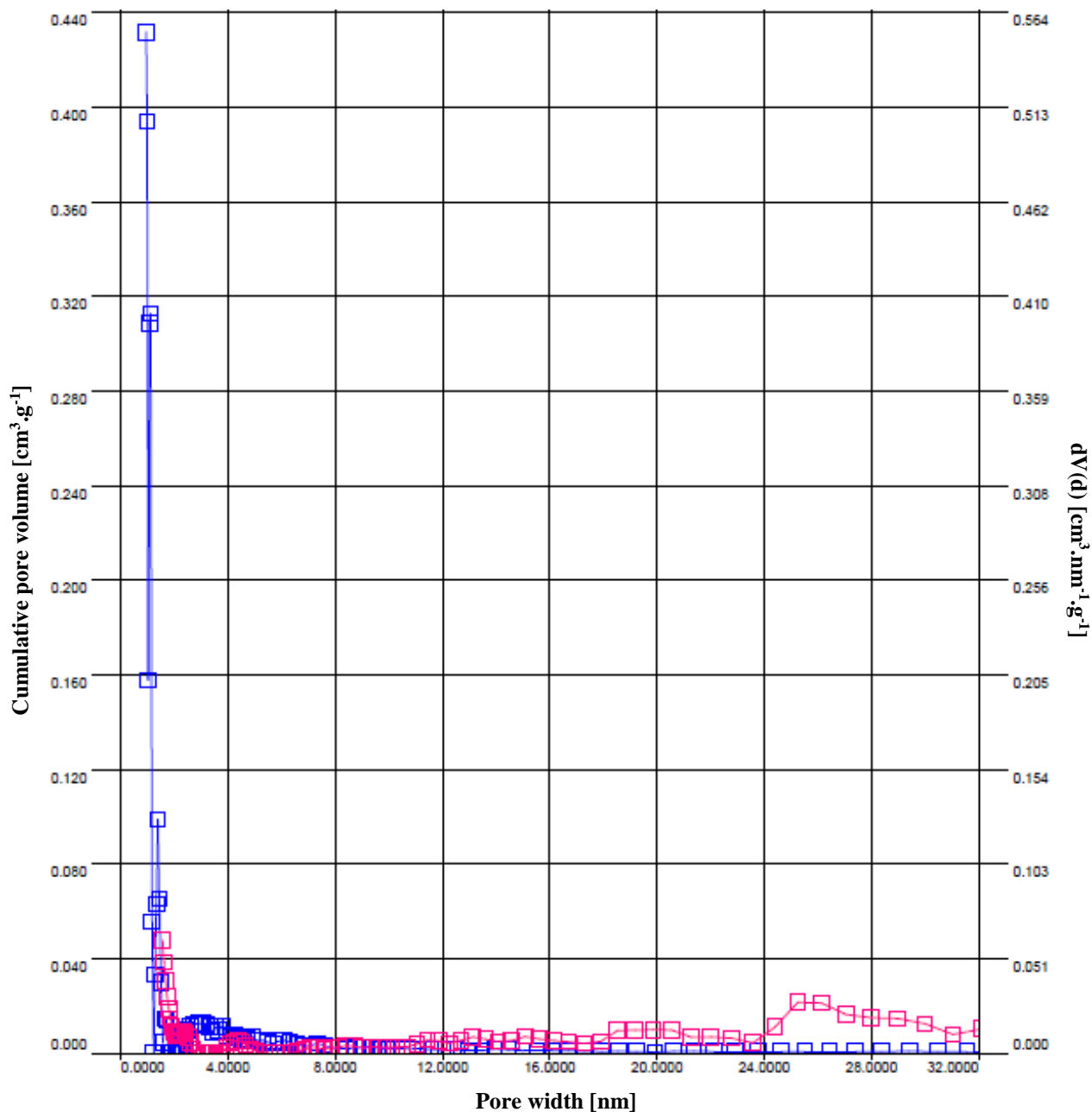


Fig. 31: The pore size distribution of JAK045A (pink) and JAK045B (blue) based on DFT.

#### 4.4.2.2. Mesoporous Carbon Material (JAK040)

Similarly to the previous case, the resulting structure of this material named JAK040 was not highly ordered. Both micropores and mesopores within a wide PSD range were present, as can be seen from SEM photographs in Fig. 32 and PSD plot in Fig. 33. In comparison to the aforementioned synthesised carbon materials, this one was extremely fluffy. Due to this feature, JAK040 was also chosen for further functionalisation.

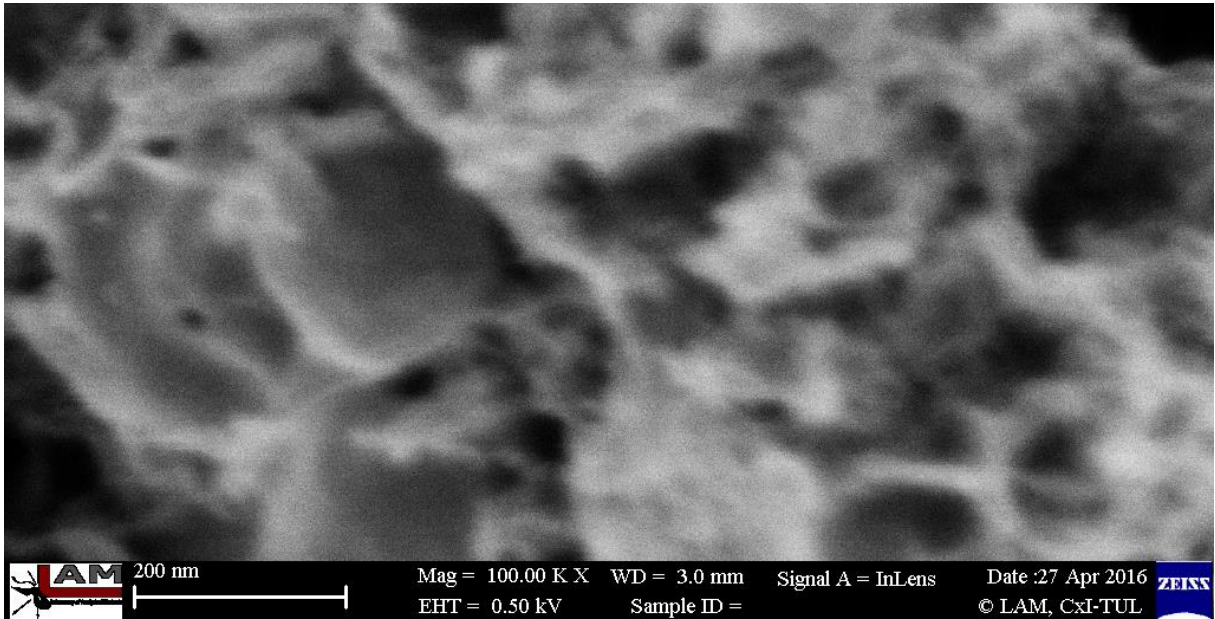


Fig. 32: SEM photograph of JAK040.

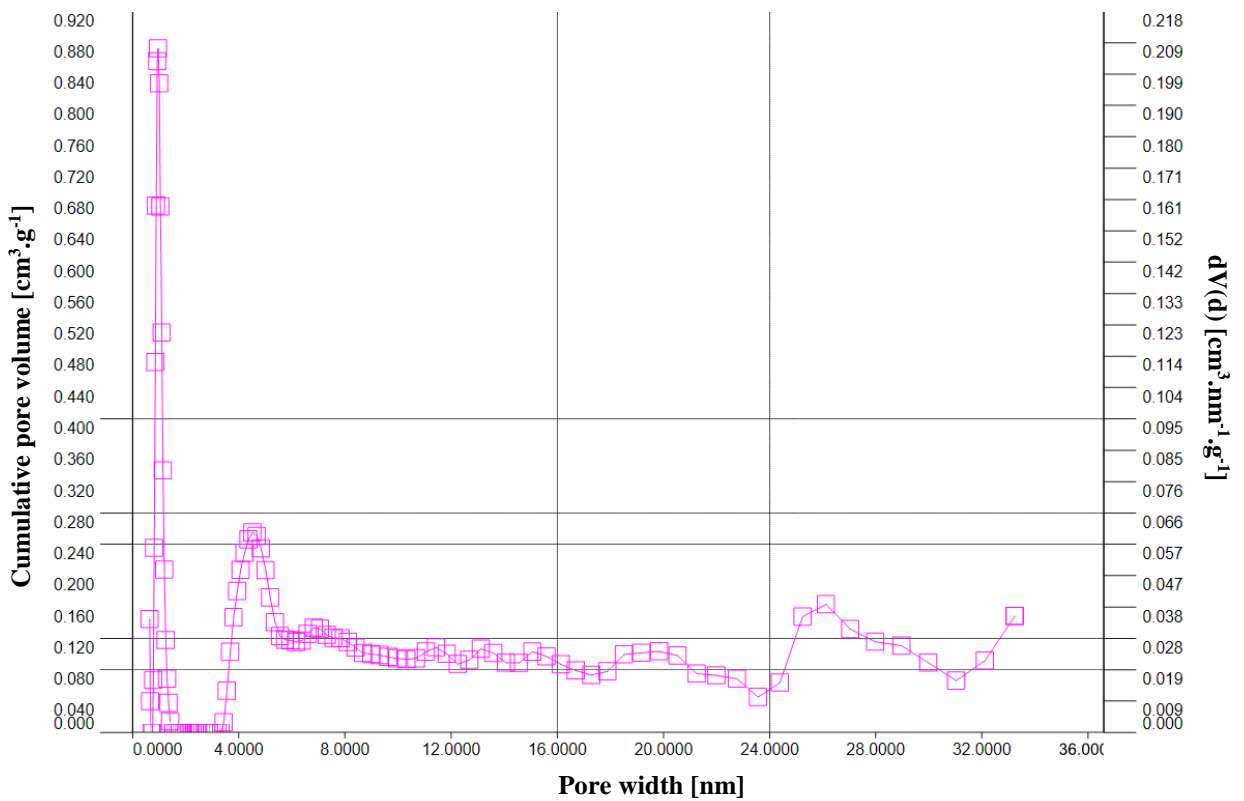


Fig. 33: The pore size distribution of JAK040.

In conclusion, hard-templated materials exhibited more ordered structures than the soft-templated ones. In addition, their preparation was reproducible, without any noticeable drawbacks. However, the procedures were lengthy, and dissolving the hard templates was an

inconvenient step indeed, after which some residues of the templates may still have stayed blocked inside the porous structures.

#### 4.4.3. Functionalised Materials

Three of the synthesised materials, namely JAK017B, JAK019 and JAK040, were functionalised with triethylenetetramine (chapter 5.6), and named JAK017B-TET, JAK019-TET and JAK040-TET.

Because of the fluffy structure of JAK040, the amount of the oxidising solution used was doubled in its case, in order to thoroughly soak the sample.

The results of the OEA in Tab. 13 show that the contents of nitrogen in JAK017B-TET and JAK019-TET were similar to that of commercially available CNPs Darco KB-G functionalised with TET (see Tab.8 in chapter 4.1.3.). For JAK040-TET, the nitrogen content was lower, which may have been influenced by the sample's fluffy structure and slightly different oxidation conditions. In addition, more sulphur, which originated from the oxidation step, was found in this sample, despite a vigorous washing procedure.

	<b>JAK017B-TET</b>	<b>JAK019-TET</b>	<b>JAK040-TET</b>
Element		<b>OEA [wt. %]</b>	
<b>C</b>	76.98	62.27	82.08
<b>N</b>	5.31	4.58	2.25
<b>S</b>	2.39	2.56	5.58
<b>H</b>	3.06	1.2	2.13

*Tab. 13: The results of OEA analysis of the synthesised materials functionalised with triethylenetetramine.*

The X-ray fluorescence revealed that all samples contained traces of chlorine (from the chlorination step), which had not been substituted with triethylenetetramine, and JAK019-TET even some silicon, which could have been caused by blocking the silica precursor inside the carbon shells of JAK019. This would also help explain the lower content of carbon in this sample.

The results of surface area analyses are summarised in Tab. 14. All functionalised samples exhibited a significant decrease in their surface areas in comparison to the pristine synthesised materials.

<b>Material</b>	<b>Surface area [m<sup>2</sup> g<sup>-1</sup>]</b>	<b>Material-TET</b>	<b>Surface area [m<sup>2</sup> g<sup>-1</sup>]</b>
JAK017B	1927	JAK017B-TET	543.6
JAK019	155.1	JAK019-TET	64.6
JAK040	565.5	JAK040-TET	235.6

*Tab. 14: Results of BET surface area analyses of the synthesised materials functionalised with triethylenetetramine.*

Pore size distribution plots of the pristine and functionalised synthesised carbon materials are shown in Fig.34-36. While the pore volumes decreased noticeably because of the decrease in surface areas, the PSDs of the pristine synthesised carbon materials did not significantly differ from the functionalised. It can be therefore assumed that the surface was functionalised homogeneously. The best correlation of the PSD curves can be seen for JAK040 and JAK040-TET in Fig. 36.

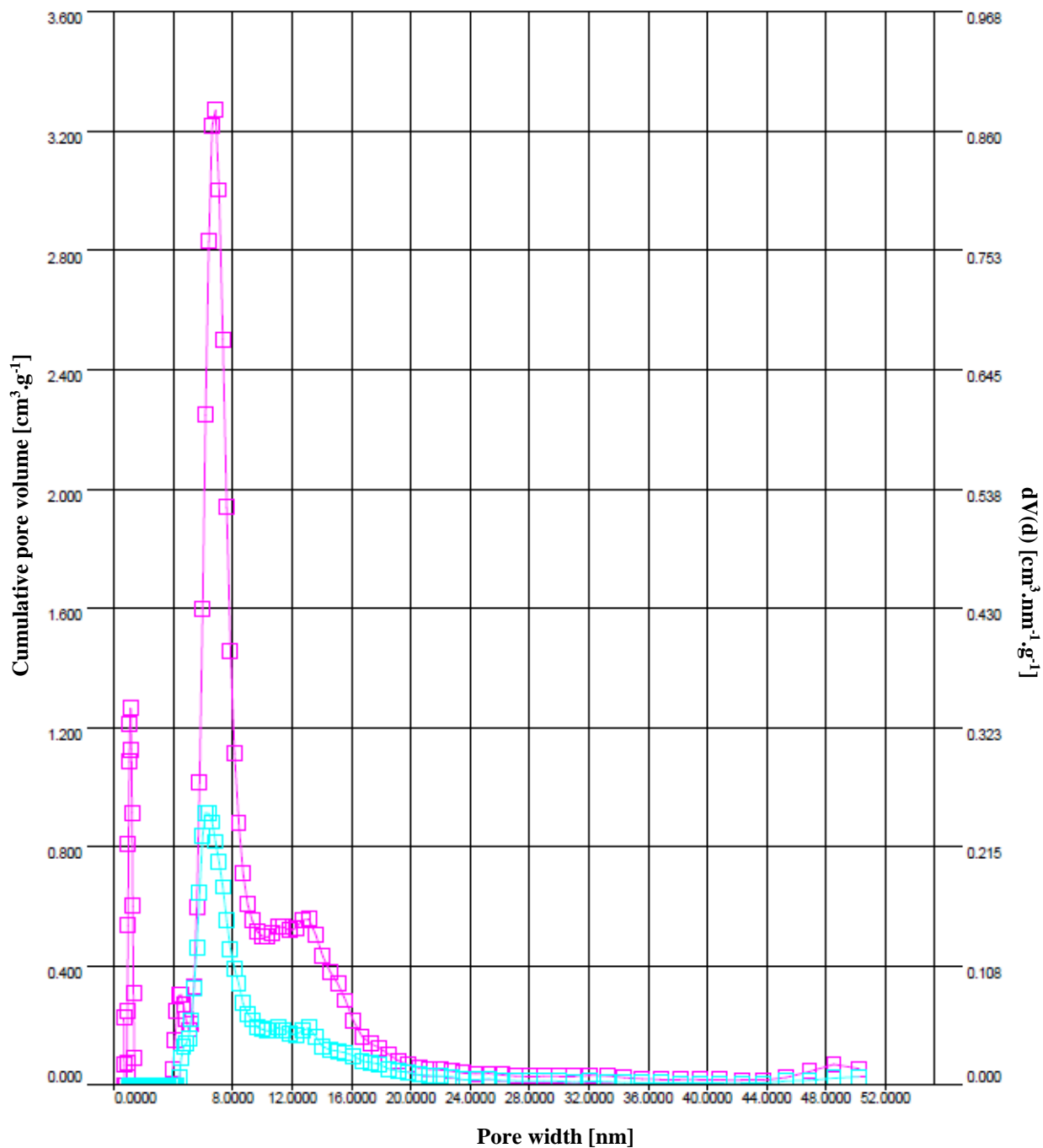


Fig. 34: The pore size distribution of JAK017B (pink) and JAK017B-TET (cyan) based on DFT.

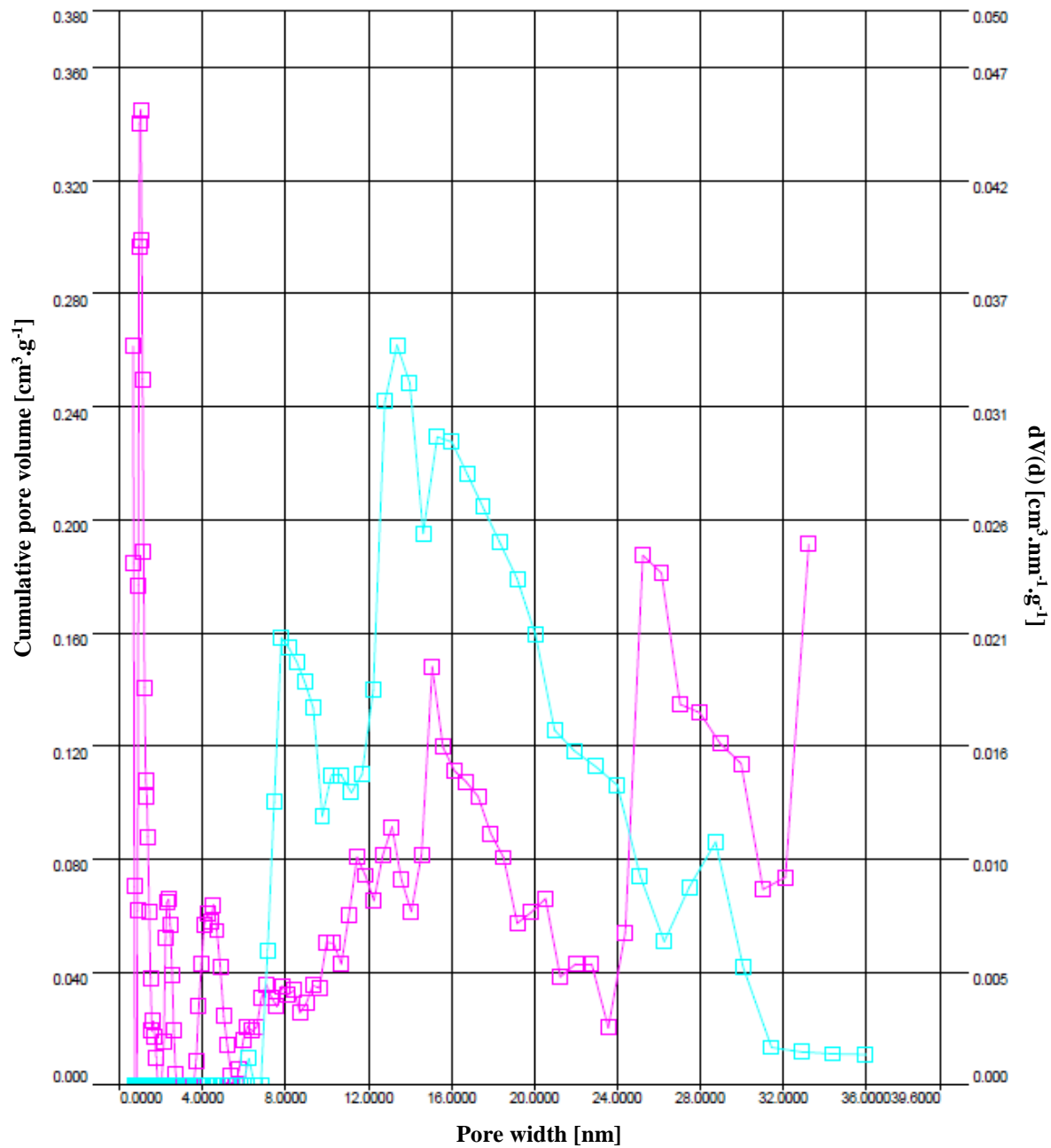


Fig. 35: The pore size distribution of JAK019 (pink) and JAK019-TET (cyan) based on DFT.

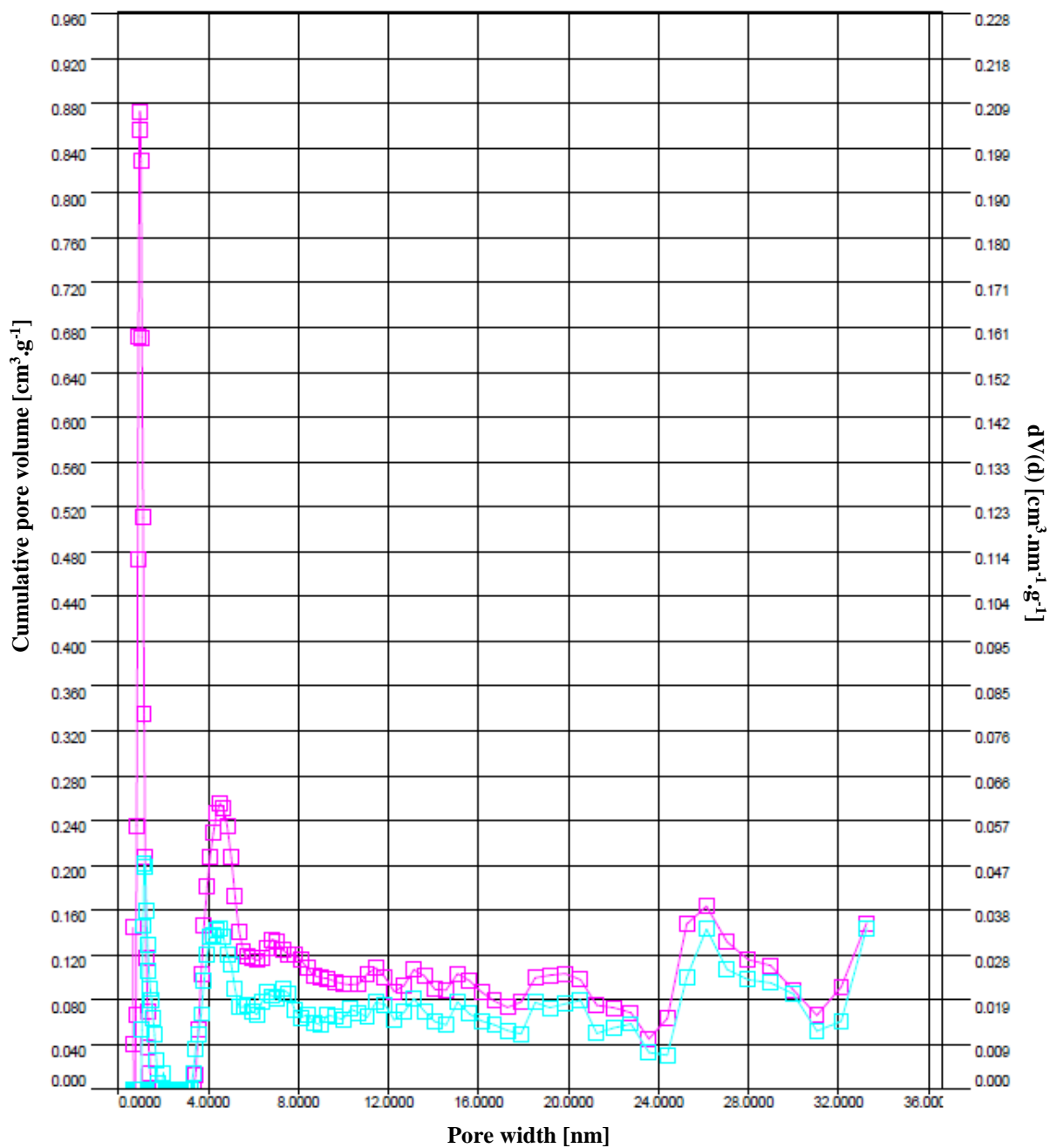


Fig. 36: The pore size distribution of JAK040 (pink) and JAK040-TET (cyan) based on DFT.

## **5. EXPERIMENTAL PART**

### **5.1. Functionalisation of Commercially Available Carbon Particles**

For the following functionalisation reactions, commercially available active carbon nanoparticles Darco KB-G from Aldrich (batch 4769TH) were used as a substrate.

#### **5.1.1. Amine formation**

The procedure was performed according to (Yantasee et al., 2004). 25 ml of concentrated sulphuric acid was slowly added to 25 ml of concentrated nitric acid at 0 °C (in an ice bath). After that, 4.5 g of CNPs Darco KB-G was slowly added and the mixture was stirred for 1 hour. It was then filtered and washed with deionized water (until the pH was neutral) and with propan-2-ol. The nitrated carbon particles were air-dried at RT for 12 hours.

The reduction step was based on (Redemann and Redemann, 1941). 2.5 g of the above prepared nitrated carbon was suspended in 25 ml of water and stirred with 10 ml of 15N ammonium hydroxide (0.15 mol) for 15 minutes. 14 g (80 mmol) of sodium hydrogensulfite ( $\text{Na}_2\text{S}_2\text{O}_4$ ) was then slowly added and the temperature of the mixture increased. 10 ml (0.175 mol) of glacial acetic acid was added and the mixture was stirred and refluxed at 100 °C for 5 hours. After cooling to RT, the suspension was centrifuged and washed several times with water and subsequently with propan-2-ol.

#### **5.1.2. Amide-amine formation**

The CNPs were first oxidised according to (Lemus-Yegres et al., 2007). CNPs Darco KB-G were added to a saturated aqueous solution of  $(\text{NH}_4)_2\text{S}_2\text{O}_8$  in 1M  $\text{H}_2\text{SO}_4$  (1g of NPs per 10 ml of the oxidising solution) and the mixture was stirred at RT for 24 hours. The CNPs were then filtered off and thoroughly washed with deionized water until the loss of acidic pH of the filtrate. Finally, the product was washed with propan-2-ol three times and dried at RT.

1 g of dried modified C-COOH NPs was suspended in 100 ml of dry toluene and 5 ml of  $\text{SOCl}_2$  was added dropwise within 5 min. The mixture was heated to reflux with exclusion of atmospheric moisture ( $\text{CaCl}_2$  adapter) for 2 hours. Next, pure toluene was added dropwise to the reaction mixture, the mixture of toluene and  $\text{SOCl}_2$  being distilled off by the same rate. The reaction suspension was cooled down to RT and was used immediately for a reaction with oligoamines.

A typical reaction with oligoamines proceeded as follows: 0.0172 mol of an amine a-f) (see Tab. 5 in chapter 4.1) was added at once to the above prepared suspension of -COCl functionalised CNPs. The mixture was stirred at RT for 12 hours, filtered off and washed with three times with 30 ml of toluene, twice with 30 ml of propan-2-ol and four times with 30 ml of absolute ethanol. Great care was taken not to expose the functionalised CNPs to any kind of acidic vapours, including e.g. carbon dioxide. The solid product was dried above KOH in vacuum at RT.

### **5.1.3. Oxidation of commercially available carbon nanoparticles**

For these experiments, a new flask of  $(\text{NH}_4)_2\text{S}_2\text{O}_8$  was always freshly opened and a saturated solution in 1M  $\text{H}_2\text{SO}_4$  was prepared. 3 grams of Darco KB-G CNPs were stirred in 30 ml of this solution for different time intervals (2, 4, 8, 12, 24 and 48 hours) without any cooling.

After these, other experiments with shortened time intervals, during which the mixture was cooled in a water bath to RT, were conducted. The reaction mixtures were stirred for 30, 60 and 90 minutes.

## **5.2. Preparation of Nanofibrous Scaffolds Containing Carbon Particles**

A solution of 16 wt% PCL in chloroform and ethanol (9:1 by weight) was prepared for electrospinning. The whole set-up consisted of an electrospinning device (needleless roller electrospinning; diameter 3 cm, length 15 cm) and a sputtering device (see Fig. 37). The roller charging was 37 kV positive and the collector charging 10 kV negative. Sputtering was conducted at a frequency of 220 Hz and 65 % amplitude. The rolling belt moved at a speed of 0.01 m/s.

The materials were produced at the temperature of 23 °C and relative humidity 45 %.

## **5.3. Cytocompatibility of Nanofibrous Scaffolds Containing Carbon Particles – MTT Assay**

3T3 mice fibroblasts (3T3 Swiss Albino, ATCC) were maintained in Dulbecco's Modified Eagle's Medium (DMEM, Lonza) with 10% (v/v) fetal bovine serum (FBS, Biosera) and 1% (v/v) penicillin / streptomycin / amphotericin B (Lonza). Cells were cultured in an incubator (37°C, 5%  $\text{CO}_2$ ). The medium was changed three times a week and the 31<sup>st</sup> passage was used for the in-vitro experiments.

Concentration of cells seeded in particular wells of 96-well plate was  $1 \cdot 10^4$ . Cell viability and proliferation was measured by MTT assay on day 1, 3, 8 and 14 after cell seeding. 50  $\mu$ l of MTT solution (Amresco) and 150  $\mu$ l of DMEM was added to all the samples and was incubated for three hours at 37°C, 5% CO<sub>2</sub>. The formazane crystals were dissolved in acidic isopropyl alcohol (IPA) and the absorbance was measured at the wavelength 570 nm with the reference wavelength at 650 nm. The samples were diluted prior to the measurement when needed (the final absorbance is related to the dilution).

After day 1, 3, 8 and 14 of cell seeding all scaffolds were processed for a microscopy analysis. All the samples were washed with PBS (phosphate buffered saline, pH 7.4) prior to fixation to remove unattached cells. The scaffolds processed for SEM were fixed with 2.5% glutaraldehyde. Samples processed for fluorescent microscopy were fixed with either 2.5% glutaraldehyde or ice-cold methanol, according to the fluorescent dye used (4',6-diamidino-2-phenylindole, i.e. DAPI, in combination with phalloidin-FITC and propidium iodide, respectively). After the fixation the samples for SEM were dried up with upgrading concentration of ethanol (60%, 70%, 80%, 90%, 95% and 100%). After drying, the samples were attached to the SEM target, sputtered with gold and analysed by scanning electron microscope (Tescan, VEGA3 SB easy probe). For the fluorescent microscopy, the samples were rinsed with PBS after the fixation and incubated for 15 minutes with PI at room temperature in the dark. After the incubation period, the samples were rinsed with PBS and analysed by the fluorescent microscope (NICON Eclipse Ti-e). When staining the samples with the combination of phalloidin-FITC and DAPI, after PBS wash samples were first permeabilised with 0.1% Triton X-100 in PBS / 0.1% BSA solution for 5 minutes. After permeabilisation, samples were washed with PBS and stained with phalloidin-FITC for 30 minutes at room temperature in the dark. After the first step of staining, the samples were washed with PBS and stained with DAPI for 5 minutes at room temperature in the dark. After staining, samples were washed in PBS and analysed by the fluorescent microscope (NICON Eclipse Ti-e).

#### **5.4. Antibacterial Testing of PCL Nanofibers and PCL+C Scaffolds**

The procedure was similar to the one described in (Padil et al., 2015). The bacterial strains of Gram-negative *Escherichia coli* (CCM 3954) and *Pseudomonas aeruginosa* (CCM 3955) and Gram-positive *Staphylococcus aureus* (CCM 3953) and *Enterococcus faecalis* (CCM 4224) used in this study were obtained from the Czech Collection of Microorganisms (Masaryk University Brno, Czech Republic). The microorganisms were cultured overnight in 5 ml of

Luria-Bertani broth in an incubation shaker at 37 °C and 150 rpm until the microbial cultures reached an OD600 (optical density) of 1.0, which corresponds to  $8 \cdot 10^8$  CFU/ml (colony forming units per ml).

All agar plates were freshly prepared before the antibacterial tests. A sterilized cotton swab was dipped into the culture suspension and the cells were spread homogeneously over the agar plates. These plates were immediately used for the antibacterial activity tests. The antibacterial activity of the plain PCL nanofibres and PCL-C scaffold was investigated by a qualitative method determining the zone of inhibition.

## **5.5. Synthesis of Templated Mesoporous Carbon Materials**

### **5.5.1. Hard-templated Materials**

#### **5.5.1.1. Ordered Mesoporous Carbon Materials Based on SBA-15 silica template (JAK017)**

First, the silica hard template SBA-15 was synthesised according to (Galarneau et al., 2003; Fulvio et al., 2005). Briefly, 4 g of P123 (Pluronic 123, poly-(ethylene glycol)-*block*-poly-(propylene glycol)-*block*-poly-(ethylene glycol), PEG20-PPG70-PEG20 from Sigma-Aldrich) was added to 144 ml of 1.7 M aqueous solution of hydrochloric acid and stirred at 40 °C for 4 hours. After that, 8.75 ml of TEOS (mass ratio of TEOS:Pluronic 123 was 2:1) was added dropwise and the mixture was stirred for two hours. Next, the mixture was transferred to a teflon-lined sealed container and kept at 130 °C for 72 hours.

The product was filtered, washed with ethanol and dried at 80 °C for 12 hours. It was then calcined at 500 °C for 6 hours, the final temperature being reached with a heating rate of approximately 1 °C/min.

Two types of mesoporous carbon materials were prepared by mixing two types of precursor solutions similarly to (Ryoo et al., 1999; Li et al., 2011). One precursor solution consisted only of sucrose (1.25 g), and distilled water (5.0 ml), the second one was enriched with 0.3 g of boric acid. Each type was then divided into two equal solutions, one solution being allowed to infiltrate the mesopores of 1 g of the SBA-15 template.

The composite materials were mixed with six drops of sulphuric acid before drying at 100 °C for 6 hours and at 160 °C for another 6 hours. The infiltration and drying processes were repeated again with additional 66% of the other precursor solution of the two equal ones and one drop of sulphuric acid.

The composites was carbonised at 850 °C for 3 hours under nitrogen flow. After that, the materials were washed twice by using volume fraction 10% HF solutions at RT. Finally, two types of mesoporous carbon material were obtained after being filtered and dried in air at 110 °C overnight.

#### **5.5.1.2. Ordered Mesoporous Carbon Materials Based on Monodisperse Silica Nanospheres (JAK019)**

The material was prepared based on (Lei et al., 2006). First, 14.4 ml of absolute ethanol, 17.1 ml of water and 8.9 ml of 25% aqueous ammonia were stirred and heated to 55 °C in a 100ml three-neck round-bottom flask with a condenser. 2 ml of freshly distilled TEOS was added to that solution and the mixture was stirred at the same temperature for 6 hours. To increase the size of the silica seeds thus obtained, 2 ml of TEOS was added seven times at the interval of 6 hours.

The solution was evaporated and the silica material obtained was then ground using a mortar. The resultant silica particles were further used as a hard template for ultra-large mesoporous carbon.

4 g of silica particles was mixed with a solution of 2 g of sucrose (the molar ratio of sucrose to silica: 0.088) in 20 ml of water and 1 ml of 96% sulphuric acid. The mixture was heated to 80 °C in 1 hour and kept at that temperature for 1 hour, then to 100 °C in 1 hour and kept at that temperature for 6 hours, followed by heating to 160 °C in 2 hours and keeping at that temperature for 6 hours.

It was then carbonised at 850 °C for 3 hours under nitrogen flow. The composite obtained was rinsed with 20% HF for 12 hours, washed with deionised water and dried at 100 °C.

## **5.5.2. Soft-templated Materials**

### **5.5.2.1. Porous Carbon Nanospheres (JAK045A, JAK045B)**

The materials were prepared according to (Fang et al., 2010). Briefly, 0.6 g of phenol, 2.1 ml of 37% formalin and 15 ml of 0.1 M NaOH solution were stirred at 70 °C. After 30 min, 0.96 g of Pluronic F127 dissolved in 15 ml of water was added to the mixture. It was then stirred at 66 °C at a speed of 340 rpm for 2 hours.

To dilute the solution, 50 ml of distilled water was added and the mixture was further stirred at 66 °C for 18 hours – no deposit was observed. The total amount of 78.5 ml was then diluted with 248 ml of distilled water and placed into the autoclave, where it was treated at 130 °C for 24 hours (set to 130 °C but oscillated between 120 °C and 143 °C). After the hydrothermal treatment, an orange precipitate appeared and was separated via centrifugation. After washing with distilled water several times, the product was dried in vacuum. It was then carbonised under nitrogen flow (40 ml/min) at 700 °C for 3 hours.

### **5.5.2.2. Mesoporous Carbon Material (JAK040)**

The material was prepared based on (Li et al., 2006). 8 g of P 123 and 2 g of sucrose were dissolved in 320 ml of 2M hydrochloric acid solution and the mixture was heated to 40 °C. After being stirred for 3 hours, 18.4 ml of TEOS was added under stirring and the mixture was left to age under a reflux condenser at 100°C for 24 hours. The resultant brown precipitate was filtered, washed and dried at room temperature. 8.627 g of silica/ P123/sucrose composite was mixed with 86.3 ml of distilled water and 8.6 ml of sulphuric acid (96%), and the mixture was stirred for 16 hours before being dried at 160 °C for 6 hours.

After carbonisation at 850 °C for 2 hours under nitrogen flow (40 ml/min), the silica was removed via rinsing in 20% HF solution for 24 hours. The carbon material obtained was washed and vacuum dried.

## **5.6. Functionalisation of the Synthesised Mesoporous Carbons**

The materials' functionalisation was performed using the procedure mentioned in chapter 5.1.2. However, the oxidation step was optimised according to chapter 5.1.3. The reaction mixture was stirred for 30 min while cooling to RT in a water bath. For sample JAK019-TET, the amount of the oxidising solution was doubled due to its fluffiness.

## 5.7. Equipment specifications

Transmission electron microscopy: JEOL JEM-1010, JEOL Ltd.

Surface element analysis: Omicron Nanotechnology ESCAProbeP spectrometer.

Organic elemental analysis: Elementar vario EL III, Elementar Analysensysteme GmbH).

Surface area, pore size distribution and total pore volume: NOVA3200, Quantachrome Instruments, and NovaWin software; Autosorb iQ, Quantachrome Instruments, and ASiQwin software.

Electrokinetic analysis (zeta potential): Zetasizer ZS90, Malvern software Ver. 6.32.

Differential Scanning Calorimetry: DSC 404C Pegasus, Netzsch GmbH, and DSC1/700, Mettler Toledo, equipped with a ceramic sensor and IntraCooler system.

Electrospinning/particle sputtering: The whole set-up consisted of an electrospinning device (needleless roller electrospinning; diameter 3 cm, length 15 cm) and a sputtering device (see Fig. 37). The roller charging was 37 kV positive and the collector charging 10 kV negative. The sputtering device, based on vibration principle, consisted of three electric motors with the cam amounting to a total length of 15 cm, the movements of which forced the particles to fall from a gap of 1 mm.

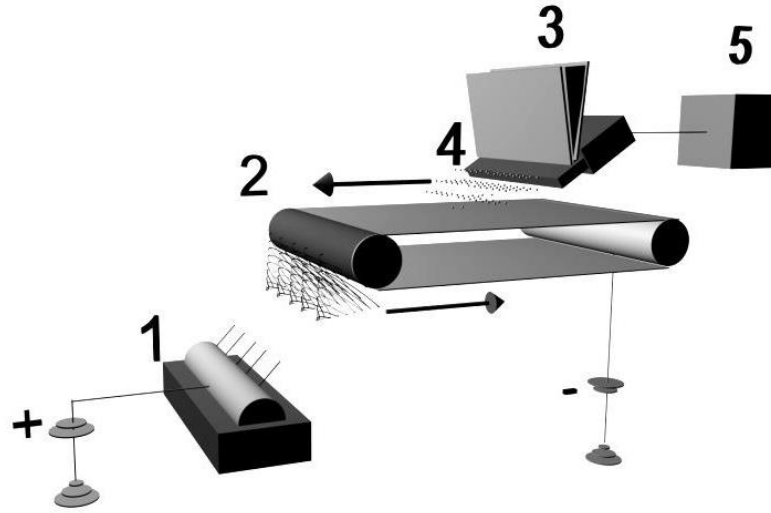


*Fig. 37: Schematic diagram of the setup for the creation of nanocomposite materials which consists of (1) needleless spinning electrode, (2) belt collector, (3) particle conveyor, (4) ultrasound sonotrode, and (5) feeder.*

Scaffolds' melting: Raman DXR microscope with objective: 10x/0.25 BD.

Scanning electron microscopy: Tescan, VEGA3 SB easy probe and UHR FE-SEM Zeiss Ultra

Plus equipped with SE2 and InLens detectors.

Thermogravimetric analysis: TGA Q500, V20.13 Build 39, TA instruments.

## 6. CONCLUSIONS

In the first part of this work, commercially available CNPs were successfully functionalised via a novel type of functionalisation, resulting in amide-amine groups on their surface. The oligoamines used varied in the length of alkyl chains and the number and type of amino groups. Although TEM images did not show any significant difference in the structure of the materials before and after functionalisation, the functionalisation modified the materials' properties to a large extent. The successful functionalisation was therefore confirmed via several analytical methods.

The wettability of the surfaces increased noticeably, and so did zeta potential. The results of XPS and OEA showed that nitrogen was present on the surface of the functionalised CNPs. The amount of nitrogen on the surface of the CNPs seemed to be influenced by the structure of the oligoamines (as more branched, secondary and tertiary amino groups containing oligoamines would not bind as easily as primary, less branched amines). The surface area and pore volume decreased distinctively after functionalisation, suggesting that pores were filled with bonded oligoamines.

Functionalised CNPs were grafted on plasma treated PET and HDPE. The polymer samples in subsequent stages of modification were characterised by various diagnostic methods. After the interaction of Ar plasma activated polymer surfaces with functionalised CNPs, an increase in nitrogen concentration on the very surface was observed. XPS, Raman spectroscopy, contact angle measurements and electrokinetic analysis confirmed that the functionalised CNPs were chemically bonded on the surface of the plasma treated polymers. Functionalised CNPs grafting on the plasma activated polymers had a positive effect on VSMCs adhesion and proliferation tested *in vitro*. The viability of cells cultivated on all grafted types of functionalised CPs was extremely high; except for the 1<sup>st</sup> day, on which the cells were still adapting to modified surface, the cell viability was above 95 %. However, differences in the numbers of cultivated cells among the individual types of the grafted CNPs were insignificant (Žáková et al., 2016). It can be therefore assumed that the structure of the amino chains did not play an important role in cell adhesion.

The aforementioned functionalised CNPs were also used to prepare composite scaffolds via sputtering the CNPs into electrospun polycaprolactone (PCL) nanofibers: three of them with

three types of functionalised CNPs and one with plain activated CNPs. Plain PCL nanofibers and the composite nanofibrous scaffold with plain activated CNPs were used as comparative samples. The structure of the materials was studied using scanning electron microscopy (SEM), which showed that the materials containing the CNPs consisted of both micro- and nanofibres, while pristine PCL samples were nanofibrous. In comparison to pristine PCL nanofibers, the specific surface area of the scaffolds containing the CNPs significantly increased.

Cytocompatibility of the materials was tested using 3T3 mouse fibroblasts. Cell viability and proliferation was measured by MTT assay on days 1, 3, 8 and 14 after cell seeding. The samples were then stained using fluorescent dyes and examined via fluorescence microscopy. During the FM analyses, all scaffolds containing CNPs underwent structural thermal degradation when irradiated with either green or blue light. No damage was caused using UV light, which is in accordance with the fact that carbon materials, especially carbon black, are widely used as UV stabilisers in polymer production. The scaffolds with functionalised CNPs showed better cytocompatibility than the scaffold with plain CNPs. Nevertheless, the performance of pristine PCL fibres was still even better than that of the scaffolds containing the functionalised CNPs.

In conclusion, functionalisation positively influenced the CNPs cytocompatibility, however, it would have been more useful to incorporate the functionalised CNPs into a material that is not as highly cytocompatible as PCL.

On the basis of the results of MTT testing, the PCL scaffold with pristine CNPs was also tested for antibacterial activity (in comparison with pristine PCL nanofibers) using the bacterial strains of *E. coli*, *S. aureus*, *P. aeruginosa* and *E. faecalis*. However, no antibacterial effect was found.

A substantial part of the thesis was also aimed at the synthesis of mesoporous carbon particles via soft- and hard-templating. Although there have been many experiments to prepare various materials, unexpected issues occurred during autoclaving and carbonisation, so there were only a few batches in relatively high yields that were sufficient for further functionalisation. The materials were analysed using SEM and gas adsorption analyses. Selected synthesised materials were functionalised using the above mentioned amide-amine functionalisation and characterised using OEA and gas adsorption. The results of the OEA confirmed a successful functionalisation, showing a distinctive increase in nitrogen concentration. In the case of one

hard-templated sample, a noticeable amount of silicon was found, which may have been caused by the presence of the residues of the spherical hard template, encapsulated inside carbon shells. The surface area of the functionalised templated materials decreased, as it had happened in the case of functionalised commercially available CNPs. The pore size distribution changed only slightly, showing similar trends and suggesting mainly micropore filling.

The templated and functionalised materials have neither been used for grafting on plasma treated polymer surfaces nor tested for cytocompatibility yet. These steps are to be conducted in the future, so that we can observe the influence of not only functionalisation but also the nano-structures.

The author performed or actively participated in the majority of the procedures and analyses throughout the study, from synthesis and functionalisation, production of fibrous materials, plasma treatment, gas physisorption, to MTT/cytocompatibility/antibacterial testing (excluding testing mentioned in (Švorčík et al., 2014; Žáková et al., 2016)) and scanning electron and fluorescence microscopy.

## 7. ABBREVIATIONS

AFM	Atomic force microscopy
AF-1	Amphiphilic fullerene-1
ARXPS	Angle resolved X-ray photoelectron spectroscopy
BET	Brunauer-Emmet-Teller
BJH	Barrett-Joyner-Halenda
BMP-2	Bone morphogenetic protein-2
BMSCs	Bone marrow stromal stem cells, BMSCs
BSA	Bovine serum albumin
C3-F-tris-MDC	C3-fullero-tris-methanodicarboxylic acid
CA	Contact angle
CaP	Calcium phosphate
CDs	Carbon dots
CFU	Colony forming unit
CNDs	Carbon nanodiamonds
CNHs	Carbon nanohorns
CNOs	Carbon nano-onions
CNPs	Carbon nanoparticles
CNTs	Carbon nanotubes
CS	Chitosan
CTAB	Cetyltrimethylammonium bromide
CVD	Chemical vapour deposition
DAPI	4',6-diamidino-2-phenylindole
DF-1	dendrofullerene-1
DFT	Density functional theory
DMEM	Dulbecco's modified Eagle's medium
ECM	Extra cellular matrix
<i>E. coli</i>	<i>Escherichia coli</i>
<i>E. faecalis</i>	<i>Enterococcus faecalis</i>
fCNTs	Functionalised carbon nanotubes
FTIR	Fourier-transform infrared
FBS	Fetal bovine serum
FM	Fluorescent microscopy

FT-NIR	Fourier transform near-infrared
gMSCs	Goat adult mesenchymal stem cells
GO	Graphene oxide
HDPE	High density polyethylene
HMDA	Hexamethylenediamine
IPA	Isopropyl alcohol
LMIC	Lipid membrane incorporated fullerenes
mAb	Monoclonal antibody
MRI	Magnetic resonance imaging
MTT	(3-(4,5-dimethylthiazol-2-yl)-2,5-diphenyltetrazolium bromide
MWCNTs	Multi-walled carbon nanotubes
NIR SERS	Near-infrared excited surface-enhanced Raman scattering
NPs	Nanoparticles
NSC	Neural stem cells
OD	Optical density
OMC	Ordered mesoporous carbon
P123	Pluronic 123
PBS	Phosphate buffered saline
PC	Phycocyanin
PDDA	Poly diallyldimethylammonium
PEB	Paclitaxel-embedded buckysomes
PEG	Poly ethylene glycol
PET	Polyethylene terephthalate
PI	Propidium iodide
PL	Phospholipid
PLL	Poly L-lysine
PLLA	Poly L-lactide
PMMA	Poly methyl methacrylate
PSD	Pore size distribution
<i>P. aeruginosa</i>	<i>Pseudomonas aeruginosa</i>
rGO	Reduced graphene oxide
rGONR	Reduced graphene oxide nanoribbon
RT	Room temperature

SBA-15	Santa Barbara amorphous
SEM	Scanning electron microscopy
SGH	Self-supporting graphene hydrogel
STP	Standard temperature and pressure
SWCNTs	Single-walled carbon nanotubes
<i>S. aureus</i>	<i>Staphylococcus aureus</i>
TEM	Transmission electron microscopy
VSMC	Vascular smooth muscle cell
XPS	X-ray photoelectron spectroscopy

## 8. REFERENCES

- Akhavan, O.; Ghaderi, E. The Use of Graphene in the Self-Organized Differentiation of Human Neural Stem Cells into Neurons under Pulsed Laser Stimulation. *J. Mater. Chem. B* **2014**, *2* (34), 5602–5611.
- Akhavan, O.; Ghaderi, E.; Shahsavari, M. Graphene Nanogrids for Selective and Fast Osteogenic Differentiation of Human Mesenchymal Stem Cells. *Carbon* **2013**, *59*, 200–211.
- Akhavan, O.; Ghaderi, E.; Abouei, E.; Hatamie, S.; Ghasemi, E. Accelerated Differentiation of Neural Stem Cells into Neurons on Ginseng-Reduced Graphene Oxide Sheets. *Carbon* **2014**, *66*, 395–406.
- Alshehri, R.; Ilyas, A. M.; Hasan, A.; Arnaout, A.; Ahmed, F.; Memic, A. Carbon Nanotubes in Biomedical Applications: Factors, Mechanisms, and Remedies of Toxicity: Miniperspective. *J. Med. Chem.* **2016**, *59* (18), 8149–8167.
- Amirshahi, N.; Alyautdin, R. N.; Sarkar, S.; Rezayat, S. M.; Orlova, M. A.; Trushkov, I. V.; Buchachenko, A. L.; Kuznetsov, D. A. Fullerene-Based Low Toxic Nanocationite Particles (Porphyrin Adducts of Cyclohexyl Fullerene-C-60) to Treat Hypoxia-Induced Mitochondrial Dysfunction in Mammalian Heart Muscle. *Arch. Med. Res.* **2008**, *39* (6), 549–559.
- Andreev, I.; Petrukhina, A.; Garmanova, A.; Babakhin, A.; Andreev, S.; Romanova, V.; Troshin, P.; Troshina, O.; DuBuske, L. Penetration of Fullerene C60 Derivatives Through Biological Membranes. *Fuller. Nanotub. Carbon Nanostructures* **2008**, *16* (2), 89–102.
- Auciello, O.; Gurman, P.; Guglielmotti, M. B.; Olmedo, D. G.; Berra, A.; Saravia, M. J. Biocompatible Ultrananocrystalline Diamond Coatings for Implantable Medical Devices. *MRS Bull.* **2014**, *39* (07), 621–629.
- Bacakova, L.; Svorcik, V. Cell Colonization Control by Physical and Chemical Modification of Materials. In *Cell Growth Process: New Research*; Nova Science Publishers, Inc., 2008.
- Bacakova, L.; Mares, V.; Bottone, M. R.; Pellicciari, C.; Lisa, V.; Svorcik, V. Fluorine Ion-Implanted Polystyrene Improves Growth and Viability of Vascular Smooth Muscle Cells in Culture. *J. Biomed. Mater. Res.* **2000**, *49* (3), 369–379.
- Bacakova, L.; Filova, E.; Kubies, D.; Machova, L.; Proks, V.; Malinova, V.; Lisa, V.; Rypacek, F. Adhesion and Growth of Vascular Smooth Muscle Cells in Cultures on Bioactive RGD Peptide-Carrying Polylactides. *J. Mater. Sci.-Mater. Med.* **2007**, *18* (7), 1317–1323.
- Bacakova, L.; Filova, E.; Parizek, M.; Ruml, T.; Svorcik, V. Modulation of Cell Adhesion, Proliferation and Differentiation on Materials Designed for Body Implants. *Biotechnol. Adv.* **2011**, *29* (6), 739–767.
- Badea, I.; Kaur, R. Nanodiamonds as Novel Nanomaterials for Biomedical Applications: Drug Delivery and Imaging Systems. *Int. J. Nanomedicine* **2013**, 203.
- Bajaj, P.; Akin, D.; Gupta, A.; Sherman, D.; Shi, B.; Auciello, O.; Bashir, R. Ultrananocrystalline Diamond Film as an Optimal Cell Interface for Biomedical Applications. *Biomed. Microdevices* **2007**, *9* (6), 787–794.
- Balavoine, F.; Schultz, P.; Richard, C.; Mallouh, V.; Ebbesen, T. W.; Mioskowski, C. Helical Crystallization of Proteins on Carbon Nanotubes: A First Step towards the Development of New Biosensors. *Angew. Chem.-Int. Ed.* **1999**, *38* (13–14), 1912–1915.
- Baptista, F. R.; Belhout, S. A.; Giordani, S.; Quinn, S. J. Recent Developments in Carbon Nanomaterial Sensors. *Chem Soc Rev* **2015**, *44* (13), 4433–4453.
- Barnes, L.-M.; Phillips, G. J.; Davies, J. G.; Lloyd, A. W.; Cheek, E.; Tennison, S. R.; Rawlinson, A. P.; Kozynchenko, O. P.; Mikhailovsky, S. V. The Cytotoxicity of Highly Porous Medical Carbon Adsorbents. *Carbon* **2009**, *47* (8), 1887–1895.
- Bartelmess, J.; Giordani, S. Carbon Nano-Onions (Multi-Layer Fullerenes): Chemistry and Applications. *Beilstein J. Nanotechnol.* **2014**, *5*, 1980–1998.
- Bhirde, A. A.; Patel, S.; Sousa, A. A.; Patel, V.; Molinolo, A. A.; Ji, Y.; Leapman, R. D.;

Gutkind, J. S.; Rusling, J. F. Distribution and Clearance of PEG-Single-Walled Carbon Nanotube Cancer Drug Delivery Vehicles in Mice. *Nanomed.* **2010**, *5* (10), 1535–1546.

Bianco, A.; Da Ros, T.; Prato, M.; Toniolo, C. Fullerene-Based Amino Acids and Peptides. *J. Pept. Sci.* **2001**, *7* (4), 208–219.

Bianco, A.; Kostarelos, K.; Partidos, C. D.; Prato, M. Biomedical Applications of Functionalised Carbon Nanotubes. *Chem. Commun.* **2005**, No. 5, 571–577.

Bisaglia, M.; Natalini, B.; Pellicciari, R.; Straface, E.; Malorni, W.; Monti, D.; Franceschi, C.; Schettini, G. C-3-Fullero-Tris-Methanodicarboxylic Acid Protects Cerebellar Granule Cells from Apoptosis. *J. Neurochem.* **2000**, *74* (3), 1197–1204.

Blazewicz, M. Carbon Mterials in the Treatent of Soft and Hard Tissue Injuries. *Eur. Cell. Mater.* **2001**, *2*, 21–29.

Bogdanovic, G.; Djordjevic, A. Carbon Nanomaterials: Biologically Active Fullerene Derivatives. *Srp. Arh. Celok. Lek.* **2016**, *144* (3–4), 222–231.

Bolotin, K. I.; Sikes, K. J.; Jiang, Z.; Klima, M.; Fudenberg, G.; Hone, J.; Kim, P.; Stormer, H. L. Ultrahigh Electron Mobility in Suspended Graphene. *Solid State Commun.* **2008**, *146* (9–10), 351–355.

Bolskar, R. D. Gadofullerene MRI Contrast Agents. *Nanomed.* **2008**, *3* (2), 201–213.

Bolskar, R. D.; Benedetto, A. F.; Husebo, L. O.; Price, R. E.; Jackson, E. F.; Wallace, S.; Wilson, L. J.; Alford, J. M. First Soluble M@C-60 Derivatives Provide Enhanced Access to Metallofullerenes and Permit in Vivo Evaluation of Gd@C-60[C(COOH)(2)](10) as a MRI Contrast Agent. *J. Am. Chem. Soc.* **2003**, *125* (18), 5471–5478.

Bottini, M.; Rosato, N.; Bottini, N. PEG-Modified Carbon Nanotubes in Biomedicine: Current Status and Challenges Ahead. *Biomacromolecules* **2011**, *12* (10), 3381–3393.

Brettreich, M.; Hirsch, A. A Highly Water-Soluble dendro[60]fullerene. *Tetrahedron Lett.* **1998**, *39* (18), 2731–2734.

Brettreich, M.; Burghardt, S.; Bottcher, C.; Bayerl, T.; Bayerl, S.; Hirsch, A. Globular Amphiphiles: Membrane-Forming Hexaadducts of C-60. *Angew. Chem.-Int. Ed.* **2000**, *39* (10), 1845–+.

Burghardt, S.; Hirsch, A.; Schade, B.; Ludwig, K.; Bottcher, C. Switchable Supramolecular Organization of Structurally Defined Micelles Based on an Amphiphilic Fullerene. *Angew. Chem.-Int. Ed.* **2005**, *44* (19), 2976–2979.

Chen, C.; Wang, H. *Biomedical Applications and Toxicology of Carbon Nanomaterials*; John Wiley & Sons, 2016.

Chen, E. Y. T.; Wang, Y.-C.; Mintz, A.; Richards, A.; Chen, C.-S.; Lu, D.; Nguyen, T.; Chin, W.-C. Activated Charcoal Composite Biomaterial Promotes Human Embryonic Stem Cell Differentiation toward Neuronal Lineage. *J. Biomed. Mater. Res. A* **2012**, *100A* (8), 2006–2017.

Chen, M.; Pierstorff, E. D.; Lam, R.; Li, S.-Y.; Huang, H.; Osawa, E.; Ho, D. Nanodiamond-Mediated Delivery of Water-Insoluble Therapeutics. *ACS Nano* **2009**, *3* (7), 2016–2022.

Crinelli, R.; Carloni, E.; Menotta, M.; Giacomini, E.; Bianchi, M.; Ambrosi, G.; Giorgi, L.; Magnani, M. Oxidized Ultrashort Nanotubes as Carbon Scaffolds for the Construction of Cell-Penetrating NF-Kappa B Decoy Molecules. *ACS Nano* **2010**, *4* (5), 2791–2803.

Crowder, S. W.; Prasai, D.; Rath, R.; Balikov, D. A.; Bae, H.; Bolotin, K. I.; Sung, H.-J. Three-Dimensional Graphene Foams Promote Osteogenic Differentiation of Human Mesenchymal Stem Cells. *Nanoscale* **2013**, *5* (10), 4171–4176.

Daroczi, B.; Kari, G.; McAleer, M. F.; Wolf, J. C.; Rodeck, U.; Dicker, A. P. In Vivo Radioprotection by the Fullerene Nanoparticle DF-1 as Assessed in a Zebrafish Model. *Clin. Cancer Res.* **2006**, *12* (23), 7086–7091.

Dellinger, A.; Zhou, Z.; Lenk, R.; MacFarland, D.; Kepley, C. L. Fullerene Nanomaterials Inhibit Phorbol Myristate Acetate-Induced Inflammation. *Exp. Dermatol.* **2009**, *18* (12), 1079–1081.

Ding, X.; Liu, H.; Fan, Y. Graphene-Based Materials in Regenerative Medicine. *Adv. Healthc. Mater.* **2015**, *4* (10), 1451–1468.

Djordjevic, A.; Srdjenovic, B.; Seke, M.; Petrovic, D.; Injac, R.; Mrdjanovic, J. Review of Synthesis and Antioxidant Potential of Fullerenol Nanoparticles. *J. Nanomater.* **2015**, *2015*, 1–15.

Doi, Y.; Ikeda, A.; Akiyama, M.; Nagano, M.; Shigematsu, T.; Ogawa, T.; Takeya, T.; Nagasaki, T. Intracellular Uptake and Photodynamic Activity of Water-Soluble [60]- and [70]Fullerenes Incorporated in Liposomes. *Chem.-Eur. J.* **2008**, *14* (29), 8892–8897.

Du, F.; Li, J.; Hua, Y.; Zhang, M.; Zhou, Z.; Yuan, J.; Wang, J.; Peng, W.; Zhang, L.; Xia, S.; et al. Multicolor Nitrogen-Doped Carbon Dots for Live Cell Imaging. *J. Biomed. Nanotechnol.* **2015**, *11* (5), 780–788.

Duan, S.; Yang, X.; Mei, F.; Tang, Y.; Li, X.; Shi, Y.; Mao, J.; Zhang, H.; Cai, Q. Enhanced Osteogenic Differentiation of Mesenchymal Stem Cells on Poly(l -Lactide) Nanofibrous Scaffolds Containing Carbon Nanomaterials: Enhanced Osteocompatibility of Nanofibrous Scaffolds. *J. Biomed. Mater. Res. A* **2015**, *103* (4), 1424–1435.

Dugan, L. L.; Turetsky, D. M.; Du, C.; Lobner, D.; Wheeler, M.; Almlı, C. R.; Shen, C. K. F.; Luh, T. Y.; Choi, D. W.; Lin, T. S. Carboxyfullerenes as Neuroprotective Agents. *Proc. Natl. Acad. Sci. U. S. A.* **1997**, *94* (17), 9434–9439.

Dutta, D.; Sundaram, S. K.; Teegarden, J. G.; Riley, B. J.; Fifield, L. S.; Jacobs, J. M.; Addleman, S. R.; Kaysen, G. A.; Moudgil, B. M.; Weber, T. J. Adsorbed Proteins Influence the Biological Activity and Molecular Targeting of Nanomaterials. *Toxicol. Sci.* **2007**, *100* (1), 303–315.

Elkhenany, H.; Amelse, L.; Lafont, A.; Bourdo, S.; Caldwell, M.; Neilsen, N.; Dervishi, E.; Derek, O.; Biris, A. S.; Anderson, D.; et al. Graphene Supports in Vitro Proliferation and Osteogenic Differentiation of Goat Adult Mesenchymal Stem Cells: Potential for Bone Tissue Engineering: Osteogenesis on Graphene. *J. Appl. Toxicol.* **2015**, *35* (4), 367–374.

Enyashin, A. N.; Ivanovskii, A. L. Structural and Electronic Properties of New 1D and 2D Carbon Allotropes with Mixed sp<sup>1</sup> – sp<sup>3</sup> Hybridization Types. *Chem. Phys. Lett.* **2014**, *609*, 15–20.

Fadeel, B.; Fornara, A.; Toprak, M. S.; Bhattacharya, K. Keeping It Real: The Importance of Material Characterization in Nanotoxicology. *Biochem. Biophys. Res. Commun.* **2015**, *468* (3), 498–503.

Falcao, E. H.; Wudl, F. Carbon Allotropes: Beyond Graphite and Diamond. *J. Chem. Technol. Biotechnol.* **2007**, *82* (6), 524–531.

Fang, Y.; Gu, D.; Zou, Y.; Wu, Z.; Li, F.; Che, R.; Deng, Y.; Tu, B.; Zhao, D. A Low-Concentration Hydrothermal Synthesis of Biocompatible Ordered Mesoporous Carbon Nanospheres with Tunable and Uniform Size. *Angew. Chem. Int. Ed.* **2010**, *49* (43), 7987–7991.

Fatouros, P. P.; Corwin, F. D.; Chen, Z.-J.; Broaddus, W. C.; Tatum, J. L.; Kettenmann, B.; Ge, Z.; Gibson, H. W.; Russ, J. L.; Leonard, A. P.; et al. In Vitro and in Vivo Imaging Studies of a New Endohedral Metallofullerene Nanoparticle. *Radiology* **2006**, *240* (3), 756–764.

Figueiredo, J. L.; Pereira, M. F. R.; Freitas, M. M. A.; Orfao, J. J. M. Modification of the Surface Chemistry of Activated Carbons. *Carbon* **1999**, *37* (9), 1379–1389.

Foley, S.; Crowley, C.; Smaihı, M.; Bonfils, C.; Erlanger, B. F.; Seta, P.; Larroque, C. Cellular Localisation of a Water-Soluble Fullerene Derivative. *Biochem. Biophys. Res. Commun.* **2002**, *294* (1), 116–119.

Frasconi, M.; Maffeis, V.; Bartelmess, J.; Echegoyen, L.; Giordani, S. Highly Surface Functionalized Carbon Nano-Onions for Bright Light Bioimaging. *Methods Appl. Fluoresc.* **2015**, *3* (4), 044005.

Fulvio, P. F.; Pikus, S.; Jaroniec, M. Tailoring Properties of SBA-15 Materials by Controlling Conditions of Hydrothermal Synthesis. *J. Mater. Chem.* **2005**, *15* (47), 5049–5053.

Galarneau, A.; Cambon, N.; Di Renzo, F.; Ryoo, R.; Choi, M.; Fajula, F. Microporosity and Connections between Pores in SBA-15 Mesoporous Silicas as a Function of the Temperature of Synthesis. *New J. Chem.* **2003**, 27 (1), 73–79.

Ge, C.; Du, J.; Zhao, L.; Wang, L.; Liu, Y.; Li, D.; Yang, Y.; Zhou, R.; Zhao, Y.; Chai, Z.; et al. Binding of Blood Proteins to Carbon Nanotubes Reduces Cytotoxicity. *Proc. Natl. Acad. Sci. U. S. A.* **2011**, 108 (41), 16968–16973.

Gharbi, N.; Pressac, M.; Hadchouel, M.; Szwarc, H.; Wilson, S. R.; Moussa, F. [60]Fullerene Is a Powerful Antioxidant in Vivo with No Acute or Subacute Toxicity. *Nano Lett.* **2005**, 5 (12), 2578–2585.

Ghosh, M.; Sonkar, S. K.; Saxena, M.; Sarkar, S. Carbon Nano-Onions for Imaging the Life Cycle of *Drosophila Melanogaster*. *Small* **2011**, 7 (22), 3170–3177.

Ghosh, S.; Dutta, S.; Gomes, E.; Carroll, D.; D’Agostino, R.; Olson, J.; Guthold, M.; Gmeiner, W. H. Increased Heating Efficiency and Selective Thermal Ablation of Malignant Tissue with DNA-Encased Multiwalled Carbon Nanotubes. *ACS Nano* **2009**, 3 (9), 2667–2673.

Giordani, S.; Bartelmess, J.; Frascioni, M.; Biondi, I.; Cheung, S.; Grossi, M.; Wu, D.; Echegoyen, L.; O’Shea, D. F. NIR Fluorescence Labelled Carbon Nano-Onions: Synthesis, Analysis and Cellular Imaging. *J Mater Chem B* **2014**, 2 (42), 7459–7463.

Gómez-Serrano, V.; Acedo-Ramos, M.; López-Peinado, A. J.; Valenzuela-Calahorra, C. Oxidation of Activated Carbon by Hydrogen Peroxide. Study of Surface Functional Groups by FT-Ir. *Fuel* **1994**, 73 (3), 387–395.

Gonzalez, K. A.; Wilson, L. J.; Wu, W. J.; Nancollas, G. H. Synthesis and in Vitro Characterization of a Tissue-Selective Fullerene: Vectoring C-60(OH)(16)AMBP to Mineralized Bone. *Bioorg. Med. Chem.* **2002**, 10 (6), 1991–1997.

Grebowski, J.; Kazmierska, P.; Krokosz, A. Fullerenols as a New Therapeutic Approach in Nanomedicine. *BioMed Res. Int.* **2013**, 2013, 1–9.

Guedidi, H.; Reinert, L.; Lévêque, J.-M.; Soneda, Y.; Bellakhal, N.; Duclaux, L. The Effects of the Surface Oxidation of Activated Carbon, the Solution pH and the Temperature on Adsorption of Ibuprofen. *Carbon* **2013**, 54, 432–443.

Guo, X.; Mei, N. Assessment of the Toxic Potential of Graphene Family Nanomaterials. *J. Food Drug Anal.* **2014**, 22 (1), 105–115.

Guseva Canu, I.; Bateson, T. F.; Bouvard, V.; Debia, M.; Dion, C.; Savolainen, K.; Yu, I.-J. Human Exposure to Carbon-Based Fibrous Nanomaterials: A Review. *Int. J. Hyg. Environ. Health* **2016**, 219 (2), 166–175.

Haydar, S.; Ferro-García, M. ; Rivera-Utrilla, J.; Joly, J. . Adsorption of P-Nitrophenol on an Activated Carbon with Different Oxidations. *Carbon* **2003**, 41 (3), 387–395.

Heo, C.; Yoo, J.; Lee, S.; Jo, A.; Jung, S.; Yoo, H.; Lee, Y. H.; Suh, M. The Control of Neural Cell-to-Cell Interactions through Non-Contact Electrical Field Stimulation Using Graphene Electrodes. *Biomaterials* **2011**, 32 (1), 19–27.

Hirsch, A. The Era of Carbon Allotropes. *Nat. Mater.* **2010**, 9 (11), 868–871.

Holt, B. D.; Dahl, K. N.; Islam, M. F. Quantification of Uptake and Localization of Bovine Serum Albumin-Stabilized Single-Wall Carbon Nanotubes in Different Human Cell Types. *Small* **2011**, 7 (16), 2348–2355.

Hong, H.; Yang, K.; Zhang, Y.; Engle, J. W.; Feng, L.; Yang, Y.; Nayak, T. R.; Goel, S.; Bean, J.; Theuer, C. P.; et al. In Vivo Targeting and Imaging of Tumor Vasculature with Radiolabeled, Antibody-Conjugated Nanographene. *ACS Nano* **2012**, 6 (3), 2361–2370.

Hu, Z.; Guan, W.; Wang, W.; Huang, L.; Xing, H.; Zhu, Z. Protective Effect of a Novel Cystine C-60 Derivative on Hydrogen Peroxide-Induced Apoptosis in Rat Pheochromocytoma PC12 Cells. *Chem. Biol. Interact.* **2007a**, 167 (2), 135–144.

Hu, Z.; Guan, W.; Wang, W.; Huang, L.; Xing, H.; Zhu, Z. Synthesis of Beta-Alanine C-60 Derivative and Its Protective Effect on Hydrogen Peroxide-Induced Apoptosis in Rat

Pheochromocytoma Cells. *Cell Biol. Int.* **2007b**, *31* (8), 798–804.

Huang, S. S.; Tsai, S. K.; Chih, C. L.; Chiang, L. Y.; Hsieh, H. M.; Teng, C. M.; Tsai, M. C. Neuroprotective Effect of Hexasulfobutylated C60 on Rats Subjected to Focal Cerebral Ischemia. *Free Radic. Biol. Med.* **2001**, *30* (6), 643–649.

Huang, W.-Y.; Yeh, C.-L.; Lin, J.-H.; Yang, J.-S.; Ko, T.-H.; Lin, Y.-H. Development of Fibroblast Culture in Three-Dimensional Activated Carbon Fiber-Based Scaffold for Wound Healing. *J. Mater. Sci.-Mater. Med.* **2012**, *23* (6), 1465–1478.

Hupert, M.; Muck, A.; Wang, J.; Stotter, J.; Cvackova, Z.; Haymond, S.; Show, Y.; Swain, G. M. Conductive Diamond Thin-Films in Electrochemistry. *Diam. Relat. Mater.* **2003**, *12* (10–11), 1940–1949.

Ikeda, A.; Sue, T.; Akiyama, M.; Fujioka, K.; Shigematsu, T.; Doi, Y.; Kikuchi, J.; Konishi, T.; Nakajima, R. Preparation of Highly Photosensitizing Liposomes with Fullerene-Doped Lipid Bilayer Using Dispersion-Controllable Molecular Exchange Reactions. *Org. Lett.* **2008**, *10* (18), 4077–4080.

Inagaki, M.; Kang, F.; Toyoda, M.; Konno, H. Chapter 1 - Introduction. In *Advanced Materials Science and Engineering of Carbon*; Inagaki, M., Kang, F., Toyoda, M., Konno, H., Eds.; Butterworth-Heinemann: Boston, 2014; pp 1–13.

Injac, R.; Boskovic, M.; Perse, M.; Koprivec-Furlan, E.; Cerar, A.; Djordjevic, A.; Strukelj, B. Acute Doxorubicin Nephrotoxicity in Rats with Malignant Neoplasm Can Be Successfully Treated with Fullerenol C-60(OH)(24) Via Suppression of Oxidative Stress. *Pharmacol. Rep.* **2008**, *60* (5), 742–749.

Isobe, H.; Tomita, N.; Jinno, S.; Okayama, H.; Nakamura, E. Synthesis and Transfection Capability of Multi-Functionalized Fullerene Polyamine. *Chem. Lett.* **2001**, No. 12, 1214–1215.

Isobe, H.; Nakanishi, W.; Tomita, N.; Jinno, S.; Okayama, H.; Nakamura, E. Nonviral Gene Delivery by Tetraamino Fullerene. *Mol. Pharm.* **2006**, *3* (2), 124–134.

Jain, S.; Sharma, A.; Basu, B. In Vitro Cytocompatibility Assessment of Amorphous Carbon Structures Using Neuroblastoma and Schwann Cells. *J. Biomed. Mater. Res. Part B-Appl. Biomater.* **2013**, *101B* (4), 520–531.

Jaramillo, J.; Álvarez, P. M.; Gómez-Serrano, V. Oxidation of Activated Carbon by Dry and Wet Methods: Surface Chemistry and Textural Modifications. *Fuel Process. Technol.* **2010**, *91* (11), 1768–1775.

Ji, H.; Yang, Z.; Jiang, W.; Geng, C.; Gong, M.; Xiao, H.; Wang, Z.; Cheng, L. Antiviral Activity of Nano Carbon Fullerene Lipidosome against Influenza Virus in Vitro. *J. Huazhong Univ. Sci. Technol.-Med. Sci.* **2008**, *28* (3), 243–246.

Kalbacova, M.; Broz, A.; Kong, J.; Kalbac, M. Graphene Substrates Promote Adherence of Human Osteoblasts and Mesenchymal Stromal Cells. *Carbon* **2010**, *48* (15), 4323–4329.

Kam, N. W. S.; Dai, H. J. Carbon Nanotubes as Intracellular Protein Transporters: Generality and Biological Functionality. *J. Am. Chem. Soc.* **2005**, *127* (16), 6021–6026.

Kam, N. W. S.; Jessop, T. C.; Wender, P. A.; Dai, H. J. Nanotube Molecular Transporters: Internalization of Carbon Nanotube-Protein Conjugates into Mammalian Cells. *J. Am. Chem. Soc.* **2004**, *126* (22), 6850–6851.

Karousis, N.; Suarez-Martinez, I.; Ewels, C. P.; Tagmatarchis, N. Structure, Properties, Functionalization, and Applications of Carbon Nanohorns. *Chem. Rev.* **2016**, *116* (8), 4850–4883.

Kim, H. J.; Kim, S. H.; Kim, M. S.; Lee, E. J.; Oh, H. G.; Oh, W. M.; Park, S. W.; Kim, W. J.; Lee, G. J.; Choi, N. G.; et al. Varying Ti-6Al-4V Surface Roughness Induces Different Early Morphologic and Molecular Responses in MG63 Osteoblast-like Cells. *J. Biomed. Mater. Res. A* **2005**, *74A* (3), 366–373.

Kim, J.; Kim, Y.-R.; Kim, Y.; Lim, K. T.; Seonwoo, H.; Park, S.; Cho, S.-P.; Hong, B. H.; Choung, P.-H.; Chung, T. D.; et al. Graphene-Incorporated Chitosan Substrata for Adhesion

and Differentiation of Human Mesenchymal Stem Cells. *J. Mater. Chem. B* **2013**, *1* (7), 933–938.

Kong, B.; Zhu, A.; Ding, C.; Zhao, X.; Li, B.; Tian, Y. Carbon Dot-Based Inorganic-Organic Nanosystem for Two-Photon Imaging and Biosensing of pH Variation in Living Cells and Tissues. *Adv. Mater.* **2012**, *24* (43), 5844–5848.

Krajcik, R.; Jung, A.; Hirsch, A.; Neuhuber, W.; Zolk, O. Functionalization of Carbon Nanotubes Enables Non-Covalent Binding and Intracellular Delivery of Small Interfering RNA for Efficient Knock-down of Genes. *Biochem. Biophys. Res. Commun.* **2008**, *369* (2), 595–602.

Ku, S. H.; Lee, M.; Park, C. B. Carbon-Based Nanomaterials for Tissue Engineering. *Adv. Healthc. Mater.* **2013**, *2* (2), 244–260.

Kuila, T.; Bose, S.; Khanra, P.; Mishra, A. K.; Kim, N. H.; Lee, J. H. Recent Advances in Graphene-Based Biosensors. *Biosens. Bioelectron.* **2011**, *26* (12), 4637–4648.

La, W.-G.; Park, S.; Yoon, H.-H.; Jeong, G.-J.; Lee, T.-J.; Bhang, S. H.; Han, J. Y.; Char, K.; Kim, B.-S. Delivery of a Therapeutic Protein for Bone Regeneration from a Substrate Coated with Graphene Oxide. *Small* **2013**, *9* (23), 4051–4060.

Lai, H. S.; Chen, W. J.; Chiang, L. Y. Free Radical Scavenging Activity of Fullerenol on the Ischemia-Reperfusion Intestine in Dogs. *World J. Surg.* **2000**, *24* (4), 450–454.

Langer, R.; Vacanti, J. P. Tissue Engineering. *Science* **1993**, *260* (5110), 920–926.

Lee, C.; Wei, X.; Kysar, J. W.; Hone, J. Measurement of the Elastic Properties and Intrinsic Strength of Monolayer Graphene. *Science* **2008**, *321* (5887), 385–388.

Lee, J. H.; Park, J. W.; Lee, H. B. Cell Adhesion and Growth on Polymer Surfaces with Hydroxyl Groups Prepared by Water Vapour Plasma Treatment. *Biomaterials* **1991**, *12* (5), 443–448.

Lee, J. H.; Jung, H. W.; Kang, I.-K.; Lee, H. B. Cell Behaviour on Polymer Surfaces with Different Functional Groups. *Biomaterials* **1994**, *15* (9), 705–711.

Lee, W. C.; Lim, C. H. Y. X.; Shi, H.; Tang, L. A. L.; Wang, Y.; Lim, C. T.; Loh, K. P. Origin of Enhanced Stem Cell Growth and Differentiation on Graphene and Graphene Oxide. *Acs Nano* **2011**, *5* (9), 7334–7341.

Lei, Z.; Xiao, Y.; Dang, L.; Lu, M.; You, W. Fabrication of Ultra-Large Mesoporous Carbon with Tunable Pore Size by Monodisperse Silica Particles Derived from Seed Growth Process. *Microporous Mesoporous Mater.* **2006**, *96* (1–3), 127–134.

Lemus-Yegres, L. J.; Such-Basáñez, I.; Román-Martínez, M. C.; de Lecea, C. S.-M. Catalytic Properties of a Rh–diamine Complex Anchored on Activated Carbon: Effect of Different Surface Oxygen Groups. *Appl. Catal. Gen.* **2007**, *331*, 26–33.

Lens, M.; Medenica, L.; Citernes, U. Antioxidative Capacity of C(60) (Buckminsterfullerene) and Newly Synthesized Fulleropyrrolidine Derivatives Encapsulated in Liposomes. *Biotechnol. Appl. Biochem.* **2008**, *51*, 135–140.

Li, L.; Song, H.; Chen, X. Ordered Mesoporous Carbons from the Carbonization of Sulfuric-Acid-Treated Silica/Triblock Copolymer/Sucrose Composites. *Microporous Mesoporous Mater.* **2006**, *94* (1–3), 9–14.

Li, N.; Zhang, Q.; Gao, S.; Song, Q.; Huang, R.; Wang, L.; Liu, L.; Dai, J.; Tang, M.; Cheng, G. Three-Dimensional Graphene Foam as a Biocompatible and Conductive Scaffold for Neural Stem Cells. *Sci. Rep.* **2013**, *3*, 1604.

Li, X.; Zhao, T.; Sun, L.; Aifantis, K. E.; Fan, Y.; Feng, Q.; Cui, F.; Watari, F. The Applications of Conductive Nanomaterials in the Biomedical Field: CONDUCTIVE NANOMATERIALS IN THE BIOMEDICAL FIELD. *J. Biomed. Mater. Res. A* **2016**, *104* (1), 322–339.

Li, Y.; Zhong, J.; Yang, X.; Lan, G.; Tang, H.; Liu, H. Simple Synthesis of Semi-Graphitized Ordered Mesoporous Carbons with Tunable Pore Sizes. *New Carbon Mater.* **2011**, *26* (2), 123–129.

Liao, X.; Zhang, B.; Wang, X.; Yan, H.; Zhang, X. Purification of C-Phycocyanin from

Spirulina Platensis by Single-Step Ion-Exchange Chromatography. *Chromatographia* **2011**, *73* (3–4), 291–296.

Lin, A. M. Y.; Chyi, B. Y.; Wang, S. D.; Yu, H. H.; Kanakamma, P. P.; Luh, T. Y.; Chou, C. K.; Ho, L. T. Carboxyfullerene Prevents Iron-Induced Oxidative Stress in Rat Brain. *J. Neurochem.* **1999**, *72* (4), 1634–1640.

Liu, K.-K.; Zheng, W.-W.; Wang, C.-C.; Chiu, Y.-C.; Cheng, C.-L.; Lo, Y.-S.; Chen, C.; Chao, J.-I. Covalent Linkage of Nanodiamond-Paclitaxel for Drug Delivery and Cancer Therapy. *Nanotechnology* **2010**, *21* (31), 315106.

Liu, Z.; Winters, M.; Holodniy, M.; Dai, H. siRNA Delivery into Human T Cells and Primary Cells with Carbon-Nanotube Transporters. *Angew. Chem.-Int. Ed.* **2007**, *46* (12), 2023–2027.

Liu, Z.; Fan, A. C.; Rakhra, K.; Sherlock, S.; Goodwin, A.; Chen, X.; Yang, Q.; Felsher, D. W.; Dai, H. Supramolecular Stacking of Doxorubicin on Carbon Nanotubes for In Vivo Cancer Therapy. *Angew. Chem.-Int. Ed.* **2009**, *48* (41), 7668–7672.

Lorena Montes-Fonseca, S.; Orrantia-Borunda, E.; Aguilar-Elguezabal, A.; Gonzalez Horta, C.; Talamas-Rohana, P.; Sanchez-Ramirez, B. Cytotoxicity of Functionalized Carbon Nanotubes in J774A Macrophages. *Nanomedicine-Nanotechnol. Biol. Med.* **2012**, *8* (6), 853–859.

Lowell, S.; Shields, J. E.; Thomas, M. A.; Thommes, M. *Characterization of Porous Solids and Powders: Surface Area, Pore Size and Density*; Springer Science & Business Media, 2012.

Lu, J.; He, Y.-S.; Cheng, C.; Wang, Y.; Qiu, L.; Li, D.; Zou, D. Self-Supporting Graphene Hydrogel Film as an Experimental Platform to Evaluate the Potential of Graphene for Bone Regeneration. *Adv. Funct. Mater.* **2013**, *23* (28), 3494–3502.

Maeda, R.; Noiri, E.; Isobe, H.; Homma, T.; Tanaka, T.; Negishi, K.; Doi, K.; Fujita, T.; Nakamura, E. A Water-Soluble Fullerene Vesicle Alleviates Angiotensin II-Induced Oxidative Stress in Human Umbilical Venous Endothelial Cells. *Hypertens. Res.* **2008**, *31* (1), 141–151.

Maeda-Mamiya, R.; Noiri, E.; Isobe, H.; Nakanishi, W.; Okamoto, K.; Doi, K.; Sugaya, T.; Izumi, T.; Homma, T.; Nakamura, E. In Vivo Gene Delivery by Cationic Tetraamino Fullerene. *Proc. Natl. Acad. Sci.* **2010**, *107* (12), 5339–5344.

Magrez, A.; Kasas, S.; Salicio, V.; Pasquier, N.; Seo, J. W.; Celio, M.; Catsicas, S.; Schwaller, B.; Forró, L. Cellular Toxicity of Carbon-Based Nanomaterials. *Nano Lett.* **2006**, *6* (6), 1121–1125.

Mallakpour, S.; Soltanian, S. Surface Functionalization of Carbon Nanotubes: Fabrication and Applications. *RSC Adv* **2016**, *6* (111), 109916–109935.

Martín, R.; Álvaro, M.; Herance, J. R.; García, H. Fenton-Treated Functionalized Diamond Nanoparticles as Gene Delivery System. *ACS Nano* **2010**, *4* (1), 65–74.

Menaa, F.; Abdelghani, A.; Menaa, B. Graphene Nanomaterials as Biocompatible and Conductive Scaffolds for Stem Cells: Impact for Tissue Engineering and Regenerative Medicine: The G Point in Stem Cell Research? *J. Tissue Eng. Regen. Med.* **2015**, *9* (12), 1321–1338.

Mochalin, V. N.; Shenderova, O.; Ho, D.; Gogotsi, Y. The Properties and Applications of Nanodiamonds. *Nat. Nanotechnol.* **2011**, *7* (1), 11–23.

Mohan, N.; Chen, C.-S.; Hsieh, H.-H.; Wu, Y.-C.; Chang, H.-C. In Vivo Imaging and Toxicity Assessments of Fluorescent Nanodiamonds in *Caenorhabditis Elegans*. *Nano Lett.* **2010**, *10* (9), 3692–3699.

Monaco, A. M.; Giugliano, M. Carbon-Based Smart Nanomaterials in Biomedicine and Neuroengineering. *Beilstein J. Nanotechnol.* **2014**, *5*, 1849–1863.

Monti, D.; Moretti, L.; Salvioli, S.; Straface, E.; Malorni, W.; Pellicciari, R.; Schettini, G.; Bisaglia, M.; Pincelli, C.; Fumelli, C.; et al. C60 Carboxyfullerene Exerts a Protective Activity against Oxidative Stress-Induced Apoptosis in Human Peripheral Blood Mononuclear Cells. *Biochem. Biophys. Res. Commun.* **2000**, *277* (3), 711–717.

Mroz, P.; Pawlak, A.; Satti, M.; Lee, H.; Wharton, T.; Gali, H.; Sarna, T.; Hamblin, M. R. Functionalized Fullerenes Mediate Photodynamic Killing of Cancer Cells: Type I versus Type II Photochemical Mechanism. *Free Radic. Biol. Med.* **2007a**, *43* (5), 711–719.

Mroz, P.; Tegos, G. P.; Gali, H.; Wharton, T.; Sarna, T.; Hamblin, M. R. Photodynamic Therapy with Fullerenes. *Photochem. Photobiol. Sci.* **2007b**, *6* (11), 1139–1149.

Murakami, T.; Sawada, H.; Tamura, G.; Yudasaka, M.; Iijima, S.; Tsuchida, K. Water-Dispersed Single-Wall Carbon Nanohorns as Drug Carriers for Local Cancer Chemotherapy. *Nanomed.* **2008**, *3* (4), 453–463.

Murthy, C. N.; Choi, S. J.; Geckeler, K. E. Nanoencapsulation of [60]fullerene by a Novel Sugar-Based Polymer. *J. Nanosci. Nanotechnol.* **2002**, *2* (2), 129–132.

Nair, R. R.; Blake, P.; Grigorenko, A. N.; Novoselov, K. S.; Booth, T. J.; Stauber, T.; Peres, N. M. R.; Geim, A. K. Fine Structure Constant Defines Visual Transparency of Graphene. *Science* **2008**, *320* (5881), 1308–1308.

Nakamura, E.; Isobe, H.; Tomita, N.; Sawamura, M.; Jinno, S.; Okayama, H. Functionalized Fullerene as an Artificial Vector for Transfection. *Angew. Chem.-Int. Ed.* **2000**, *39* (23), 4254–+.

Nayak, T. R.; Andersen, H.; Makam, V. S.; Khaw, C.; Bae, S.; Xu, X.; Ee, P.-L. R.; Ahn, J.-H.; Hong, B. H.; Pastorin, G.; et al. Graphene for Controlled and Accelerated Osteogenic Differentiation of Human Mesenchymal Stem Cells. *Acs Nano* **2011**, *5* (6), 4670–4678.

Novoselov, K. S.; Jiang, Z.; Zhang, Y.; Morozov, S. V.; Stormer, H. L.; Zeitler, U.; Maan, J. C.; Boebinger, G. S.; Kim, P.; Geim, A. K. Room-Temperature Quantum Hall Effect in Graphene. *Science* **2007**, *315* (5817), 1379–1379.

Oberdörster, G.; Oberdörster, E.; Oberdörster, J. Nanotoxicology: An Emerging Discipline Evolving from Studies of Ultrafine Particles. *Environ. Health Perspect.* **2005**, *113* (7), 823–839.

Orecchioni, M.; Bedognetti, D.; Sgarrella, F.; Marincola, F. M.; Bianco, A.; Delogu, L. G. Impact of Carbon Nanotubes and Graphene on Immune Cells. *J. Transl. Med.* **2014**, *12*, 138.

Padil, V. V. T.; Nguyen, N. H. A.; Ševců, A.; Černík, M. Fabrication, Characterization, and Antibacterial Properties of Electrospun Membrane Composed of Gum Karaya, Polyvinyl Alcohol, and Silver Nanoparticles. *J. Nanomater.* **2015**, 2015.

Pantarotto, D.; Singh, R.; McCarthy, D.; Erhardt, M.; Briand, J. P.; Prato, M.; Kostarelos, K.; Bianco, A. Functionalized Carbon Nanotubes for Plasmid DNA Gene Delivery. *Angew. Chem.-Int. Ed.* **2004a**, *43* (39), 5242–5246.

Pantarotto, D.; Briand, J. P.; Prato, M.; Bianco, A. Translocation of Bioactive Peptides across Cell Membranes by Carbon Nanotubes. *Chem. Commun.* **2004b**, No. 1, 16–17.

Parizek, M.; Kasalkova, N.; Bacakova, L.; Slepicka, P.; Lisa, V.; Blazkova, M.; Svorcik, V. Improved Adhesion, Growth and Maturation of Vascular Smooth Muscle Cells on Polyethylene Grafted with Bioactive Molecules and Carbon Particles. *Int. J. Mol. Sci.* **2009**, *10* (10), 4352–4374.

Park, S. Y.; Park, J.; Sim, S. H.; Sung, M. G.; Kim, K. S.; Hong, B. H.; Hong, S. Enhanced Differentiation of Human Neural Stem Cells into Neurons on Graphene. *Adv. Mater.* **2011**, *23* (36), H263–+.

Partha, R.; Conyers, J. L. Biomedical Applications of Functionalized Fullerene-Based Nanomaterials. *Int. J. Nanomedicine* **2009**, *4*, 261–275.

Partha, R.; Mitchell, L. R.; Lyon, J. L.; Joshi, P. P.; Conyers, J. L. Buckysomes: Fullerene-Based Nanocarriers for Hydrophobic Molecule Delivery. *Acs Nano* **2008**, *2* (9), 1950–1958.

Peñalver, J. L.; Linares-Fernández, J.-L.; Fariás, V. de A.; López-Ramón, M. V.; Tassi, M.; Oliver, F. J.; Moreno-Castilla, C.; Almodóvar, J. M. R. de. Activated Carbon Cloth as Support for Mesenchymal Stem Cell Growth and Differentiation to Osteocytes. *Carbon* **2009**, *47* (15), 3574–3577.

Perevedentseva, E.; Cheng, C.-Y.; Chung, P.-H.; Tu, J.-S.; Hsieh, Y.-H.; Cheng, C.-L. The Interaction of the Protein Lysozyme with Bacteria *E. Coli* Observed Using Nanodiamond Labelling. *Nanotechnology* **2007**, *18* (31), 315102.

Perevedentseva, E.; Lin, Y.-C.; Jani, M.; Cheng, C.-L. Biomedical Applications of Nanodiamonds in Imaging and Therapy. *Nanomed.* **2013**, *8* (12), 2041–2060.

Piperigkou, Z.; Karamanou, K.; Engin, A. B.; Gialeli, C.; Docea, A. O.; Vynios, D. H.; Pavão, M. S. G.; Golokhvast, K. S.; Shtilman, M. I.; Argiris, A.; et al. Emerging Aspects of Nanotoxicology in Health and Disease: From Agriculture and Food Sector to Cancer Therapeutics. *Food Chem. Toxicol.* **2016**, *91*, 42–57.

Porter, A. E.; Gass, M.; Bendall, J. S.; Muller, K.; Goode, A.; Skepper, J. N.; Midgley, P. A.; Welland, M. Uptake of Noncytotoxic Acid-Treated Single-Walled Carbon Nanotubes into the Cytoplasm of Human Macrophage Cells. *ACS Nano* **2009**, *3* (6), 1485–1492.

Portney, N. G.; Ozkan, M. Nano-Oncology: Drug Delivery, Imaging, and Sensing. *Anal. Bioanal. Chem.* **2006**, *384* (3), 620–630.

Price, R. L.; Ellison, K.; Haberstroh, K. M.; Webster, T. J. Nanometer Surface Roughness Increases Select Osteoblast Adhesion on Carbon Nanofiber Compacts. *J. Biomed. Mater. Res. A* **2004**, *70A* (1), 129–138.

Qi, W.; Yuan, W.; Yan, J.; Wang, H. Growth and Accelerated Differentiation of Mesenchymal Stem Cells on Graphene Oxide/Poly-L-Lysine Composite Films. *J. Mater. Chem. B* **2014**, *2* (33), 5461–5467.

Qu, X.; Komatsu, T.; Sato, T.; Glatter, O.; Horinouchi, H.; Kobayashi, K.; Tuchida, E. Structure, Photophysical Property, and Cytotoxicity of Human Serum Albumin Complexed with tris(dicarboxymethylene)[60]fullerene. *Bioconjug. Chem.* **2008**, *19* (8), 1556–1560.

Rancan, F.; Rosan, S.; Boehm, F.; Cantrell, A.; Brellreich, M.; Schoenberger, H.; Hirsch, A.; Moussa, F. Cytotoxicity and Photocytotoxicity of a Dendritic C-60 Mono-Adduct and a Malonic Acid C-60 Tris-Adduct on Jurkat Cells. *J. Photochem. Photobiol. B-Biol.* **2002**, *67* (3), 157–162.

Ratner, B. D. *Biomaterials Science: An Introduction to Materials in Medicine*; Academic Press, 2004.

Ratner, B. D.; Hoffman, A. S.; Schoen, F. J.; Lemons, J. E.; Dyro, J.; Martinsen, O. G.; Kyle, R.; Preim, B.; Bartz, D.; Grimnes, S.; et al. *Biomedical Engineering E-Mega Reference*; Academic Press, 2009.

Redemann, C. T.; Redemann, C. E. *Organic Syntheses Collective Volume 1*; Wiley: New York, 1941; Vol. 1.

Reznickova, A.; Kolska, Z.; Siegel, J.; Svorcik, V. Grafting of Gold Nanoparticles and Nanorods on Plasma-Treated Polymers by Thiols. *J. Mater. Sci.* **2012**, *47* (17), 6297–6304.

Rodil, S. E.; Olivares, R.; Arzate, H. In Vitro Cytotoxicity of Amorphous Carbon Films. *Biomed. Mater. Eng.* **2005**, *15* (1–2), 101–112.

Rosso, F.; Giordano, A.; Barbarisi, M.; Barbarisi, A. From Cell–ECM Interactions to Tissue Engineering. *J. Cell. Physiol.* **2004**, *199* (2), 174–180.

Ryoo, R.; Joo, S. H.; Jun, S. Synthesis of Highly Ordered Carbon Molecular Sieves via Template-Mediated Structural Transformation. *J. Phys. Chem. B* **1999**, *103* (37), 7743–7746.

Santos, S. G.; Santana, J. V.; Maia, F. F.; Lemos, V.; Freire, V. N.; Caetano, E. W. S.; Cavada, B. S.; Albuquerque, E. L. Adsorption of Ascorbic Acid on the C-60 Fullerene. *J. Phys. Chem. B* **2008**, *112* (45), 14267–14272.

Schipper, M. L.; Nakayama-Ratchford, N.; Davis, C. R.; Kam, N. W. S.; Chu, P.; Liu, Z.; Sun, X.; Dai, H.; Gambhir, S. S. A Pilot Toxicology Study of Single-Walled Carbon Nanotubes in a Small Sample of Mice. *Nat. Nanotechnol.* **2008**, *3* (4), 216–221.

Shadjou, N.; Hasanzadeh, M. Graphene and Its Nanostructure Derivatives for Use in Bone Tissue Engineering: Recent Advances: Graphene and Its Nanostructure Derivatives for Use in

Bone Tissue Engineering. *J. Biomed. Mater. Res. A* **2016**, *104* (5), 1250–1275.

Shershakova, N.; Baraboshkina, E.; Andreev, S.; Purgina, D.; Struchkova, I.; Kamyshnikov, O.; Nikonova, A.; Khaitov, M. Anti-Inflammatory Effect of Fullerene C60 in a Mice Model of Atopic Dermatitis. *J. Nanobiotechnology* **2016**, *14* (1).

Shvedova, A.; Pietrojusti, A.; Kagan, V. Nanotoxicology Ten Years Later: Lights and Shadows. *Toxicol. Appl. Pharmacol.* **2016**, *299*, 1–2.

Silva, W. M.; Ribeiro, H.; Seara, L. M.; Calado, H. D. R.; Ferlauto, A. S.; Paniago, R. M.; Leite, C. F.; Silva, G. G. Surface Properties of Oxidized and Aminated Multi-Walled Carbon Nanotubes. *J. Braz. Chem. Soc.* **2012**, *23* (6), 1078–+.

Singh, R.; Pantarotto, D.; McCarthy, D.; Chaloin, O.; Hoebeke, J.; Partidos, C. D.; Briand, J. P.; Prato, M.; Bianco, A.; Kostarelos, K. Binding and Condensation of Plasmid DNA onto Functionalized Carbon Nanotubes: Toward the Construction of Nanotube-Based Gene Delivery Vectors. *J. Am. Chem. Soc.* **2005**, *127* (12), 4388–4396.

Singh, S.; Vardharajula, S.; Tiwari, P.; Erdal Eroğlu; Komal Vig; Dennis, V.; Ali. Functionalized Carbon Nanotubes: Biomedical Applications. *Int. J. Nanomedicine* **2012**, 5361.

Sitharaman, B.; Tran, L. A.; Pham, Q. P.; Bolskar, R. D.; Muthupillai, R.; Flamm, S. D.; Mikos, A. G.; Wilson, L. J. Gadofullerenes as Nanoscale Magnetic Labels for Cellular MRI. *Contrast Media Mol. Imaging* **2007**, *2* (3), 139–146.

Sitharaman, B.; Zakharian, T. Y.; Saraf, A.; Misra, P.; Ashcroft, J.; Pan, S.; Pham, Q. P.; Mikos, A. G.; Wilson, L. J.; Engler, D. A. Water-Soluble Fullerene (C60) Derivatives as Nonviral Gene-Delivery Vectors. *Mol. Pharm.* **2008**, *5* (4), 567–578.

Stoller, M. D.; Park, S.; Zhu, Y.; An, J.; Ruoff, R. S. Graphene-Based Ultracapacitors. *Nano Lett.* **2008**, *8* (10), 3498–3502.

Sun, X.; Liu, Z.; Welsher, K.; Robinson, J. T.; Goodwin, A.; Zaric, S.; Dai, H. Nano-Graphene Oxide for Cellular Imaging and Drug Delivery. *Nano Res.* **2008**, *1* (3), 203–212.

Švorčík, V.; Makajová, Z.; Slepíčková Kasálková, N.; Kolská, Z.; Žáková, P.; Karpíšková, J.; Stibor, I.; Slepíčka, P. Cytocompatibility of Polymers Grafted by Activated Carbon Nano-Particles. *Carbon* **2014**, *69*, 361–371.

Tatavarty, R.; Ding, H.; Lu, G.; Taylor, R. J.; Bi, X. Synergistic Acceleration in the Osteogenesis of Human Mesenchymal Stem Cells by Graphene Oxide-Calcium Phosphate Nanocomposites. *Chem. Commun.* **2014**, *50* (62), 8484–8487.

Thommes, M.; Kaneko, K.; Neimark, A. V.; Olivier, J. P.; Rodriguez-Reinoso, F.; Rouquerol, J.; Sing, K. S. W. Physisorption of Gases, with Special Reference to the Evaluation of Surface Area and Pore Size Distribution (IUPAC Technical Report). *Pure Appl. Chem.* **2015**, *87* (9–10).

Toth, E.; Bolskar, R. D.; Borel, A.; Gonzalez, G.; Helm, L.; Merbach, A. E.; Sitharaman, B.; Wilson, L. J. Water-Soluble Gadofullerenes: Toward High-Relaxivity, pH-Responsive MRI Contrast Agents. *J. Am. Chem. Soc.* **2005**, *127* (2), 799–805.

Trostová, S.; Stibor, I.; Karpíšková, J.; Kolská, Z.; Švorčík, V. Characterization of Surface Chemical Modified Carbon Nano-Particles. *Mater. Lett.* **2013**, *102–103*, 83–86.

Trpkovic, A.; Todorovic-Markovic, B.; Trajkovic, V. Toxicity of Pristine versus Functionalized Fullerenes: Mechanisms of Cell Damage and the Role of Oxidative Stress. *Arch. Toxicol.* **2012**, *86* (12), 1809–1827.

Tsai, M. C.; Chen, Y. H.; Chiang, L. Y. Polyhydroxylated C-60, Fullerenol, a Novel Free-Radical Trapper, Prevented Hydrogen Peroxide- and Cumene Hydroperoxide-Elicited Changes in Rat Hippocampus in-Vitro. *J. Pharm. Pharmacol.* **1997**, *49* (4), 438–445.

Tykhomyrov, A. A.; Nedzvetsky, V. S.; Klochkov, V. K.; Andrievsky, G. V. Nanostructures of Hydrated C-60 Fullerene (C(60)HyFn) Protect Rat Brain against Alcohol Impact and Attenuate Behavioral Impairments of Alcoholized Animals. *Toxicology* **2008**, *246* (2–3), 158–165.

Ugarte, D. Curling and Closure of Graphitic Networks under Electron-Beam Irradiation. *Nature*

1992, 359 (6397), 707–709.

Wang, J.; Qiu, J. A Review of Carbon Dots in Biological Applications. *J. Mater. Sci.* **2016**, *51* (10), 4728–4738.

Wang, J.; Zhang, P.; Huang, C.; Liu, G.; Leung, K. C.-F.; Wang, Y. X. J. High Performance Photoluminescent Carbon Dots for In Vitro and In Vivo Bioimaging: Effect of Nitrogen Doping Ratios. *Langmuir* **2015**, *31* (29), 8063–8073.

Wang, R.; Mikoryak, C.; Li, S.; Bushdiecker, D.; Musselman, I. H.; Pantano, P.; Draper, R. K. Cytotoxicity Screening of Single-Walled Carbon Nanotubes: Detection and Removal of Cytotoxic Contaminants from Carboxylated Carbon Nanotubes. *Mol. Pharm.* **2011**, *8* (4), 1351–1361.

Wang, Y.; Lee, W. C.; Manga, K. K.; Ang, P. K.; Lu, J.; Liu, Y. P.; Lim, C. T.; Loh, K. P. Fluorinated Graphene for Promoting Neuro-Induction of Stem Cells. *Adv. Mater.* **2012**, *24* (31), 4285–.

Webster, T. J.; Siegel, R. W.; Bizios, R. Osteoblast Adhesion on Nanophase Ceramics. *Biomaterials* **1999**, *20* (13), 1221–1227.

Wen, D.; Deng, L.; Zhou, M.; Guo, S.; Shang, L.; Xu, G.; Dong, S. A Biofuel Cell with a Single-Walled Carbon Nanohorn-Based Bioanode Operating at Physiological Condition. *Biosens. Bioelectron.* **2010**, *25* (6), 1544–1547.

Whitney, J.; DeWitt, M.; Whited, B. M.; Carswell, W.; Simon, A.; Rylander, C. G.; Rylander, M. N. 3D Viability Imaging of Tumor Phantoms Treated with Single-Walled Carbon Nanohorns and Photothermal Therapy. *Nanotechnology* **2013**, *24* (27), 275102.

Whitney, J. R.; Sarkar, S.; Zhang, J.; Do, T.; Young, T.; Manson, M. K.; Campbell, T. A.; Poretzky, A. A.; Rouleau, C. M.; More, K. L.; et al. Single Walled Carbon Nanohorns as Photothermal Cancer Agents. *Lasers Surg. Med.* **2011**, *43* (1), 43–51.

Wick, P.; Manser, P.; Limbach, L. K.; Dettlaff-Weglikowska, U.; Krumeich, F.; Roth, S.; Stark, W. J.; Bruinink, A. The Degree and Kind of Agglomeration Affect Carbon Nanotube Cytotoxicity. *Toxicol. Lett.* **2007**, *168* (2), 121–131.

Xu, J.; Yudasaka, M.; Kouraba, S.; Sekido, M.; Yamamoto, Y.; Iijima, S. Single Wall Carbon Nanohorn as a Drug Carrier for Controlled Release. *Chem. Phys. Lett.* **2008**, *461* (4–6), 189–192.

Xu, X.; Ray, R.; Gu, Y.; Ploehn, H. J.; Gearheart, L.; Raker, K.; Scrivens, W. A. Electrophoretic Analysis and Purification of Fluorescent Single-Walled Carbon Nanotube Fragments. *J. Am. Chem. Soc.* **2004**, *126* (40), 12736–12737.

Yamashita, T.; Yamashita, K.; Nabeshi, H.; Yoshikawa, T.; Yoshioka, Y.; Tsunoda, S.; Tsutsumi, Y. Carbon Nanomaterials: Efficacy and Safety for Nanomedicine. *Materials* **2012**, *5* (2), 350–363.

Yang, D.; Li, T.; Xu, M.; Gao, F.; Yang, J.; Yang, Z.; Le, W. Graphene Oxide Promotes the Differentiation of Mouse Embryonic Stem Cells to Dopamine Neurons. *Nanomed.* **2014a**, *9* (16), 2445–2455.

Yang, F.; Han, J.; Zhuo, Y.; Yang, Z.; Chai, Y.; Yuan, R. Highly Sensitive Impedimetric Immunosensor Based on Single-Walled Carbon Nanohorns as Labels and Bienzyme Biocatalyzed Precipitation as Enhancer for Cancer Biomarker Detection. *Biosens. Bioelectron.* **2014b**, *55*, 360–365.

Yang, J.; Alemany, L. B.; Driver, J.; Hartgerink, J. D.; Barron, A. R. Fullerene-Derivatized Amino Acids: Synthesis, Characterization, Antioxidant Properties, and Solid-Phase Peptide Synthesis. *Chem.-Eur. J.* **2007a**, *13* (9), 2530–2545.

Yang, J.; Wang, K.; Driver, J.; Yang, J.; Barron, A. R. The Use of Fullerene Substituted Phenylalanine Amino Acid as a Passport for Peptides through Cell Membranes. *Org. Biomol. Chem.* **2007b**, *5* (2), 260–266.

Yang, W.; Auciello, O.; Butler, J. E.; Cai, W.; Carlisle, J. A.; Gerbi, J. E.; Gruen, D. M.;

Knickerbocker, T.; Lasseter, T. L.; Russell, J. N.; et al. DNA-Modified Nanocrystalline Diamond Thin-Films as Stable, Biologically Active Substrates. *Nat. Mater.* **2002**, *1* (4), 253–257.

Yantasee, W.; Lin, Y. H.; Fryxell, G. E.; Alford, K. L.; Busche, B. J.; Johnson, C. D. Selective Removal of copper(II) from Aqueous Solutions Using Fine-Grained Activated Carbon Functionalized with Amine. *Ind. Eng. Chem. Res.* **2004**, *43* (11), 2759–2764.

Zakharian, T. Y.; Seryshev, A.; Sitharaman, B.; Gilbert, B. E.; Knight, V.; Wilson, L. J. A Fullerene–Paclitaxel Chemotherapeutic: Synthesis, Characterization, and Study of Biological Activity in Tissue Culture. *J. Am. Chem. Soc.* **2005**, *127* (36), 12508–12509.

Žáková, P.; Slepíčková Kasálková, N.; Kolská, Z.; Leitner, J.; Karpíšková, J.; Stibor, I.; Slepíčka, P.; Švorčík, V. Cytocompatibility of Amine Functionalized Carbon Nanoparticles Grafted on Polyethylene. *Mater. Sci. Eng. C* **2016**, *60*, 394–401.

Zhang, J.; Yuan, Y.; Liang, G.; Yu, S.-H. Scale-Up Synthesis of Fragrant Nitrogen-Doped Carbon Dots from Bee Pollens for Bioimaging and Catalysis. *Adv. Sci.* **2015**, *2* (4), 1500002.

Zhang, R.; Olin, H. Carbon Nanomaterials as Drug Carriers: Real Time Drug Release Investigation. *Mater. Sci. Eng. C-Mater. Biol. Appl.* **2012**, *32* (5), 1247–1252.

Zhang, Y.; Xu, Y.; Li, Z.; Chen, T.; Lantz, S. M.; Howard, P. C.; Paule, M. G.; Slikker, W.; Watanabe, F.; Mustafa, T.; et al. Mechanistic Toxicity Evaluation of Uncoated and PEGylated Single-Walled Carbon Nanotubes in Neuronal PC12 Cells. *ACS Nano* **2011**, *5* (9), 7020–7033.

Zhao, G.; Schwartz, Z.; Wieland, M.; Rupp, F.; Geis-Gerstorfer, J.; Cochran, D. L.; Boyan, B. D. High Surface Energy Enhances Cell Response to Titanium Substrate Microstructure. *J. Biomed. Mater. Res. A* **2005**, *74A* (1), 49–58.

Zhu, C.; Du, D.; Lin, Y. Graphene and Graphene-like 2D Materials for Optical Biosensing and Bioimaging: A Review. *2D Mater.* **2015**, *2* (3), 032004.

*Carbon Nanomaterials for Biomedical Applications*; Zhang, M., Naik, R. R., Dai, L., Eds.; Springer Series in Biomaterials Science and Engineering; Springer International Publishing: Cham, 2016; Vol. 5.

## 9. LIST OF PUBLICATIONS

**h-index:** 3

**Impacted articles:** 4

**Oral presentations at international conferences (abroad):** 5 (4)

**Poster presentations at international conferences (abroad):** 4 (2)

### 9.1. Articles in impacted journals

a) Žáková, P., Slepíčková Kasálková, N., Kolská, Z., Leitner, J., Karpíšková, J., Stibor, I., Slepíčka, P., Švorčík, V.: Cytocompatibility of Amine Functionalized Carbon Nanoparticles Grafted on Polyethylene. *Materials Science and Engineering: C* 60 (1 March 2016): 394–401. doi:10.1016/j.msec.2015.11.058.

b) Švorčík, V., Makajová, Z., Slepíčková Kasálková, N., Kolská, Z., Žáková, P., Karpíšková, J., Stibor, I., Slepíčka, P.: Cytocompatibility of Polymers Grafted by Activated Carbon Nanoparticles. *Carbon* 69 (April 2014): 361–71. doi:10.1016/j.carbon.2013.12.037.

c) Trostová, S., Stibor, I., Karpíšková, J., Kolská, Z., Švorčík, V.: Characterization of surface chemical modified carbon nano-particles, *Materials Letters*, Volumes 102–103, July 2013, 83–86. doi:10.1016/j.matlet.2013.03.119.

d) Šlamborová, I., Zajícová, V., Karpíšková, J., Exnar, P., Stibor, I.; New type of protective hybrid and nanocomposite hybrid coatings containing silver and copper with an excellent antibacterial effect especially against MRSA, *Materials Science and Engineering: C*, Volume 33, Issue 1, 1 January 2013, 265–273, ISSN 0928-4931. doi: 10.1016/j.msec.2012.08.039

### 9.2. Articles in non-impacted journals

a) Šlamborová, I., Zajícová, V., Karpíšková, J. a Exnar, P.: Immobilisation of antibiotic tetracycline on silica nanofibres. *Vlákna a Textil.* 2012, 19(2), 3–9. ISSN 1335-0617.

### 9.3. Conferences

- oral presentations:

a) Karpiskova, J., Pilarova, K., Jencova, V., Stibor, I., Chvojka, J., Mikes, P., Nguyen, H. A. N.: Cytocompatibility of Polycaprolactone Nano-Microfibrous Scaffolds Loaded with Amide-Amine Functionalised Carbon Nanoparticles, *6<sup>th</sup> EuCheMS 2016 Chemistry Congress, Seville, Spain*. September 11–15 2016

b) Karpiskova, J., Pilarova, K., Jencova, V., Stibor, I., Chvojka, J., Mikes, P., Nguyen, H. A. N.: Cytocompatibility of Polycaprolactone Nano-Microfibrous Scaffolds Loaded with Amide-Amine Functionalised Carbon Nanoparticles, *NANOinBIO 2016: Advances for life & Materials Science, Guadeloupe*. May–June 2016.

c) Karpiskova, J., Pilarova, K., Jencova, V., Stibor, I., Chvojka, J., Mikes, P.: Polycaprolactone Nanofibrous Scaffolds Loaded with Amide-Amine Functionalised Carbon Nanoparticles and

Their Effect on 3T3 Mouse Fibroblasts. *International Conference on Nanoscience, Nanotechnology and Advanced Materials NANOS15, Visakhapatnam, India*. December 2015

d) Karpiskova, J., Pilarova, K., Jencova, V., Stibor, I., Chvojka, J., Mikes, P.: Polycaprolactone Micro-Nanofibrous Scaffolds Loaded with Amide-Amine Functionalised Carbon Particles and Their Effect on 3T3 Mouse Fibroblasts. *NANOCON 2015, 7th International Conference, Brno*, 14-16 October 2015

e) Karpiskova, J., Pilarova, K., Jencova, V., Stibor, I., Chvojka, J., Mikes, P.: Polycaprolactone Nanofibrous Scaffolds Loaded with Amide-Amine Functionalised Carbon Nanoparticles and Their Effect on 3T3 Mouse Fibroblasts. *2nd Annual International Conference on Nanoscience and Nanotechnology (ICNSNT) 2015, Colombo, Sri Lanka*. September 2015

-posters and other:

a) Žáková, P., Slepíčková Kasálková, N., Slepíčka, P., Švorčík, V.: Cell adhesion and proliferation on amine functionalized carbon nanoparticles grafted biopolymer. *NANOCON 2015, 7th International Conference, Brno*, 14-16 October 2015 – article in conference proceedings and poster

b) Karpíšková, J., Stibor, I., Švorčík, V., Makajová, Z., Slepíčková Kasálková, N., Kolská, Z., Žáková, P., Slepíčka, P.: Polymer Surfaces Grafted With Functionalized Carbon Nanoparticles For Cell Culturing. *5th EuCheMS Chemistry Congress, Istanbul, Turkey*, 31 August-4 September 2014 – poster

c) Karpíšková, J., Stibor, I., Švorčík, V., Makajová, Z., Slepíčková Kasálková, N., Kolská, Z., Žáková, P., Slepíčka, P.: Cytocompatibility Of Polymer Surfaces Grafted With Amid-Amine Functionalized Carbon Nanoparticles, *Challenges in Nanoscience ISACS 15, San Diego, California*, 17-20 August 2014 – poster

d) Karpíšková, J., Stibor, I., Švorčík, V., Makajová, Z., Slepíčková Kasálková, N., Kolská, Z., Žáková, P., Slepíčka, P.: Surfaces with Carbon Nanoparticles for Medical Applications, *5<sup>th</sup> International Conference Nanocon, Brno*, 16-18 October 2013 – article in conference proceedings and poster

e) Švorčík, V., Makajova, Z., Slepíčková Kasálková, N., Kolská, Z., Stibor, I., Karpíšková, J., Žáková, P., Slepíčka, P.: Cytocompatibility of polymers grafted by activated carbon nanoparticles, *XVII Eur. Conf. Anal. Chem., Warsaw, Poland*, 25-29 August 2013 – poster

f) Šlamborová, I., Zajícová, V., Stibor, I., Karpíšková, J., Exnar, P.: High Protective Hybrid Coating Containing Silver, Copper and Zinc Ions with an Excellent Antibacterial Effect Especially Against Bacterial Strains of MRSA. *Potential and Application of Nanotreatment of Medical Surfaces – Book of Extended Abstracts Liberec – TUL2012*, 4, ISBN: 978-80-7372-890-8. – article in conference proceedings

g) Karpíšková, J.: Antibiotické látky ve vybraných rostlinách. *Jelenia Gora: 5th International Conference of Young Scientists, 2011*. ISBN 978-83-62708-21-5 – 1<sup>st</sup> award winning article in conference proceedings

- h) Karpíšková, J.: Zkoumání antibiotických látek v rostlinách. *Sborník přednášek z mezinárodní konference Trojanovice*. September 29 – October 1 2010. Přírodovědecká Fakulta Ostravské univerzity v Ostravě, edit.: A. Chupáč, J. Vermířovský. ISBN 978-80-7368-426-6. – article in conference proceedings
- i) Grégr, J., Karpíšková, J., Kopecká, V., Slavík, M.: ICT pro řešení problémů chemie rostlinných látek, *Aktuální trendy ICT ve výuce chemie – Current trends of ICT in chemistry education XX, Book of abstracts*, p. 47, ISBN 978-80-7041-082-5.
- j) Grégr, J., Karpíšková, J., Kopecká, V., Slavík, M., Šlamborová, I.: ICT pro řešení problémů chemie rostlinných látek – ICT for Solving Problems of Herbal Chemistry, *Media4u Magazine X3/2010*, str. 186, ISSN 1214-9187.
- k) Jodas, B., Grégr, J., Karpíšková, J., Slavík, M.: Problémové úlohy v chemii řešené pomocí molekulární vizualizace, *Sborník přednášek 19. mezinárodní konference o výuce chemie*, 2. část: Přehledové studie a krátké informace, Hradec Králové, IX-2009, edit.: M. Bílek, str. 247-250, ISBN 978-80-7041-839-0.